
Centro Brasileiro de Pesquisas Físicas
Programa de Mestrado

Mariana Teixeira Santos

# Irreversibility of Effective Dynamics in Closed Quantum Systems

Rio de Janeiro/RJ

2026

# Irreversibility of Effective Dynamics in Closed Quantum Systems

Mariana Teixeira Santos

Dissertação de mestrado submetida a coordenação de formação científica do Centro Brasileiro de Pesquisas Físicas como parte dos requisitos para a obtenção do título de Mestre em Física.
Orientador: Dr. Fernando de Melo
Coorientador: Dr. Raúl Vallejos

Rio de Janeiro/RJ

2026

"IRREVERSIBILITY OF EFFECTIVE DYNAMICS IN CLOSED QUANTUM SYSTEMS"

**MARIANA TEIXEIRA SANTOS**

Dissertação de Mestrado em Física apresentada no Centro Brasileiro de Pesquisas Físicas do Ministério da Ciência Tecnologia e Inovação. Fazendo parte da banca examinadora os seguintes professores:

Fernando da Rocha Vaz Bandeira de Melo - Orientador/CBPF

Raul Oscar Vallejos – Coorientador/ CBPF

Marcelo Paleólogo Elefteriadis de França Santos – UFRJ

Welles Antonio Martinez Morgado – PUC/RJ

Rio de Janeiro, 29 de abril de 2026.

# Abstract

Effective macroscopic descriptions of quantum systems may involve loss of information and can exhibit irreversibility, even when the underlying microscopic dynamics is unitary. This motivates the investigation of how irreversibility can emerge from fundamentally reversible theories. In classical statistical mechanics, Boltzmann entropy quantifies the volume of microscopic phase space compatible with a macroscopic state. We extend this notion to quantum systems by defining and computing the corresponding volume in Hilbert space for specific quantum preparations and we use this volume to link to irreversibility in closed systems undergoing effective evolution. Irreversibility here is defined by the distance between effective states. We first examine the link between volume growth and irreversibility using coarse-graining maps, which explicitly implement the micro-to-macro assignment and induce effective irreversible dynamics. The same relation emerges for ensembles of microstates constrained only by sharing the same expectation value of an observable. Analogous to classical statistical mechanics, these results suggest irreversibility arises from the growth of the volume of Hilbert microstates compatible with the observed macrostate.

**Keywords**: Irreversibility. Effective descriptions. Coarse-graining maps.

# Resumo

Descrições macroscópicas efetivas de sistemas quânticos podem envolver perda de informação e exibir irreversibilidade, mesmo quando a dinâmica microscópica subjacente é unitária. Isso motiva a investigação de como a irreversibilidade pode emergir a partir de teorias fundamentalmente reversíveis. Na mecânica estatística clássica, a entropia de Boltzmann quantifica o volume do espaço de fase microscópico compatível com um estado macroscópico. Estendemos essa noção para sistemas quânticos ao definir e calcular o volume correspondente no espaço de Hilbert para preparações quânticas específicas e relacionamos esse volume com irreversibilidade em sistemas fechados submetidos à evolução efetiva. Irreversibilidade aqui é definida pela distância de estados efetivos. Inicialmente, examinamos a relação entre o crescimento do volume e a irreversibilidade por meio de mapas de coarse-graining, que implementam explicitamente a atribuição do nível microscópico ao macroscópico e induzem uma dinâmica efetiva irreversível. A mesma relação emerge para conjuntos de microestados restritos apenas pelo compartilhamento do mesmo valor esperado de um observável. De modo análogo à mecânica estatística clássica, esses resultados sugerem que a irreversibilidade surge do crescimento do volume de microestados no espaço de Hilbert compatíveis com o macroestado observado.

**Palavras-chave**: Irreversibilidade. Descrição efetiva. Mapas coarse-graining.

# Agradecimentos

Primeiro agradeço ao *Universo* por todas as oportunidades dadas para que eu chegasse até aqui. Não foi fácil. Vim de uma família com poucos recursos, em que títulos acadêmicos são raros e na qual a carreira acadêmica, embora admirada, não é muito bem compreendida.

Segundo, agradeço à minha família: meus pais, avós, irmãos e primos pelo apoio. Em especial à minha mãe, Ana Regina, meu exemplo, que sempre me incentivou a galgar passos cada vez maiores. E à minha avó, por todo o suporte dado. Agradeço também ao meu parceiro de vida, Yudi, por todo o apoio e companheirismo.

Agradeço aos professores Fernando e Raul por toda a orientação, paciência e zelo nesses dois anos de supervisão acadêmica e também por todos os esforços e incentivos investidos em mim durante esse período. Agradeço também a José Leon e Isadora Veeren pela colaboração com o grupo de pesquisa.

Agradeço aos meus amigos de Salvador e do Rio de Janeiro pelo acolhimento, bate-papos, cafés e muretas, e por acreditarem em mim e me incentivarem a continuar.

Agradeço à CAPES pelo financiamento e aos professores, servidores e terceirizados do CBPF pela estrutura e pelas oportunidades.

# Contents

# 1 Introduction

I grew up in a world profoundly shaped by technology while still being surrounded by nature. This coexistence between rapid technological development and natural phenomena fostered in me a curiosity about how the physical world operates at its most fundamental level. During adolescence, this curiosity naturally led me to study physics.

While exploring different research areas, I became particularly fascinated by quantum information (QI). At first, the notion of "information" seemed disconnected from the quantum mechanical systems I was studying: potential wells, hydrogen atoms, and Schrödinger's equation. At that time, I understood information in its everyday sense as accumulated knowledge about a topic or the clarification of existing knowledge [1]. How could information be embedded in such systems? A course in the history of science clarified this connection and revealed how deeply intertwined the concept of information is with the foundations of quantum theory. From that point onward, I decided to focus my academic work on this field during my master's program.

During the first year of my master's studies, I concentrated on quantum information, open quantum systems and generalized subsystems, in which a system of dimension $d$ provides an effective description of a larger system of dimension $D$, with $D > d$. In the second year, building upon these concepts, our research group refined the central question that motivates this work: can irreversibility emerge from the effective dynamics of closed quantum systems? This question is particularly intriguing because it touches upon the interplay between irreversibility and closed quantum systems.

The main objective of this work is to investigate whether effective dynamics in closed quantum systems can exhibit irreversible behavior. More specifically, we aim to review an entropy measure defined through the volume of the set of microscopic states in Hilbert space that are compatible with a given effective description; to define irreversibility in terms of a distance between effective states; and to relate the growth of the volume of compatible microstates under effective dynamics to the distinguishability of effective states.

The motivation for this investigation lies in the fundamental importance of the second law of thermodynamics. The development of physics is often closely connected to its historical context. During the Industrial Revolution in the 18th and 19th centuries, the emergence of heat engines raised fundamental questions about the limits of efficiency in cyclic processes. In particular, it was asked whether a heat engine could achieve 100% efficiency, operating indefinitely without energy dissipation.

To address this question, Carnot demonstrated that the efficiency of a heat engine

reaches its maximum only when the cycle is reversible and that any irreversibility necessarily reduces its efficiency [2]. Later, Clapeyron provided an algebraic formulation of what are now known as Carnot cycles. In the mid-19th century, Kelvin and Clausius extended these ideas beyond cyclic engines to natural processes. Clausius introduced entropy as a state function and established that, for isolated systems, entropy increases in irreversible processes, leading to a formulation of the second law of thermodynamics [2].

The success of thermodynamics motivated the search for a microscopic foundation of its macroscopic laws. This effort gave rise to statistical mechanics, developed by Maxwell, Boltzmann, and Gibbs [2]. In Boltzmann's formulation, a single macrostate corresponds to a collection of microstates, and the concept of entropy is related to the number of microscopic configurations ($W$) compatible with a given macroscopic description

$$S = k_B \ln W, \tag{1.1}$$

where $k_B$ is the so-called Boltzman's constant introduced by Planck [3]. In classical statistical mechanics, each microstate of the system is associated with a point in phase space, and the system evolves according to Hamiltonian dynamics. The number of microstates compatible with a macrostate is therefore measured by the volume containing these accessible microstates [4].

In classical mechanics framework a point in phase space specifies the positions $q \in \mathbf{R}^3$ and momenta $p \in \mathbf{R}^3$ of all particles, thereby defining a microscopic state $x = (q_1, ..., q_N, p_1, ..., p_N)$. Since considering both position and momentum as three-dimensional variables, the phase space of the system is $R^{6N}$.

In statistical mechanics, the probability associated with a macroscopic preparation of a classical system composed of N particles is related to the size of the accessible region in phase space compatible with it: low-probability preparations correspond to small regions, whereas highly probable preparations, such as thermal equilibrium, correspond to much larger regions.

Let $x(0)$ be a microstate compatible with a low-probability preparation. Under Hamiltonian dynamics, this microstate evolves through phase space. Although the microscopic evolution is reversible, the evolved state is, in general, associated with macroscopic preparations compatible with much larger regions of phase space. Since these regions overwhelmingly dominate the accessible volume, the probability of the system spontaneously returning to the initial small region becomes negligible.

In this sense, reversible microscopic dynamics generally gives rise to irreversible macroscopic behavior. Irreversibility emerges because the number of microstates compatible with the evolved macroscopic preparation is most of the time much larger than the number compatible with the initial one. Figure 1 (taken from [5]) illustrates this idea through a two-dimensional schematic representation of microscopic evolution in phase space, with

scales omitted for simplicity.

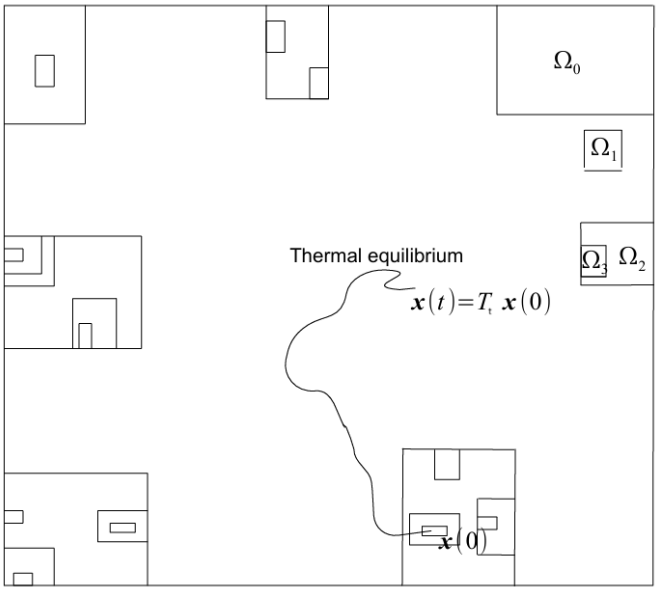


Figure 1 – A possible evolution of a microstate $x(t) = T_t\, x(0)$ in phase space a representation not drawn to scale. Small acessible regions correspond to low-probability preparation of a classical system composed of N particles and large acessible regions to highly probable preparation. Figure taken from [5].

In Boltzmann's framework, entropy is overwhelmingly likely to increase for typical initial conditions and this statistical interpretation troubled several of Boltzmann's contemporaries [6]. One of the earliest conceptual challenges to Boltzmann's statistical interpretation of the second law was raised by Loschmidt in 1876 [7], Thomson in 1874 [8] and Zermelo in 1886 [9]. Boltzmann's $H$-theorem suggested that a certain quantity associated with the microscopic distribution of particles decreases monotonically in time, indicating a preferred direction for the time evolution. Loschmidt pointed out, however, that the microscopic laws governing particle dynamics are time-reversal invariant. If a system evolves from an initial state at time $t = 0$ to a state at time $t$, reversing all particle velocities should lead the system to retrace its trajectory and return to the original configuration. In this reversed evolution the quantity $H$ would increase, apparently contradicting the monotonic behaviour predicted by the $H$-theorem. This argument, known as the reversibility paradox, highlights the tension between the time-symmetric character of microscopic laws and the irreversible behaviour observed at the macroscopic level [3].

A discussion of Boltzmann's response to these objections can be found in Ref. [3], where the statistical nature of macroscopic irreversibility is emphasized. As pointed out in that reference,

> In other words, the impossibility of observing macroscopic phenomena that run backwards with respect to those that are actually observed is, in the last

> analysis, due to the large number of molecules present even in macroscopically small volumes [3].

The German mathematician and philosopher Ernst Zermelo, on the other hand, based on Poincaré's recurrence, stated that "a bounded world, governed by the laws of mechanics, will always pass through a state very close to its initial state" (Zermelo quoted in [3]). Boltzmann replied to Zermelo in 1897 [10] as quoted in [3] :

> Thus when Zermelo concludes, from the theoretical fact that the initial states in a gas must recur — without having calculated how long a time this will take —, that the hypotheses of gas theory must be rejected or else fundamentally changed, he is just like a dice player who has calculated that the probability of a sequence of 1000 one's is not zero, and then concludes that his dice must be loaded since he has not yet observed such a sequence! [3]

These discussions highlight the statistical nature of the second law: macroscopic irreversibility does not contradict the reversibility of microscopic dynamics, but instead reflects the overwhelmingly larger number of microscopic configurations associated with macroscopic states of higher entropy.

While Boltzmann's entropy was originally formulated to describe the number of microscopic configurations compatible with a macroscopic state, J. W. Gibbs introduced an alternative formulation based on statistical ensembles. In Gibbs's approach, a physical system is represented by a large collection of identically prepared copies. Rather than counting microstates compatible with a macrostate, this description is given in terms of a probability density over the phase space and thermodynamic quantities are represented as ensemble averages.

Gibbs entropy is [11]

$$S(\rho) = -k_b \int_\Gamma dx \rho(x) \log\left(\rho(x)\right) \tag{1.2}$$

where $k_B$ is Boltzmann's constant, $\Gamma = \mathbf{R}^{6N}$ is the phase space of the physical system for N point particles in $\mathbf{R}^3$ with positions $\mathbf{q}_i$ and momentos $\mathbf{p}_i$, $dx = N!^{-1} d^3\mathbf{q}_1 d^3\mathbf{p}_1 ... d^3\mathbf{q}_N d^3\mathbf{p}_N$ is the phase space volume measure and $\rho(x)$ is the probability distribution on $\Gamma$.

In the 1940s, Claude Shannon, motivated by problems in communication theory, introduced a mathematical measure of information based on probability distributions [12]. Consider a discrete random variable with outcomes $\{x_i\}$ occurring with probabilities $\{p_i\},\ i = 1, ..., M$. Its entropy is defined as

$$S = -\sum_{i=1}^{M} p_i \ln p_i, \tag{1.3}$$

which quantifies the uncertainty associated with the probability distribution over $\{x_i\}$ [12, 13].

In quantum mechanics, classical probability distributions are replaced by density operators. The von Neumann entropy is defined as

$$S(\rho) = -\mathrm{tr}(\rho \ln \rho), \tag{1.4}$$

or, equivalently, in terms of the eigenvalues of $\rho$,

$$S(\lambda_i) = -\sum_i \lambda_i \ln \lambda_i, \tag{1.5}$$

and constitutes the natural quantum generalization of Shannon entropy [14]. When the density operator is diagonal in a given basis, the von Neumann entropy reduces to the classical expression.

In the von Neumann framework, the entropy reflects the uncertainty encoded in the eigenvalue distribution, i.e. the lack of knowledge about which eigenstate would be obtained in a measurement performed in the eigenbasis. Under unitary evolution, which governs closed quantum systems through the Schrödinger equation, the von Neumann entropy remains constant, reflecting the reversibility of closed quantum evolution [12, 14, 15]. In contrast, under effective dynamics, a useful indicator of irreversibility is how the evolution modifies the spectrum of the state, leading to changes in entropy and purity.

The fundamental laws of physics are reversible, yet macroscopic dynamics is generally not. How then can irreversibility emerge from fundamental laws? As mentioned earlier, this work focuses on effective dynamics and more precisely, we analyze the evolution of effective (macroscopic) descriptions associated with constrained sets of microstates. Although the underlying dynamics take place in closed quantum systems, the passage from a microscopic description to a macroscopic one cannot be neglected. In general, this reduction to an effective description is accompanied by a loss of accessible information and, consequently, by an increase in uncertainty about the underlying microstates.

Since our goal is to analyze entropy in the quantum domain while allowing for information loss at the level of effective dynamics, we review an entropy formulation analogous to Boltzmann's, in which the counting of microstates compatible with a given macrostate, represented here by an effective state, is performed directly in Hilbert space [16, 17]:

$$S(\rho) \propto \log(\mathcal{V}(\rho)). \tag{1.6}$$

This definition employs the volume of microscopic states associated with an effective description, $\mathcal{V}(\rho)$, and will serve as the basis for our analysis of irreversibility.

The effective dynamics considered here describe the evolution of macroscopic states, that is, the level at which experimental access is available. We represent these macroscopic

states through a collection of fixed expectation values of relevant observables. When the chosen set is tomographically complete, these expectation values uniquely determine an effective density operator.

The preparation of such an effective state can be interpreted as defining a collection of compatible microscopic states in a higher dimensional Hilbert space. The connection between microscopic and macroscopic levels is established through a dimension-reduction map, which associates microscopic descriptions with their corresponding effective representations.

In this framework, Ref. [18–20] consider that the effective dynamics, i.e. the dynamics of the effective description $\rho$ or even a fixed expectation value, are given by the composition of three operations: an assignment map, which associates a macroscopic state with a set of compatible microscopic states; a unitary evolution, which governs the closed-system dynamics from an initial time $t = 0$ to a later time $t$; and a coarse-graining map, which projects the evolved microscopic description back onto the reduced macroscopic level. This structure is illustrated in Fig. 2.

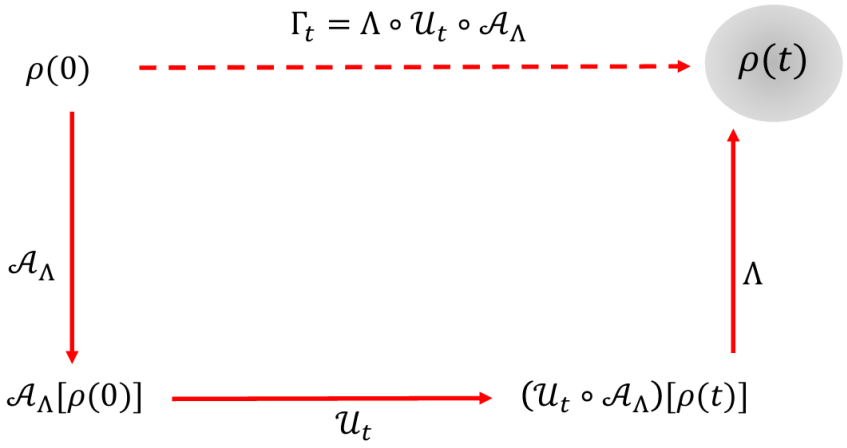


Figure 2 – A macroscopic effective dynamics represented by a composition of quantum operations: assignment map ($\mathcal{A}_\Lambda : \mathcal{L}(\mathcal{H}_d) \to \mathcal{L}(\mathcal{H}_D)$), unitary evolution ($\mathcal{U}_t : \mathcal{L}(\mathcal{H}_D) \to \mathcal{L}(\mathcal{H}_D)$) and coarse-graining map ($\Lambda : \mathcal{L}(\mathcal{H})_D \to \mathcal{L}(\mathcal{H}_d) \quad D > d$).

As effective dynamics provide the framework used throughout this thesis, we briefly introduce their fundamental operations here. The following chapter will illustrate how these operations arise in different scenarios.

We begin by introducing coarse-graining maps, following Refs. [19, 21, 22]. Let $\mathcal{H}_D$ be a Hilbert space of dimension $D$, and let $\mathcal{L}(\mathcal{H}_D)$ denote the set of linear operators acting on this space. A linear map

$$\Lambda : \mathcal{L}(\mathcal{H}_D) \to \mathcal{L}(\mathcal{H}_d)$$

is said to be completely positive and trace preserving (CPTP) if it satisfies the following two properties [12]:

1. Trace preservation:
$$\mathrm{tr}\Big[\Lambda(\psi)\Big] = \mathrm{tr}[\psi] \quad \forall\, \psi \in \mathcal{L}(\mathcal{H}_D),$$
which guarantees that probabilities are conserved under the action of the map.

2. Complete positivity: for any auxiliary Hilbert space $\mathcal{H}_Z$ of arbitrary dimension $Z$, the extended map
$$\Lambda \otimes \mathbf{1}_Z : \mathcal{L}(\mathcal{H}_D \otimes \mathcal{H}_Z) \to \mathcal{L}(\mathcal{H}_d \otimes \mathcal{H}_Z)$$
maps positive operators to positive operators, i.e.,
$$(\Lambda \otimes \mathbf{1}_Z)[\psi] \geq 0 \quad \text{whenever } \psi \geq 0.$$
This condition ensures that states are mapped into states even when the map acts locally on a subsystem.

A linear map is complete positive trace-preserving (CPTP) if and only if it admits a Kraus representation [12, 19, 22],

$$\Lambda[\psi] = \sum_{i=1}^{N} K_i \psi K_i^\dagger, \qquad \sum_{i=1}^{N} K_i^\dagger K_i = \mathbf{1}_D, \tag{1.7}$$

where the operators $\{K_i\}_{i=1}^N$, known as Kraus operators, satisfy $K_i : \mathcal{H}_D \to \mathcal{H}_d$. This representation is not unique [19]: two sets $\{K_i\}$ and $\{K_i'\}$ describe the same CPTP map if and only if they are related by a unitary transformation acting on the Kraus index, i.e.,

$$K_i' = \sum_j u_{ij} K_j, \tag{1.8}$$

where $U = (u_{ij})$ is a unitary matrix.

A coarse-graining map is a CPTP map that reduces the dimension of the Hilbert space,

$$\Lambda : \mathcal{L}(\mathcal{H}_D) \to \mathcal{L}(\mathcal{H}_d), \quad D > d,$$

and is typically used when fine-grained information about the underlying microscopic description is either inaccessible or intentionally averaged out [19]. The partial trace provides a standard example of a coarse-graining CPTP map, since it reduces dimension while preserving positivity and trace.

In this work, following Refs. [17–20, 23], we also consider coarse-graining maps associated with blurred and saturated detectors. In such cases, the effective description

cannot be reduced to a simple partial trace and reflects more general forms of information loss.

The second operation to be specified based on Refs. [17, 18, 20] is the averaging assignment map. This map connects a macroscopic description to a compatible microscopic one,

$$\mathcal{A}_\Lambda : \mathcal{L}(\mathcal{H}_d) \to \mathcal{L}(\mathcal{H}_D), \quad D > d.$$

Consider a macroscopic constraint given by a set of mean values $\mathcal{O} = \{o_i\}_{i=1}^N$, obtained from measuring observables $\{O_i\}$ with $O_i \in \mathcal{L}(\mathcal{H}_d)$, such that $o_i = \mathrm{tr}\,(O_i\rho_d) \quad \forall\, i \in [1, ..., |\mathcal{O}|]$ and $\rho_d$ is a density matrix in $\mathcal{L}(\mathcal{H}_d)$ [20]. Let $\psi = |\psi\rangle\langle\psi|$ be a microscopic pure state in $\mathcal{L}(\mathcal{H}_D)$. The macroscopic data satisfy:

$$o_i = \mathrm{tr}\Big[\Lambda(\psi)O_i\Big], \quad \forall\, i \in [N]\,.$$

Preparing the macroscopic data $\mathcal{O}$ defines a set of compatible microscopic states,

$$\Omega_\Lambda(\mathcal{O}) = \Big\{\psi \in \mathcal{L}(\mathcal{H}_D) \,\Big|\, \mathrm{tr}\Big[\Lambda(\psi)O_i\Big] = o_i,\ \forall\, i \in [N]\Big\}\,. \tag{1.9}$$

An averaging assignment map associates the average over the compatible microscopic states [18] with the macroscopic description,

$$\mathcal{A}_\Lambda[\mathcal{O}] = \int d\mu_\psi\ \mathrm{Pr}_\Lambda(\psi \mid \mathcal{O})\,\psi, \tag{1.10}$$

where $d\mu_\psi$ denotes the uniform Haar measure over pure states, and $\mathrm{Pr}_\Lambda(\psi \mid \mathcal{O})$ is the probability density of the microscopic state $\psi$ conditioned on the macroscopic constraints $\mathcal{O}$ and the coarse-graining map. In general, this assignment map is neither linear nor CPTP. However, it provides an average microscopic description compatible with the given macrostate, yielding a physically meaningful state.

Notice that the effective dynamics

$$\Gamma_t = \Lambda \circ \mathcal{U}_t \circ \mathcal{A}_\Lambda$$

cannot, in general, be represented by a unitary evolution, even though the underlying microscopic evolution is unitary and takes place in a closed quantum system. The composition of assignment, unitary evolution, and coarse-graining maps defines a reduced dynamics that requires a notion of entropy that allows the loss of accessible information in the dynamical process, thereby enabling a meaningful analysis of the emergence of irreversibility.

Macroscopic states can also be described through a collection of fixed expectation values of relevant observables and the effective dynamics, in this case, are represented by the evolution of expectation values. Consider $A$ an observable and the set

$$\Omega_A = \{\phi \in \mathcal{L}(\mathcal{H}_D) | \langle\phi|A|\phi\rangle = a_0\}. \tag{1.11}$$

In this scenario, aiming to a more analytical description, we employ the concept of dynamical typicality, introduced by Bartsch and Gemmer in Ref. [24]. Microscopic states constrained to yield the same expectation value at time $t = 0$, $a_0$, produce concentrated (typical) expectation values at later times. Consequently, the microscopic evolution can be characterized, with high accuracy, solely through the evolution of these typical expectation values, as illustrated in Fig. 3.

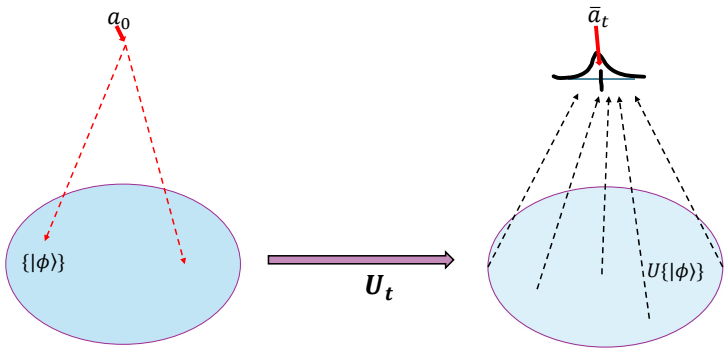


Figure 3 – A macroscopic forward dynamics of expectation values. The bar over $\bar{a}(t)$ represents the average over all pure microscopic states that evolved from the set defined by $a_0$.

Dynamical typicality is essential for characterizing the evolution of expectation values, which, in this context, play the role of an effective dynamics. Although a single expectation value does not uniquely determine a density matrix, we adopt the same conceptual structure of effective states: the expectation value specifies the macroscopic description, while the set of compatible pure states constitutes the underlying microscopic set.

In this work, we investigate effective dynamics in two complementary scenarios. First, when the set of observables is tomographically complete, the dynamics are described through the composition of coarse-graining, assignment, and unitary maps. Second, when the effective description is specified by a collection of relevant expectation values, we analyze the dynamics at the level of these expectation values.

As the main objective of this work is to investigate whether effective dynamics in closed quantum systems can exhibit irreversible behavior, we recall the second law of

thermodynamics states: for an isolated system undergoing a process,

$$\Delta S \geq 0, \tag{1.12}$$

its entropy never decreases [25]. Within our framework, considering an analogue of thermodynamics, entropy growth can be analyzed by comparing the volumes of the corresponding sets of microscopic states before and after the effective evolution.

However irreversibility can be defined directly at the level of effective descriptions, without explicit reference to the full microscopic ensemble. This is achieved by analyzing the distinguishability between macroscopic states, as schematically represented in Fig. 4.

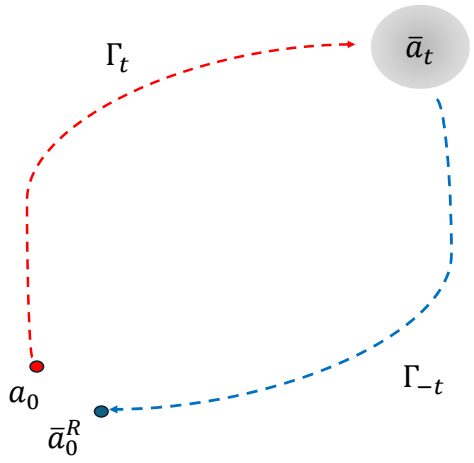


Figure 4 – A macroscopic arbitray dynamics represented by $\Gamma_t$ in red. Backward dynamics in blue represent by $\Gamma_{-t}$. If $\bar{a}_0^R$ and $a_0$ cannot be distinguished the process is irreversible.

If the process is reversible, the initial expectation value $a_0$ and the recovered one, obtained after forward and backward evolution denoted $\bar{a}_0^R$, are indistinguishable for the observable we are using. Conversely, if these expectation values can be distinguished, the process is irreversible. Since quantum states can be discriminated through distance measures, the distinguishability between $a_0$ and $\bar{a}_0^R$ provides an operational criterion for irreversibility: a nonzero distance signals the impossibility of fully recovering the initial macroscopic description. When the chosen set of observables is tomographically complete, these expectation values uniquely determine an effective density operator. Than we compare the initial effective state, $\rho(0)$, and the state obtained after a forward and

backward dynamics $\rho_R(0)$. The process is irreversible if the distance between $\rho(0)$ and $\rho_R(0)$ is not null and reversible otherwise.

The advantage of formulating irreversibility in terms of distance between effective states is that it does not require explicit reference to the microscopic level. While the macroscopic description arises from microscopic degrees of freedom, experimentally accessible quantities are naturally expressed at the effective level.Moreover, another question arises: can we define irreversibility through the behavior of the volume associated with the preparation before and after evolution in Hilbert space? We will show results that suggest this relation.

When referring to volume behavior, we have in mind a picture analogous to the classical one shown in Fig. 1. Consider a set of observed quantities of an observable, $\mathcal{O} = \{o_i\}_{i=1}^{N}$, obtained from measurements of observables $\{O_i\}$ with $O_i \in \mathcal{L}(\mathcal{H}_d)$. For a given low-probability outcome $o_1$, let $\Omega(o_1)$ denote the set of microscopic states compatible with that observation. The volume associated with $o_1$ is then defined as the measure of $\Omega(o_1)$

$$\Omega(o_1) = \{\psi(0) \in \mathcal{L}(\mathcal{H}_D) | \mathrm{tr}\left(\Lambda[\psi(0)]O_1\right) = o_1\}. \tag{1.13}$$

Let $\psi(0)$ be a microstate compatible with a low-probability preparation $o_1$. Under unitary dynamics, this microstate evolves through Hilbert space. Although microscopic evolution is reversible, the evolved microscopic state is generally associated with macroscopic preparations compatible with much larger regions of phase space; i.e., there are more accessible microstates available besides $\psi(0)$. Since these regions largely dominate the accessible volume, the probability of the system spontaneously returning to the small initial region becomes negligible.

In Fig. 5 we show a representation not drawn to scale of two dimensional Hilbert space of this microscopic evolution. We use Hilbert space rather than quantum phase space because it is a quantum mechanics natural space and it is not possible to define trajectories in the quantum version of phase space.

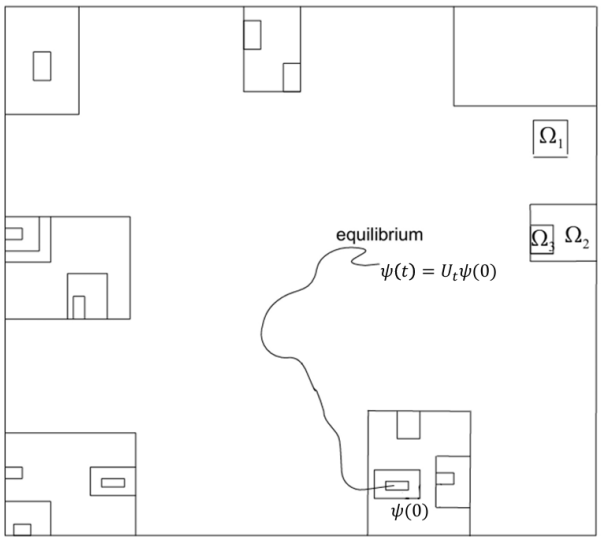


Figure 5 – Possible microscopic evolution $\psi(t) = U_t\ \psi(0)$ in Hilbert space. Small regions correspond to low-probability preparation of a classical system composed of N particles and large regions to highly probable preparation.

Our goal is to characterize irreversibility through the behavior of the volume associated with a preparation before and after evolution in Hilbert space, reflecting the fact that a reversible microscopic evolution may give rise to an irreversible effective evolution.

This work is organized as follows. In the chapter 2, we analyze the dynamics of effective states induced by coarse-graining maps, assignment maps, and unitary evolution. Two different coarse-graining maps are discussed: the partial trace and the so-called detector coarse-grainings. We also review the notion of volume in Hilbert space, representing the uncertainty associated with a given effective preparation through the number of compatible microscopic states. The trace distance between effective states is then introduced as a criterion for irreversibility. A connection between these two quantities is established, constituting one of the original contributions of this thesis.

Chapter 3 presents the formalism of dynamical typicality and applies it to the effective dynamics of expectation values. We compute the volume associated with sets of states defined by a given expectation value, as well as the distance between initial and recovered expectation values obtained through forward and backward evolution. Finally, we analyze irreversibility in terms of distance between expectation values and the relation between distance and volume ratio. Finally, chapter 4 summarizes the main results obtained throughout this work, highlights the original contributions, and discusses possible extensions and open questions that may guide future developments.

# 2 Effective dynamics induced by coarse-graining maps

This chapter is motivated by the connection between microscopic and macroscopic descriptions. When a system is described in terms of quantities accessible to our senses, a macroscopic description is employed, as in thermodynamics. On the other hand, statistical mechanics defines a set of microstates compatible with the accessible macroscopic properties, called a statistical ensemble, allowing one to predict macroscopic behavior from microscopic quantities [25, 26].

The second law of thermodynamics states that the entropy of an isolated system never decreases [25]. In the thermodynamic limit, fluctuations become negligible, and entropy is therefore expected to increase monotonically toward equilibrium. In classical mechanics the counting of microstates compatible with the accessible macroscopic properties is done in phase space. Here, we introduce a quantity analogous to the Boltzmann entropy by quantifying the volume in Hilbert space associated with a given quantum preparation. This volume is then used to characterize irreversibility in closed quantum systems undergoing unitary evolution in a manner analogous to that used in thermodynamics.

The effective dynamics employed in this work are given by the composition of three quantum operations already specified in Sec. 1, but presented here for the sake of completeness, following [17–20]: 1) a coarse-graining map, which is a completely positive and trace-preserving (CPTP) map that reduces the dimension of the system and ensures that the resulting state is a physical state:

$$\Lambda : \mathcal{L}(\mathcal{H}_D) \to \mathcal{L}(\mathcal{H}_d), \quad D > d, \tag{2.1}$$

here, $\mathcal{L}(\mathcal{H})$ denotes the set of linear operators acting on $\mathcal{H}$. Notice that the coarse-graining operation does not correspond to a measurement; we just map microscopic state to a macroscopic one, otherwise there would be no uncertainty associated with the effective description. 2) a unitary evolution, since we consider a closed quantum system at microscopic level

$$\mathcal{U}_t : \mathcal{L}(\mathcal{H}_D) \to \mathcal{L}(\mathcal{H}_D); \tag{2.2}$$

and 3) an averaging assignment map, which connects the macroscopic and microscopic levels, i.e., assigns to each macrostate a microscopic description obtained by averaging over all pure states compatible with that macrostate:

$$\mathcal{A}_\Lambda : \mathcal{L}(\mathcal{H}_d) \to \mathcal{L}(\mathcal{H}_D). \tag{2.3}$$

The composition

$$\Gamma_t = \Lambda \circ \mathcal{U}_t \circ \mathcal{A}_\Lambda \tag{2.4}$$

defines the effective dynamics of the system.

In this chapter, we consider two effective descriptions of a closed system composed of a system of interest and irrelevant degrees of freedom, obtained through coarse-graining maps. The first description employs the partial trace map, one of the best-known coarse-graining maps, in which the reduced density matrix is obtained by tracing out the environmental degrees of freedom [14]. The second description applies when tracing out is no longer appropriate; in this case, we may describe the system of interest as a generalized subsystem defined through a quantum map [17–20, 23, 27].

Fig. 2 illustrates both scenarios. In the partial trace case, the degrees of freedom are divided into those associated with the system of interest and those corresponding to irrelevant degrees of freedom. In contrast, in the generalized subsystem case, there is no such clear distinction between system and environment. As a consequence, it becomes necessary to employ a more general coarse-graining map, leading to a generalized subsystem description.

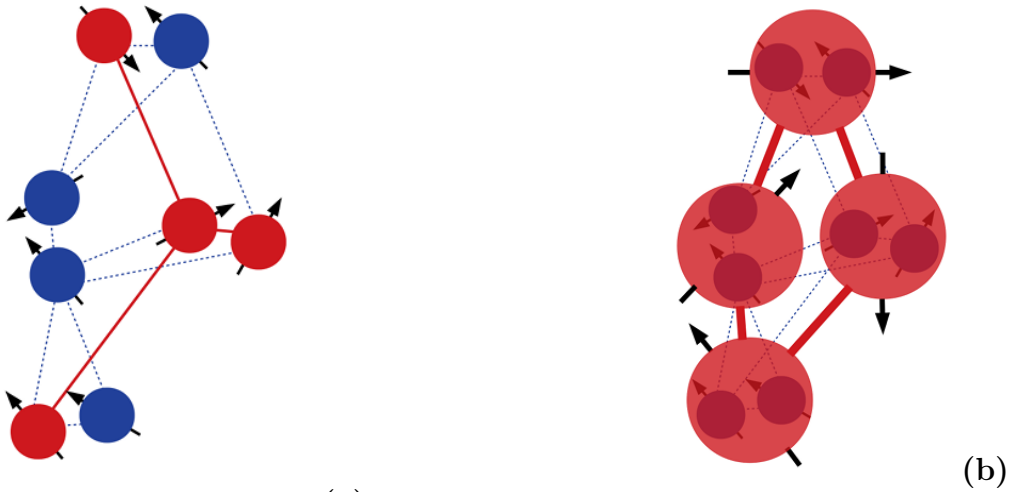


Figure 6 – A representation of partial trace (a) and generalized subsystems (b) taken from [20]. In (a) the degrees of freedom are split into those that identify the system of interest, represented by red spins, and those that are irrelevant degrees of freedom, represented in blue. The red and blue degrees of freedom interact weakly, allowing the elimination of the irrelevant degrees of freedom through the partial trace map. In contrast, in (b) there is no clear-cut separation between red and blue. In this case it is necessary to employ a more general coarse-graining map, leading to a generalized subsystem description, the one to which we have acess, represented by effective spins.

This chapter is organized as follows. First, we present the effective dynamics, illustrating the evolution under two different descriptions: partial trace and generalized subsystems, induced by coarse-graining maps, unitary evolution, and assignment maps. Next, we introduce the corresponding notion of volume in Hilbert space, which represents the uncertainty associated with a given effective preparation, quantified by the number of microscopic states compatible with it. Up to this point, no original results are presented; the discussion aims to establish the necessary framework.

We then introduce the trace distance between effective states as a criterion for the distinguishability of the states as will be explained below and discuss irreversibility in terms of it and the associated volumes. A connection between volume and distance is established, which constitutes one of the original contributions of this thesis. Finally, we summarize the main results and present the conclusions of the chapter.

## 2.1 Effective dynamics

The results presented in this section were previously developed in Refs. [17–20] and are reviewed here for completeness. The purpose of this section is to establish the conceptual and technical framework that will be used to develop the original results presented in the subsequent sections.

A coarse-grained description is determined by the relevant or available physical criteria of the system and characterizes our access to the microscopic world. Within this perspective, the macroscopic dynamics can be represented by the effective dynamics induced by coarse-graining maps introduced in this section.

Suppose that the effective description of a system is associated with a Hilbert space $\mathcal{H}_d$. When an initial effective state $\rho(0) \in \mathcal{L}(\mathcal{H}_d)$ is prepared, one may interpret this preparation as corresponding to a microscopic pure state $|\psi(0)\rangle \in \mathcal{H}_D$, with $D \geq d$. At the microscopic level, however, the preparation is not uniquely specified: there exists an intrinsic uncertainty regarding which microscopic state actually realizes the effective state. In other words, many microscopic states are compatible with the same effective description.

If the preparation of $\rho(0)$ is repeated several times, each run may correspond to a different microscopic state. Collectively, these realizations define a restricted set of microscopic states $\Omega$ that all produce the same effective state through the coarse-graining map $\Lambda : \mathcal{L}(\mathcal{H}_D) \to \mathcal{L}(\mathcal{H}_d)$

$$\Omega(\rho(0)) = \{\psi(0) \in \mathcal{L}(\mathcal{H}_D) \mid \Lambda[\psi(0)] = \rho(0), \quad \psi(0) = |\psi(0)\langle\psi(0)|\rangle\} \tag{2.5}$$

Here $\psi(0)$ is considered to be pure assuming the microscopic system is very well isolated so that any uncertainty about its state can be attributed to classical ignorance.

In Fig. 7, taken from [18], a representation of this process is shown: once an effective state is prepared, a corresponding set of random microscopic states whose effective description is $\rho(0)$ is defined.

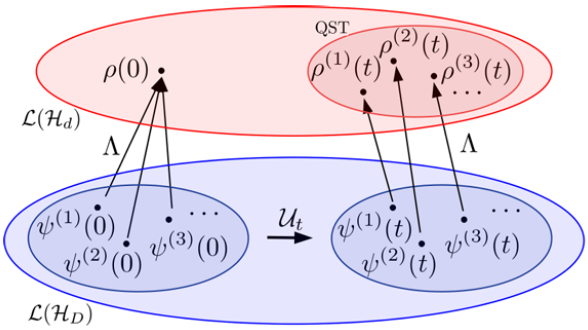


Figure 7 – In each $i$-th run, an initial effective state $\rho(0)$ is prepared, which can be thought of as the preparation of a random microscopic state $\psi^{(i)}(0)$. Through the coarse-graining map $\Lambda$, the effective description of each $\psi^{(i)}(0)$ is exactly $\rho(0)$. The unitary evolution of each microscopic state generally leads to a different final effective state, given by $\rho^{(i)}(t) = (\Lambda \circ \mathcal{U}_t)[\psi^{(i)}(0)]$. Figure taken from [18].

Following Ref. [18], a preparation of $\rho(0)$ prepares a random microscopic state from the set defined by Eq. (2.5), $\psi^{(i)}(0) \in \Omega(\rho(0))$, with probability $Pr(\psi^{(i)}(0) \mid \rho(0))$. Notice that if $\psi^{(i)}(0) \notin \Omega(\rho(0))$ then $Pr(\psi^{(i)}(0) \mid \rho(0)) = 0$. This state evolves according to the Schrödinger equation via a unitary map $\mathcal{U}_t : \mathcal{L}(\mathcal{H}_D) \to \mathcal{L}(\mathcal{H}_D)$. The microscopic state at time $t$ is

$$\psi^{(i)}(t) = \mathcal{U}_t[\psi^{(i)}(0)]. \tag{2.6}$$

Each of these evolved microscopic states (Eq. (2.6)) generates a corresponding effective state via coarse-graining map, such that the effective state associated with $\psi^{(i)}(t)$ is given by:

$$\rho^{(i)}(t) = \Lambda[\psi^{(i)}(t)] \tag{2.7}$$

or even

$$\rho^{(i)}(t) = (\Lambda \circ \mathcal{U}_t)[\psi^{(i)}(0)]. \tag{2.8}$$

when we desire to connect the effective state at time $t$ with initial microscopic state.

By evolving each microscopic state from $\Omega$ and applying the same procedure, the final effective state can be seen to correspond to the average over the microscopic states,

$$\rho(t) = \int d\mu_{\psi(0)} Pr\left(\psi(0)|\rho(0)\right) \left(\Lambda \circ \mathcal{U}_t\right) \left[\psi(0)\right] \tag{2.9}$$

$$= (\Lambda \circ \mathcal{U}t) \int d\mu_{\psi(0)} Pr\left(\psi(0)|\rho(0)\right) \left[\psi(0)\right] \tag{2.10}$$

$$= \left(\Lambda \circ \mathcal{U}_t \circ \mathcal{A}_\Lambda\right) \left[\rho(0)\right], \tag{2.11}$$

where [18] defined

$$\mathcal{A}_\Lambda = \int d\mu_{\psi(0)} Pr\left(\psi(0)|\rho(0)\right)\ \psi(0), \tag{2.12}$$

the average assignment map. In Eq. (2.12) $d\mu_{\psi(0)}$ is a uniform measure over pure states in $\mathcal{L}(\mathcal{H}_D)$ and $Pr\left(\psi(0)|\rho(0)\right)$ is a probability density of having the microscopic state $\psi(0)$ given the preparation of $\rho(0)$. Notice that Eq. (2.12) defines an average over the pure states compatible with a given macrostate. This averaging reflects the fact that the macroscopic description does not uniquely determine the underlying microstate. The Haar measure is employed because it is invariant under unitary transformations and expresses the absence of any preferred pure state $\psi(0)$. The conditional probability encodes the microscopic constraint, while $\mathcal{A}_\Lambda$ denotes the average over all pure states $\psi(0)$ conditioned on compatibility with the macroscopic restriction.

The map $\mathcal{A}_\Lambda : \mathcal{L}(\mathcal{H}_d) \to \mathcal{L}(\mathcal{H}_D)$ is the assignment map that connects macro to micro levels. The effective dynamics induced by coarse-graining maps [18–20] is then

$$\Gamma_t = \Lambda \circ \mathcal{U}_t \circ \mathcal{A}_\Lambda, \tag{2.13}$$

a composition of maps, as illustrated in Figure 8.

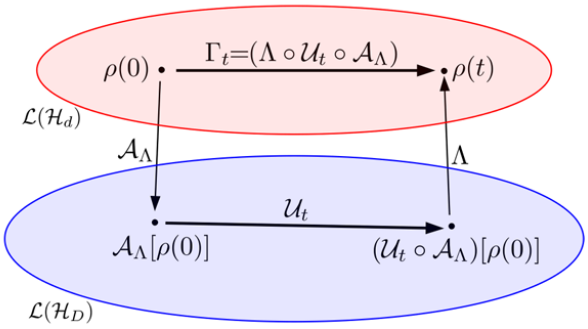


Figure 8 – A macroscopic evolution represented by the effective dynamics through a composition of quantum operations. This figure is taken from [18].

The effective dynamics analyzed here are induced by two different coarse-grained maps: the partial trace –tracing out the environment –and $\Lambda_{BnS}$ –which provides us the description of a generalized subsystem.

### 2.1.1 Partial trace

Consider a system of interest that is in contact with an environment that may have reservoir properties or even another system with unknown degress of freedom such that the entire system is isolated. The system is considered to be open [14, 28].

The total closed quantum system lives in $\mathcal{L}(\mathcal{H}_D) = \mathcal{L}(\mathcal{H}_d \otimes \mathcal{H}_E)$, a composite of system–environment Hilbert space. The density matrix of the system of interest $\rho$ is obtained by tracing out the environment $E$. In this case, the coarse-graining map connecting subsystem is the partial trace, $\Lambda_{tr_E} : \mathcal{L}(\mathcal{H}_d \otimes \mathcal{H}_E) \to \mathcal{L}(\mathcal{H}_d)$, and the effective state is

$$\rho = \Lambda_{tr_E}[\rho_{dE}], \quad \rho \in \mathcal{L}(\mathcal{H}_d), \tag{2.14}$$

where $\rho_{dE} \in \mathcal{L}(\mathcal{H}_D) = \mathcal{L}(\mathcal{H}_d \otimes \mathcal{H}_E)$ is the total density matrix and $\rho \in \mathcal{L}(\mathcal{H}_d)$ is the system of interest.

The set of fine-grained states constrained by the same effective description $\rho \in \mathcal{L}(\mathcal{H}_d)$ is

$$\Omega_{\Lambda_{tr_E}}(\rho) = \{\psi \in \mathcal{L}(\mathcal{H}_d \otimes \mathcal{H}_E) \mid \Lambda_{tr_E}[\psi] = \rho, \quad \psi = |\psi\rangle\langle\psi|\}. \tag{2.15}$$

To complete the effective dynamics in the partial trace case, it is necessary to define the connection between the macroscopic and microscopic levels. This connection is provided by the averaging assignment map, which is computed using (2.12) definition.

The conditional probability density of finding a microscopic state $\psi$ given an effective state $\rho$, denoted by $Pr_{tr_E}(\psi \mid \rho)$, is nonzero only on the set defined in Eq. (2.15). All states in $\Omega_{\Lambda_{tr_E}}$ (see Eq. (2.15)) are assigned equal weight since, according to Laplace's principle of indifference, there is no justification for favoring one compatible microscopic state over another. This allows us to take the probability density as being proportional to $\delta(\Lambda_{tr_E}[\psi] - \rho)$. The delta functional simply enforces the restriction. According to [20], the assignment map can be written more explicitly as

$$\mathcal{A}_{\Lambda_{tr_E}}(\rho) = \int d\mu_\psi \; Pr_{tr_E}(\psi|\rho)\; \psi = \int d\mu_\psi \delta\left(\Lambda_{tr_E}[\psi] - \rho\right) \psi. \tag{2.16}$$

Following Ref. [18], the conditional probability distribution $Pr_{tr_E}(\psi|\rho)$ is invariant by unitary transformations in the "environment" part, that is

$$Pr_{tr_E}(\psi|\rho) = Pr_{tr_E}(\mathbf{1} \otimes U_E \; \psi \mathbf{1} \otimes U_E^\dagger|\rho), \quad \forall\, U_E \in \mathcal{U}(d_E). \tag{2.17}$$

Since all purifications of a given density matrix are related by a unitary transformation acting on the purifying subsystem, the states in Eq. (2.15) are connected by local unitary transformations on $\mathcal{H}_E$. This invariance implies that, in the absence of additional constraints, all states in Eq. (2.15) are equally likely.

Since the Haar measure $d\mu_\psi$ is also invariant under unitary transformations, the average state for the partial trace case can be equivalently written by changing the variables $|\psi\rangle \to \mathbf{1} \otimes U_E|\psi\rangle$ as

$$\mathcal{A}_{\Lambda_{tr_E}}(\rho) = \int d\mu_\psi \; Pr_{tr_E}(\psi|\rho)\; \mathbf{1} \otimes U_E \; \psi \mathbf{1} \otimes U_E^\dagger. \tag{2.18}$$

Since no unitary transformation is preferred, we may average over the unitary group to obtain

$$\mathcal{A}_{\Lambda_{tr_E}}(\rho) = \int d\mu_\psi \; Pr_{tr_E}(\psi|\rho) \; \overline{\mathbf{1} \otimes U_E \; \psi \mathbf{1} \otimes U_E^\dagger}^{\mu_{U_E}}. \tag{2.19}$$

To evaluate the Haar average over the unitary group $\mathcal{U}(d_E)$, we employ the Schmidt decomposition of $|\psi\rangle$, writing in the environment and system bases:

$$|\psi\rangle = \sum_\alpha \sqrt{\lambda}_\alpha |s_\alpha\rangle \otimes |e_\alpha\rangle, \tag{2.20}$$

in a way that the Haar average over the unitary group becomes:

$$\begin{aligned}\int d\mu_{U_E} \; \mathbf{1} \otimes U_E \; \psi \mathbf{1} \otimes U_E^\dagger &= \sum_\alpha \sum_\beta \sqrt{\lambda}_\alpha \sqrt{\lambda}_\beta |s_\alpha\rangle\langle s_\beta| \otimes \int d\mu_{U_E} \; U_E |e_\alpha\rangle\langle e_\beta| U_E^\dagger \\ &= \sum_\alpha \sum_\beta \sqrt{\lambda}_\alpha \sqrt{\lambda}_\beta |s_\alpha\rangle\langle s_\beta| \otimes E_{\alpha\beta}\end{aligned} \tag{2.21}$$

with $E_{\alpha\beta} = \int d\mu_{U_E} \; U_E |e_\alpha\rangle\langle e_\beta| U_E^\dagger$. The defining property of the Haar measure is left/right invariance with respect to shifts via multiplication: let $V\mathcal{U}(d_E)$ be a fixed unitary, then [**?**]:

$$\begin{aligned}V_E E_{\alpha\beta} V_E^\dagger &= \int d\mu_{U_E} \; V_E U_E |e_\alpha\rangle\langle e_\beta| U_E^\dagger V_E^\dagger \\ &= \int d\mu_{W_E} \; W_E |e_\alpha\rangle\langle e_\beta| W_E^\dagger = E_{\alpha\beta},\end{aligned} \tag{2.22}$$

where $W_E = V_E U_E$ and $\int d\mu_{U_E} \equiv \int d\mu_{V_E^\dagger W_E} \equiv \int d\mu_{W_E}$.

As

$$V_E E_{\alpha\beta} V_E^\dagger = E_{\alpha\beta}, \tag{2.23}$$

commutes with every unitary operator on $\mathcal{H}_E$ so $E_{\alpha\beta} = c_{\alpha\beta} \mathbf{1}_{d_E}$. To determine $c_{\alpha\beta}$ we perform:

$$\mathrm{tr}\,[E_{\alpha\beta}] = \int d\mu_{U_E} \; \mathrm{tr}\left[U_E |e_\alpha\rangle\langle e_\beta| U_E^\dagger\right] = \mathrm{tr}\,[|e_\alpha\rangle\langle e_\beta|] \int d\mu_{U_E} = \delta_{\alpha\beta}, \tag{2.24}$$

since the Haar measure integral is normalized to unit. On the other hand

$$\mathrm{tr}\,[E_{\alpha\beta}] = c_{\alpha\beta} \mathrm{tr}\,[\mathbf{1}_{d_E}] = c_{\alpha\beta} d_E. \tag{2.25}$$

Equating the Eq. (2.24) to Eq. (2.25) we find:

$$c_{\alpha\beta} = \frac{\delta_{\alpha\beta}}{d_E} \tag{2.26}$$

and $E_{\alpha\beta} = \frac{\delta_{\alpha\beta}}{d_E} \mathbf{1}_{d_E}$. Recovering Eq. (2.19),

$$\begin{aligned}\int d\mu_{U_E} \; \mathbf{1} \otimes U_E \; \psi \mathbf{1} \otimes U_E^\dagger &= \sum_\alpha \sum_\beta \sqrt{\lambda}_\alpha \sqrt{\lambda}_\beta |s_\alpha\rangle\langle s_\beta| \otimes \frac{\delta_{\alpha\beta}}{d_E} \mathbf{1}_{d_E} \\ &= \sum_\alpha \lambda_\alpha |s_\alpha\rangle\langle s_\alpha| \otimes \frac{\mathbf{1}_{d_E}}{d_E}.\end{aligned} \tag{2.27}$$

Notice that the first factor on the right-hand side of Eq. (2.27) is precisely the reduced state obtained by tracing out the environment. As we consider $\mathrm{tr}_E[\psi] = \rho$, we rewrite Eq. (2.19) and the averaging assignment map for the partial trace case is given by as [18, 20]:

$$\mathcal{A}_{\Lambda tr_E}[\rho(0)] = \rho(0) \otimes \frac{\mathbf{1}_{d_E}}{d_E}, \tag{2.28}$$

where $d_E$ is the environment dimension.

Therefore the effective evolved state $\rho(t)$ is [18]

$$\rho(t) = (\Lambda_{tr_E} \circ \mathcal{U}_t) \left[\rho(0) \otimes \frac{\mathbf{1}_{d_E}}{d_E}\right]. \tag{2.29}$$

In this case the effective dynamics is linear in $\rho(0)$, inasmuch as both $\mathcal{U}_t$ and $\Lambda_{tr_E}$ are linear operations. Since $\mathcal{U}_t$ and $\Lambda_{tr_E}$ are completely positive, the resulting map $\Gamma_t$ is also completely positive. Thus, the effective dynamics $\Gamma_t$ induced by partial trace coarse-graining map is a CPTP map.

Moreover, the transformation $\Gamma_t = \Lambda_{tr_E} \circ \mathcal{U}_t \circ \mathcal{A}_{\Lambda_{tr_E}}$ is unital. A transformation $T: \mathcal{L}(\mathcal{H}_d) \to \mathcal{L}(\mathcal{H}_d)$ is unital if it maps the identity operator to itself [21]:

$$T[\mathbf{1}_d] = \mathbf{1}_d. \tag{2.30}$$

Thus, $\Gamma_t$ in Eq.(2.29) is unital if the composition $\Lambda_{tr_E} \circ \mathcal{U}_t \circ \mathcal{A}_{\Lambda tr_E}$ is unital:

$$\begin{aligned} \Gamma_t[\mathbf{1}_d] &= \Lambda_{tr_E}\left[\mathcal{U}\left(\mathbf{1}_d \otimes \frac{\mathbf{1}_{d_E}}{d_E}\right)\mathcal{U}^\dagger\right] \\ &= \Lambda_{tr_E}\left[\left(\mathbf{1}_d \otimes \frac{\mathbf{1}_{d_E}}{d_E}\right)\right] \qquad (2.31) \\ &= \mathbf{1}_d \otimes \Lambda_{tr_E}\left[\frac{\mathbf{1}_{d_E}}{d_E}\right] = \mathbf{1}_d. \qquad (2.32) \end{aligned}$$

The importance of this transformation being unital will be discussed later in the irreversibility section. Notice also that if we consider a local unitary of the form $\mathcal{U}_d \otimes \mathcal{U}_E$, the effective evolved state becomes

$$\rho(t) = (\Lambda_{tr_E} \circ \mathcal{U}_d \otimes \mathcal{U}_E)\left[\rho(0) \otimes \frac{\mathbf{1}_{d_E}}{d_E}\right] = \mathcal{U}_d[\rho(0)], \tag{2.33}$$

and the effective dynamics reduce to the unitary map ($\Gamma_t = \mathcal{U}_d$). This case is trivially reversible.

### 2.1.2 Blurred and saturated detector

An interesting case that cannot be reduced to a partial-trace scenario is a quantum system observed by a blurred and saturated detector [17–20, 27]. In this case, the coarse-graining map is inspired by the experimental setting. In this type of experiment, cold

atoms are stored in optical lattices, which are arrays of minimum potential traps formed by laser light, and the measurement is done by state dependent fluorescence [29]. We can consider a simplified case previously analyzed by [17–20, 27]: two neighboring qubits trapped in a double-well potential and measured by a blurred and saturated detector. When measuring the state of an atom through fluorescence, the atom is illuminated with light. If the atom is in the excited state $|1\rangle$, it scatters light; if it is in the ground state $|0\rangle$, no light is observed.

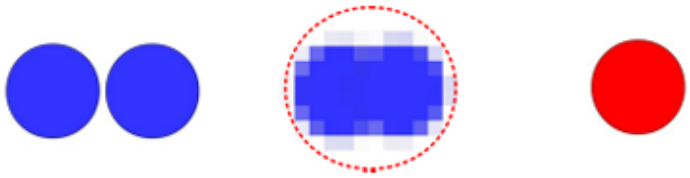

Figure 9 – Representation of the blurred detector experiment. The detector becomes saturated by the light emitted by a single excited atom, not being possible to resolve the joint excitation of the atoms when light is shone on them. So, the effective description is a generalized subsystem. Figure taken from [27].

Consider the mathematical example of measurement of two neighbouring atoms, as illustrated in Fig. 9. Due to the characteristics of the detector, it cannot distinguish between the single-excitation states $|10\rangle$ and $|01\rangle$. And since the detector becomes saturated by the light emitted from a single excited atom, it is also unable to resolve the joint excitation state $|11\rangle$.

Consequently, the detector can only determine whether the system is in the ground state or in any excited state. Therefore, in this coarse-grained description, the two-atom system is effectively reduced to a two-level subsystem (see Fig. 10).

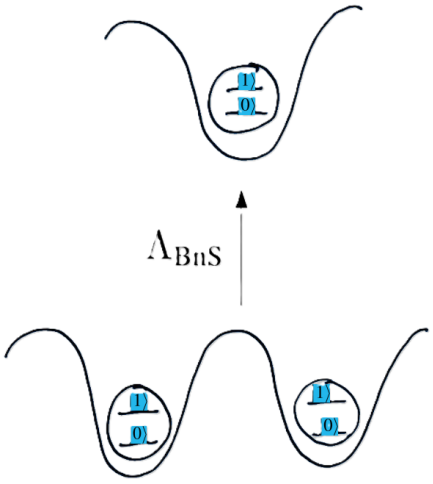


Figure 10 – Due to the characteristics of the detector during measurement, two atoms are effectively reduced to the description of a single atom.

Figure 10 shows a toy model that neither resolves photon number nor possesses sufficient spatial resolution to identify the source of the detected excitation. It is a toy model.

This dimensional reduction can also be represented as a reduction from a four-level system to a two-level system, as shown in Fig. 11. In this interpretation, the detector is unable to spectrally resolve the incoming signal, and the blurred behavior arises from this lack of spectral resolution.

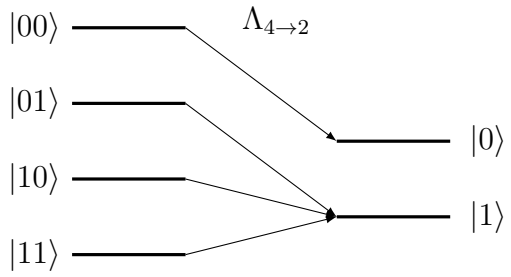


Figure 11 – Diagram of the coarse-graining map action, $\Lambda$ reducing from 4 levels to 2 level system. The map is illustrated only for product basis states $|ij\rangle\langle ij|$ with $i, j \in \{0, 1\}$.

This situation represents a case in which the coarse-graining operation does not reduce to tracing out a subsystem, as we will discuss below. Instead, the appropriate effective description is given by a single two-level system within the generalized subsystems framework. The coarse-graining map that models this reduction from a four-level system to a two-level system, in which coherences between the excited states are not preserved, is defined in Eq. (2.34). Further details can be found in [18–20, 27]:

$$\begin{aligned}
\Lambda_{4\to2}[|00\rangle\langle 00|] &= |0\rangle\langle 0| & \Lambda_{4\to2}[|10\rangle\langle 00|] &= \tfrac{1}{\sqrt{3}}|1\rangle\langle 0| \\
\Lambda_{4\to2}[|00\rangle\langle 01|] &= \tfrac{1}{\sqrt{3}}|0\rangle\langle 1| & \Lambda_{4\to2}[|10\rangle\langle 01|] &= 0 \\
\Lambda_{4\to2}[|00\rangle\langle 10|] &= \tfrac{1}{\sqrt{3}}|0\rangle\langle 1| & \Lambda_{4\to2}[|10\rangle\langle 10|] &= |1\rangle\langle 1| \\
\Lambda_{4\to2}[|00\rangle\langle 11|] &= \tfrac{1}{\sqrt{3}}|0\rangle\langle 1| & \Lambda_{4\to2}[|10\rangle\langle 11|] &= 0 \\
\Lambda_{4\to2}[|01\rangle\langle 00|] &= \tfrac{1}{\sqrt{3}}|1\rangle\langle 0| & \Lambda_{4\to2}[|11\rangle\langle 00|] &= \tfrac{1}{\sqrt{3}}|1\rangle\langle 0| \\
\Lambda_{4\to2}[|01\rangle\langle 01|] &= |1\rangle\langle 1| & \Lambda_{4\to2}[|11\rangle\langle 01|] &= 0 \\
\Lambda_{4\to2}[|01\rangle\langle 10|] &= 0 & \Lambda_{4\to2}[|11\rangle\langle 10|] &= 0 \\
\Lambda_{4\to2}[|01\rangle\langle 11|] &= 0 & \Lambda_{4\to2}[|11\rangle\langle 11|] &= |1\rangle\langle 1|
\end{aligned} \tag{2.34}$$

We can notice in Eq.(2.34) that the ground state ($|00\rangle\langle 00|$) of the four-level system is mapped to the ground state in two level ($|0\rangle\langle 0|$), while all excited-state populations are mapped onto a single effective excited state ($|1\rangle\langle 1|$). In the effective description, no

coherence is preserved among the states $|01\rangle$, $|10\rangle$, and $|11\rangle$ due to the detector's inability to distinguish them [19]. For this reason,

$$\Lambda_{4\to2}[|01\rangle\langle10|] = \Lambda_{4\to2}[|01\rangle\langle11|] = \Lambda_{4\to2}[|10\rangle\langle11|] = 0 \tag{2.35}$$

as well as their corresponding Hermitian conjugates. Moreover, the factor $\frac{1}{\sqrt{3}}$ is the maximal value that ensures that $\Lambda_{4\to2}$ defines a completely positive and trace-preserving (CPTP) map.

The generalized character of the coarse-graining map presented in Eq. (2.34) can be clearly demonstrated by examining its diagonal elements. In particular,

$$\Lambda_{4\to2}[|01\rangle\langle01|] = \Lambda_{4\to2}[|10\rangle\langle10|] = \Lambda_{4\to2}[|11\rangle\langle11|] = |1\rangle\langle1|. \tag{2.36}$$

This behavior is incompatible with a partial trace description, since tracing out either the first or the second subsystem would not lead to equivalent results.

One possible set of Kraus operators associated with the level-reduction process presented above from two two-level atoms, denoted here as $4 \to 2$, which provides an operator-sum representation of the coarse-graining map $\Lambda_{4\to2}$, is given by

$$K_1 = \begin{bmatrix} 1 & 0 & 0 & 0 \\ 0 & \frac{1}{\sqrt{3}} & \frac{1}{\sqrt{3}} & \frac{1}{\sqrt{3}} \end{bmatrix}, \tag{2.37}$$

$$K_2 = \begin{bmatrix} 0 & 0 & 0 & 0 \\ 0 & -\frac{1}{\sqrt{2}} & 0 & \frac{1}{\sqrt{2}} \end{bmatrix}, \tag{2.38}$$

$$K_3 = \begin{bmatrix} 0 & 0 & 0 & 0 \\ 0 & -\frac{1}{\sqrt{6}} & \sqrt{\frac{2}{3}} & -\frac{1}{\sqrt{6}} \end{bmatrix} \tag{2.39}$$

In order to complete the effective dynamics in this case, one must define the averaging assignment map associated with the $4 \to 2$ level-reduction process,

$$\mathcal{A}_{\Lambda_{4\to2}}(\rho) = \int d\mu_\psi Pr_{\Lambda_{4\to2}}(\psi|\rho)\,\psi. \tag{2.40}$$

Similarly to the partial trace case, the conditional probability of finding a microscopic state $\psi$ given an effective state $\rho$ is nonzero only on the set of fine-grained states constrained by the effective description $\rho \in \mathcal{L}(\mathcal{H}_2)$, such as

$$\Omega_{\Lambda_{4\to2}}(\rho) = \{\psi \in \mathcal{L}(\mathcal{H}_4) \mid \Lambda_{4\to2}[\psi] = \rho, \quad \psi = |\psi\rangle\langle\psi|\} \tag{2.41}$$

and as no additional microscopic information is available beyond the effective constraint all states in $\Omega_{\Lambda_{4\to2}}$ are taken with the same weight what allows to consider the probability density to be proportional to $\delta(\Lambda_{4\to2}[|\psi\rangle\langle\psi|] - \rho)$ that enforces the restriction.

The assignment expression for the dimension reduction case $4 \to 2$

$$\mathcal{A}_{\Lambda_{4\to2}}(\rho) = \int d\mu_\psi \delta\left(\Lambda_{4\to2}[\psi] - \rho\right)\psi \tag{2.42}$$

was previously computed in [18, 20], where the symmetry-group method for pure states was employed. By averaging over the symmetry group with respect to the Haar measure, assuming no preferred unitary transformation, and expressing the assignment map in terms of the effective state, the authors obtained the following expression:

$$\mathcal{A}_{\Lambda_{4\to2}}(\rho) = \begin{bmatrix} \rho_{00} & \frac{\rho_{01}}{\sqrt{3}} & \frac{\rho_{01}}{\sqrt{3}} & \frac{\rho_{01}}{\sqrt{3}} \\ \frac{\rho_{01}^*}{\sqrt{3}} & \frac{\rho_{11}}{3} & \frac{|\rho_{01}|^2}{2\rho_{00}} - \frac{\rho_{11}}{6} & \frac{|\rho_{01}|^2}{2\rho_{00}} - \frac{\rho_{11}}{6} \\ \frac{\rho_{01}^*}{\sqrt{3}} & \frac{|\rho_{01}|^2}{2\rho_{00}} - \frac{\rho_{11}}{6} & \frac{\rho_{11}}{3} & \frac{|\rho_{01}|^2}{2\rho_{00}} - \frac{\rho_{11}}{6} \\ \frac{\rho_{01}^*}{\sqrt{3}} & \frac{|\rho_{01}|^2}{2\rho_{00}} - \frac{\rho_{11}}{6} & \frac{|\rho_{01}|^2}{2\rho_{00}} - \frac{\rho_{11}}{6} & \frac{\rho_{11}}{3} \end{bmatrix}. \tag{2.43}$$

Therefore, the evolved effective description at time $t$ obtained using the map defined by Kraus operators (Eq. (2.37)–Eq. (2.39)) together with the assignment map given in Eq.(2.43), is

$$\rho(t) = (\Lambda_{4\to2} \circ \mathcal{U}_t \circ \mathcal{A}_{\Lambda_{4\to2}})\,[\rho(0)]. \tag{2.44}$$

Ref. [17] also introduces a second example of dimension reduction, which leaves no doubt that the resulting coarse-graining channel does not correspond to a partial trace, as we will discuss. Now, imagine a simplified model of an individual three-level system trapped in a potential minimum and measured by a blurred and saturated detector.

Similarly to $4 \to 2$ dimension reduction case, when the state is measured through fluorescence the atom is illuminated with light. If the atom is in one of the excited states, $|2\rangle$ or $|1\rangle$, it scatters light; if it is in the ground state $|0\rangle$, no light is observed. However, suppose that even a small amount of light is enough to saturate the detector and it cannot distinguish between the excited states, determining only whether the atom is in an excited state or not. Again, this is a mathematical example of detection, similar to the one presented in the previous case, where coherence is not preserved between excited levels, as will be explained later. See Fig. 12

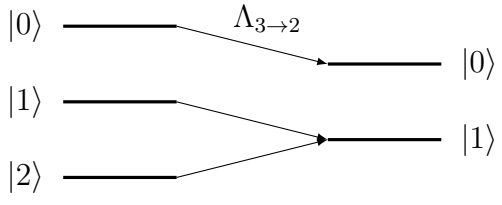


Figure 12 – Diagram of the coarse-graining map action, $\Lambda$ reducing from 3 levels to 2 level system. $|0\rangle$ refers to the ground state, while $|1\rangle$ and $|2\rangle$ are excited states. The map is illustrated only for computational base $|0\rangle, |1\rangle, |2\rangle$.

The detector cannot distinguish between the excited states; it can only determine whether the system is in the ground state or in some excited state. Thus, in a coarse-

grained description, the three-level system is effectively reduced to a two-level subsystem (see fig.12).

The action of this map can be represented by

$$\begin{aligned}
\Lambda_{3\to2}[|0\rangle\langle 0|] &= |0\rangle\langle 0| \\
\Lambda_{3\to2}[|0\rangle\langle 1|] &= \frac{1}{\sqrt{2}}|0\rangle\langle 1| \\
\Lambda_{3\to2}[|0\rangle\langle 2|] &= \frac{1}{\sqrt{2}}|0\rangle\langle 1| \\
\Lambda_{3\to2}[|1\rangle\langle 0|] &= \frac{1}{\sqrt{2}}|1\rangle\langle 0| \\
\Lambda_{3\to2}[|1\rangle\langle 1|] &= |1\rangle\langle 1| \\
\Lambda_{3\to2}[|1\rangle\langle 2|] &= 0 \\
\Lambda_{3\to2}[|2\rangle\langle 0|] &= \frac{1}{\sqrt{2}}|1\rangle\langle 0| \\
\Lambda_{3\to2}[|2\rangle\langle 1|] &= 0 \\
\Lambda_{3\to2}[|2\rangle\langle 2|] &= |1\rangle\langle 1|
\end{aligned} \tag{2.45}$$

In Eq.(2.46) the ground state remains unchanged. But both excited states populations are mapped to the same effective state and as the detector cannot distinguish $|1\rangle$ and $|2\rangle$ there's no coherence between them. Furthermore, the $\frac{1}{\sqrt{2}}$ factor is to guarantee the $\Lambda_{3\to2}$ is a CPTP map.

One possible set of Kraus operators representing that level reduction $3 \to 2$ which provides the operator-sum representation of the coarse-graining map $\Lambda_{3\to2}$ are [17]

$$K_1 = \begin{bmatrix} 1 & 0 & 0 \\ 0 & \frac{1}{\sqrt{2}} & \frac{1}{\sqrt{2}} \end{bmatrix}, \quad K_2 = \begin{bmatrix} 0 & 0 & 0 \\ 0 & \frac{1}{\sqrt{2}} & -\frac{1}{\sqrt{2}} \end{bmatrix}. \tag{2.46}$$

In this case, the set of microscopic states constrained to yield the same effective description is

$$\Omega_{\Lambda_{3\to2}}(\rho) = \{\psi \in \mathcal{L}(\mathcal{H}_3) \mid \Lambda_{3\to2}[\psi] = \rho,\ \psi = |\psi\rangle\langle\psi|\}, \tag{2.47}$$

and $\rho \in \mathcal{L}(\mathcal{H}_2)$. The conditional probability of finding $\psi$ given $\rho$ is not null only on the set defined by Eq.(2.47). And all states in $\Omega_{\Lambda_{3\to2}}$ are taken with the same weight, because we assume that no additional microscopic information is available beyond the effective constraint and the probability density is proportional to $\delta(\Lambda_{3\to2}[\psi] - \rho)$ that enforces the restriction.

The connection of the effective system to the microscopic one, taking an average

over pure states, is in this case [17]

$$\mathcal{A}_{\Lambda_{3\to2}}(\rho) = \begin{bmatrix} (1+z)/2 & \frac{(x-iy)/2}{\sqrt{2}} & \frac{(x-iy)/2}{\sqrt{2}} \\ \frac{(x+iy)/2}{\sqrt{2}} & \frac{(1-z)/2}{2} & \frac{\left|\frac{x-iy}{2}\right|^2}{(z+1)/2} - \frac{(1-z)/2}{2} \\ \frac{(x+iy)/2}{\sqrt{2}} & \frac{\left|\frac{x-iy}{2}\right|^2}{(z+1)/2} - \frac{(1-z)/2}{2} & \frac{(1-z)/2}{2} \end{bmatrix}, \tag{2.48}$$

where $x, y, z$ are $\rho$ coordinates in Bloch sphere and they used the symmetry-group method for pure states, averaging over this group to reflect the absence of any preferred unitary transformation, and expressing the assignment map in terms of the effective state.

Thus, the effective evolved state at time $t$, obtained using the map defined in Eq.(2.46) together with the assignment map given in Eq.(2.48), is

$$\rho(t) = \left(\Lambda_{3\to2} \circ \mathcal{U}_t \circ \mathcal{A}_{\Lambda_{3\to2}}\right)[\rho(0)]. \tag{2.49}$$

with $\Lambda_{3\to2}$ and $\mathcal{A}_{\Lambda_{3\to2}}$ defined above.

## 2.2 Volumes

The results presented in this section summarize a framework previously proposed in [17] in which the uncertainty of which microstates generates the effective preparation is quantified. This uncertainty increases as the number of microscopic states yielding the same effective density matrix $\rho$ grows [17]. The formal developments and explicit calculations were carried out in Refs. [17, 18, 20] and are presented here for completeness and to establish the conceptual basis for the subsequent analysis.

In this context, we propose that entropy is directly related with the volume of the set of microscopic states compatible with it, $\mathcal{V}_\Lambda(\rho)$:

$$S(\rho) \propto \log(\mathcal{V}_\Lambda(\rho)). \tag{2.50}$$

Motivated by this perspective, [17] proposed to quantify such uncertainty by counting the number of microscopic pure states compatible with a given effective description $\rho$. This set is defined as previously,

$$\Omega_\Lambda(\rho) = \{\psi \in \mathcal{L}(\mathcal{H}_D) \mid \Lambda[\psi] = \rho, \quad \psi = |\psi\rangle\langle\psi|\}. \tag{2.51}$$

Each microstate $\psi \in \Omega_\Lambda(\rho)$ is equivalent to a volume element of the Hilbert space and since this space is continuous, the counting of compatible microstates is quantified by the volume of $\Omega(\rho)$. Assuming all compatible pure states to be equally probable, once there is no preference among $\psi$ and the probability to find $\psi$ given $\rho$ is not null only inside the set of Eq. (2.51), we induce a Haar measure over pure states restricted by the effective description given by $\rho$, this volume is given by [16, 18, 20]

$$\mathcal{V}_\Lambda(\rho) = \int d_{\mu_\psi} \delta\left(\Lambda[\psi] - \rho\right), \tag{2.52}$$

where the integration is taken over pure states $\psi \in \mathcal{L}(\mathcal{H}_D)$ with the uniform (Haar) measure.

The quantity defined in Eq.(2.52) is the volume of the Hilbert space occupied by microstates associated with the effective state $\rho \in \mathcal{L}(\mathcal{H}_d)$. In this section, we review results for the two coarse-graining schemes (partial trace and blurred and saturated detectors) introduced previously in [17] and [20]. In the following section, we will relate the behave of this volume under coarse-grained dynamics to the emergence of irreversibility.

### 2.2.1 Partial trace

In this case, we aim to compute the Hilbert space volume associated with an effective state $\rho \in \mathcal{L}(\mathcal{H}_d)$ which emerges from tracing out the environment $\mathcal{H}_E$ from the total Hilbert space ($\mathcal{H}_D = \mathcal{H}_E \otimes \mathcal{H}_d$).

The volume of microstates compatible with the constraint $\Lambda_{tr_E}[\psi] = \rho$ is

$$\mathcal{V}_{\Lambda_{tr_E}}(\rho) = \int d\mu_\psi \delta\left(\Lambda_{tr_E}[\psi] - \rho\right), \tag{2.53}$$

where $d\mu_\psi$ denotes the Haar measure on $\mathcal{H}_d \otimes \mathcal{H}_E$.

The detailed derivation is presented in Ref. [17], where a change of variables based on the symmetries of $\Lambda_{\mathrm{tr_E}}$was performed, a basis in which $\rho$ is diagonal was chosen, and $|\psi\rangle$ was parameterized in terms of the degrees of freedom of the system and environment. It was shown that the volume of the set $\Omega_{\Lambda_{tr_E}}$ is

$$\mathcal{V}_{\Lambda_{tr_E}}(\rho) \propto \det[\rho]^{d_E - d}, \tag{2.54}$$

where $\det[\rho]$ is the density matrix determinant.

In Eq.(2.54), when $d = d_E$ the volume becomes independent of $\rho$, indicating that all effective full rank states have the same volume [17]. However we shall use expression (2.54) only in the regime $d < d_E$ consistent with the interpretation of $\mathcal{H}_E$ as an environment.

Thus, for $d < d_E$, Eq. (2.54) attains its maximum at the maximally mixed state

$$\rho = \frac{\mathbf{1}_d}{d}. \tag{2.55}$$

This means that, in the partial trace case, the number of compatible microscopic states is maximized when the state is maximally mixed.

### 2.2.2 Blurred and saturated detector

In the generalized subsystem scenario induced by the blurred and saturated detector, we aim to review the volume associated with an effective state $\rho \in \mathcal{L}(\mathcal{H}_2)$ which emerges

from two distinct coarse-graining maps, namely $\Lambda_{4\to2}$, and $\Lambda_{3\to2}$ introduced previously by [20] and [17] respectively.

The volume associated with the blurred and saturated detector is

$$\mathcal{V}_{\Lambda_{BnS}}(\rho) = \int d\mu_\psi \delta\left(\Lambda_{BnS}[\psi] - \rho\right), \tag{2.56}$$

where the explicit form of the coarse-graining map $\Lambda_{BnS}$ must be specified in order to compute the integral.

The procedure to compute the volume of microscopic states compatible with a given effective description $\rho \in \mathcal{L}(\mathcal{H}_2)$ is very similar for both level-reduction schemes ($4 \to 2$ and $3 \to 2$) [17,18,20]. The derivation proceeds by expressing $\rho$ in the Bloch-vector representation, parameterizing the matrix elements of the microscopic pure states, and applying Laplace and Fourier transforms together with their inverse transformations.. For the $4 \to 2$ dimension reduction the volume of the set $\Omega_{\Lambda_{4\to2}}$ is [20]

$$\mathcal{V}_{\Lambda_{4\to2}}(\rho) = \frac{\pi^5(1 - x^2 - y^2 - z^2)}{(1+z)^2}., \tag{2.57}$$

where $x = \mathrm{tr}(\rho\sigma_x)$, $y = \mathrm{tr}(\rho\sigma_y)$, $z = \mathrm{tr}(\rho\sigma_z)$ and $\sigma_x$, $\sigma_y$ are Pauli matrices. Notice when $x^2 + y^2 + z^2 = 1$ we are in Bloch sphere superfice and the state is pure. As we are not dealing with effective pure states, we never catch it. On the other hand, Eq. (2.57) develops a singular behavior near $z = -1$, corresponding to the effective state $|1\rangle$. This reflects the large number of microscopic states mapped to the same effective description.

For the $3 \to 2$ dimension reduction the volume of the set $\Omega_{\Lambda_{3\to2}}$ is computed as before [17]

$$\mathcal{V}_{\Lambda_{3\to2}}(\rho) = \frac{2\pi^5}{1+z}. \tag{2.58}$$

In $3 \to 2$ case the associated volume never vanishes for any effective state $\rho$. The volume of accessible microstates increases as $\rho$ approaches the south pole of the Bloch sphere, diverging in the limit $z \to -1$, representing the big amount of microstates mapped to the state $|1\rangle$. Note however that this singularity is integrable.

## 2.3 Distance between effective states

The effective dynamics induced by a coarse-graining map, as discussed in Sec. 2.1, is given by

$$\Gamma_t = \Lambda \circ \mathcal{U}_t \circ \mathcal{A}_\Lambda \tag{2.59}$$

which corresponds to the composition of a coarse-graining map, a unitary evolution, and an averaging assignment map [18–20].

Consequently for a given initial effective state ($\rho(t=0)$), the effective state at a later time $t$ is

$$\rho(t) = \Gamma_t[\rho(0)]. \tag{2.60}$$

This procedure leads to a new effective state $\rho(t)$ which is associated with the set

$$\Omega(\rho(t)) = \{\psi(t) \in \mathcal{L}(\mathcal{H}_D) \mid \Lambda[\psi(t)] = \rho(t), \quad \psi(t) = |\psi(t)\rangle\langle\psi(t)|\} \tag{2.61}$$

One may then perform a backward evolution in time, denoted by $\Gamma_{-t}$. This procedure consists of applying the assignment map to $\rho(t)$, evolving it backward in time via the inverse unitary operation $\mathcal{U}_{-t}$, and finally mapping through the coarse-graining map. The resulting effective state is referred to here as the recovered state, denoted by $\rho_R(0)$ (see Fig. 13).

This backward dynamics corresponds to a time-reversed evolution, defined as [17]

$$\Gamma_{-t} = \Lambda \circ \mathcal{U}_{-t} \circ \mathcal{A}, \tag{2.62}$$

such that

$$\rho_R(0) = \Gamma_{-t}[\rho(t)]. \tag{2.63}$$

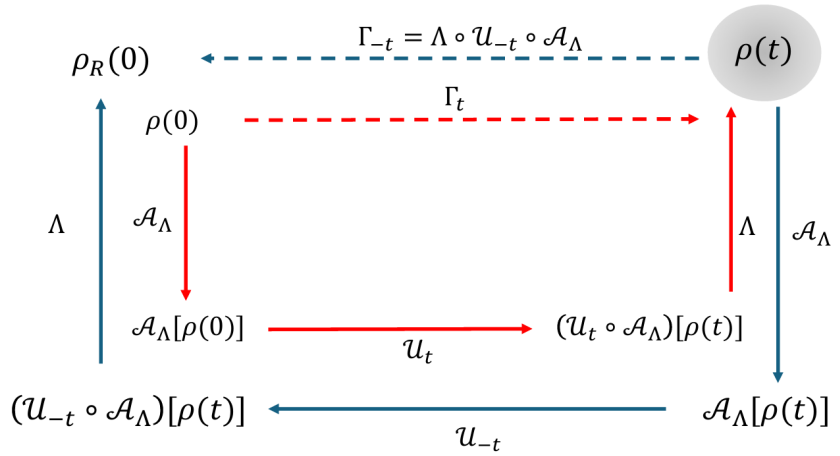


Figure 13 – A macroscopic backward dynamics represented by a composition of quantum operations. Forward dynamics in red and backward dynamics in blue.

Fig. 13 shows the forward dynamics in red given an initial effective state $\rho(0)$ and a backward evolution, considering $\rho(t) = \Gamma_t[\rho(0)]$ as a new preparation. Our aim here is to calculate the distance between the initial state ($\rho(0)$) and the "recovered" state $\rho_R(0)$ in order to assess their distinguishability. Consequently, we classify the process as irreversible if the distance between them is non-null.

Our idea is that these states can be distinguished because the microscopic set associated with $\rho(t)$ (in orange in Fig. 14) is not necessarily identical to the set of microscopic states obtained by evolving forward the microscopic preparation corresponding to $\rho(0)$ (in purple). In other words, there may exist microscopic states whose effective description is $\rho(t)$ but which do not belong to the evolved image of the initial set $\Omega_\Lambda(\rho(0))$. Consequently, when this larger set of compatible microscopic states is evolved backward in time, its effective description may no longer be $\rho(0)$. The Fig. 14 illustrates the possible difference between microscopic sets.

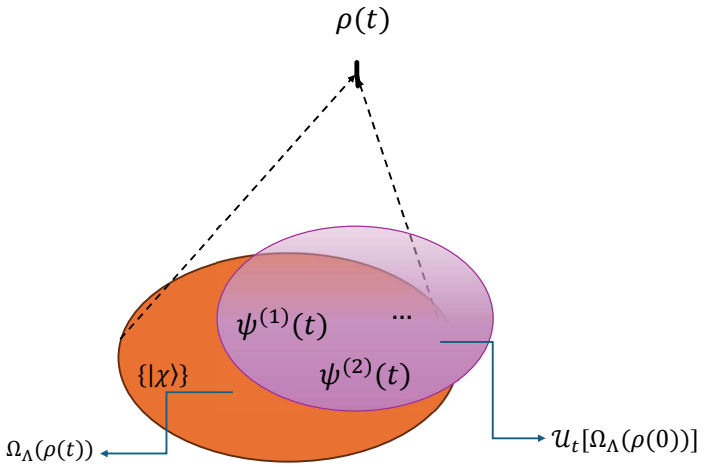


Figure 14 – The microscopic ensemble associated with the preparation of $\rho(0)$ evolves in time and yields in average the effective state $\rho(t)$ under coarse-graining map. Nevertheless, the set of microscopic states compatible with $\rho(t)$ may include states that do not belong to the forward-evolved image of $\Omega_\Lambda(\rho(0))$. Hence, $\Omega_\Lambda(\rho(t))$ can be larger than the evolved microscopic ensemble originating from $\rho(0)$.

The distance between two quantum states $\rho$ and $\sigma$ can be defined by trace distance [12, 21] and it is

$$\mathcal{D}(\rho,\sigma) = \frac{1}{2}\left\|\rho-\sigma\right\|_1 . \tag{2.64}$$

where the 1-norm $\|A\|_1 := \mathrm{tr}(\sqrt{A^\dagger A})$ for a given operator A.

Therefore, the quantity to be computed here is

$$\mathcal{D}(\rho_R(0), \rho(0)) = \frac{1}{2} \|\rho_R(0) - \rho(0)\|_1 , \tag{2.65}$$

and the recovered effective state ($\rho_R(0)$) would be obtained either through partial trace map or blurred and saturated detector map plus assignment and unitary.

### 2.3.1 Partial Trace

Consider an initial effective state $\rho(0)$ prepared in the laboratory. Under the partial-trace coarse-graining, assuming weak coupling between the system and the environment and no access to the environmental degrees of freedom, the effective state at time $t$ can be written as

$$\rho(t) = tr_E \left[ U \left( \rho(0) \otimes \frac{\mathbf{1}_{d_E}}{d_E} \right) U^\dagger \right] \quad \approx_{d_E \gg d} \quad \frac{\mathbf{1}_d}{d}, \tag{2.66}$$

where $d_E$ and $d$ denote the dimensions of the environment and the system of interest, respectively. The approximation holds when the environment is much larger than the system ($d_E \gg d$) and the unitary $U$ is sufficiently mixing. In this regime, typical unitary evolutions drive the state of the system toward the maximally mixed state. We employ random unitaries in our analysis because they are representative of generic mixing dynamics.

The hypothesis is that starting from an initial state $\rho(0)$, the effective unitary dynamics couples the subsystem to an environment. For sufficiently mixing interactions, the information initially encoded in the subsystem becomes distributed into system–environment correlations. Consequently, when $d_E \gg d$ the state at time $t$ becomes approximately close to the maximally mixed state.

Consider an initial state ($\rho(0)$) given by a statistical mixture,

$$\rho(0) = (1-p)|\psi(0)\rangle\langle\psi(0)| + p\frac{\mathbf{1}_d}{d} \tag{2.67}$$

where $p \in [0, 1]$ is a mixing parameter that controls the purity of the state. The cases $p = 0$ and $p = 1$ correspond to a pure state and to the maximally mixed state, respectively. The states $p = 1$ are known as depolarized pure states, a particular class of mixed states. This choice allows us to explore a continuous family of states whose determinant ranges from zero (at $p = 0$) to its maximal value $(1/d)^d$, attained at $p = 1$.

Since our goal is to quantify the distance between the initial and recovered effective states, it is convenient to write the recovered state $\rho_R(0)$ as a function of the initial state ($\rho(0)$) via composition of effective forward dynamics $\Gamma_t$ and backward dynamics $\Gamma_{-t}$, as follows

$$\rho_R(0) = \Gamma_{-t}[\rho(t)] = \Gamma_{-t} \circ \Gamma_t[\rho(0)] = \bar{\Gamma}_t[\rho(0)] \tag{2.68}$$

where $\bar{\Gamma}_t = \Gamma_{-t} \circ \Gamma_t$ is a linear map in the case of partial trace dynamics.

Using the linearity of $\bar{\Gamma}_t$ and substituting Eq. (2.67), the recovered effective state can be written as

$$\rho_R(0) = (1-p)\bar{\Gamma}_t|\psi(0)\rangle\langle\psi(0)| + p\frac{\mathbf{1}_d}{d}. \tag{2.69}$$

The trace distance between the recovered and initial states then reads

$$D(\rho_R(0), \rho(0)) = \frac{1}{2}(1-p)\left\|\bar{\Gamma}_t\left[|\psi(0)\rangle\langle\psi(0)|\right] - |\psi(0)\rangle\langle\psi(0)|\right\|_1, \tag{2.70}$$

where the identity contributions cancel exactly.

Since no additional constraints are imposed beyond the macroscopic description, we may take $|\psi(0)\rangle$ to be an arbitrary pure state. Recall that the 1-norm of an operator $A$ is defined as

$$\|A\|_1 := \mathrm{tr}\left(\sqrt{A^\dagger A}\right). \tag{2.71}$$

If $A$ is Hermitian, this reduces to

$$\|A\|_1 = \sum_i |\lambda_i|, \tag{2.72}$$

where $\lambda_i$ are the eigenvalues of $A$.

Then, for the hermitian operator in Eq. (2.70)

$$\bar{\Gamma}_t[|\psi(0)\rangle\langle\psi(0)|] - |\psi(0)\rangle\langle\psi(0)|, \tag{2.73}$$

the trace distance can be written as

$$\frac{1}{2}\left\|\bar{\Gamma}_t[|\psi(0)\rangle\langle\psi(0)|] - |\psi(0)\rangle\langle\psi(0)|\right\|_1 = \frac{1}{2}\sum_{i=1}^{d}|\lambda_i|, \tag{2.74}$$

where $\lambda_i$ are the eigenvalues of

$$\bar{\Gamma}_t[|\psi(0)\rangle\langle\psi(0)|] - |\psi(0)\rangle\langle\psi(0)|, \tag{2.75}$$

and $d$ denotes the dimension of the system of interest.

Therefore, the distance between $\rho_R(0)$ and $\rho(0)$ under our assumptions, substituting (2.74) in (2.70), is given by the expression

$$\mathcal{D}(\rho_R(0), \rho(0)) = \frac{(1-p)}{2}\sum_{i=0}^{d}|\lambda_i|. \tag{2.76}$$

It is straightforward to note that the distance in Eq. (2.76) vanishes when the initial effective state is maximally mixed ($p = 1$). As the dynamic is unital, if the initial

state is maximally mixed it will be map to another maximally mixed state and it is not possible to distinguish them.

On the other hand, if we consider the effective dynamics induced by the partial trace when it reduces to a unitary map ($\Gamma_t = \mathcal{U}_d$, which occurs when the total evolution is governed by a local unitary), the recovered state coincides exactly with the initial state,

$$\begin{aligned} \rho_R(0) &= \Lambda_{tr_E} \circ \mathcal{U}_{-t} \circ \mathcal{A}\{\Lambda_{tr_E} \circ \mathcal{U}_t \circ \mathcal{A}[\rho(0)]\} \\ &= (\mathbf{1}_d \otimes \mathrm{tr}_E)\ (U_d^\dagger \otimes U_E^\dagger) \left[U_d \rho(0) U_d^\dagger \ \otimes \ \frac{\mathbf{1_{d_E}}}{d_E}\right] (U_d \otimes U_E) \\ &= \rho(0) \end{aligned} \tag{2.77}$$

And

$$D(\rho_R(0), \rho(0)) = 0 \tag{2.78}$$

The cases of zero distances between the initial and recovered effective states ($\rho(0), \rho_R(0)$ respectively) indicate that these states cannot be distinguished and correspond to a reversible process.

### 2.3.2 Blurred and saturated detector

As before in partial trace case, we evolved the initial effective state $\rho(0)$ through the effective dynamics induced by the blurred–saturated detector coarse-graining map, defining the evolved effective state $\rho(t)$. Subsequently, we evolve this state backward in time, obtaining the recovered state $\rho_R(0)$.

The trace distance between $\rho(0)$ and $\rho_R(0)$ in this case is

$$D(\rho_R(0), \rho(0)) = \frac{1}{2} ||\bar{\Gamma}_t[\rho(0)] - \rho(0)||_1. \tag{2.79}$$

Although no further analytical simplification is available in this case, the general form above is sufficient to establish irreversibility through state distinguishability.

For a random $\rho(0)$ and random unitary, the dynamics will generally be irreversible, as we will show later with the numerical results.

## 2.4 Irreversibility

According to the second law of thermodynamics, the entropy of an isolated system does not decrease in the thermodynamic limit. In this sense, a transformation is reversible if the entropy remains unchanged, and irreversible if the final entropy is greater than the initial one [13, 25, 26, 30–33]. In the present framework, we relate the entropy to the volume of the Hilbert space associated with an effective state. Consequently, a possible

signature of irreversibility is the volume of the microscopic set associated with $\rho(0)$ (the initial effective state) being grater than the one associated to the effective description $\rho(t)$ (the evolved effective state at time t),

$$\frac{\mathcal{V}_\Lambda(\rho(t))}{\mathcal{V}_\Lambda(\rho(0))} > 1, \tag{2.80}$$

where the volume is computed as Eq. (2.52) and $\mathcal{V}_\Lambda(\rho(t))$ is the volume of the set associated to the effective description $\rho(t)$ and $\mathcal{V}_\Lambda(\rho(0))$ is the volume of the microscopic set associated with $\rho(0)$.

Irreversibility, on the other hand, can be defined through the trace distance between the initial state $\rho(0)$ and the recovered state ($\rho_R(0) = \bar{\Gamma}_t[\rho(0)]$). The trace distance allows one to distinguish between effective states in the following way: if $D(\rho_R(0), \rho(0)) = 0$ the two states are indistinguishable and the dynamics is reversible, if $D(\rho_R(0), \rho(0)) > 0$ both states can be distinguished and the dynamics is irreversible.

We expect these two indicators of irreversibility (volume growth and trace-distance increase) can be directly connected. In particular, an increase in the volume of the Hilbert space associated with the effective state after evolution is accompanied in most cases by an increase in the distance between the initial and recovered states, characterizing the irreversibility of the physical process. In this section, we demonstrate analytically and numeracally this correlation for effective dynamics induced by the partial trace and by the blurred and saturated detector coarse-graining map and we show numerical results for each case.

### 2.4.1 Partial trace

In this case, the volume associated with the microscopic states whose effective description is $\rho$, as discussed previously, is,

$$\mathcal{V}_{\Lambda_{PT}}(\rho) \propto \det[\rho]^{d_E - d}, \tag{2.81}$$

and this volume grows in time under the effective dynamics whenever the environment dimension is greater than the system of interest dimension ($d_E > d$).

To prove this growth analitically, Ref. [17] considered two quantum states $\sigma_1$ and $\sigma_2$ of the same dimension. $\sigma_1$ can be converted to $\sigma_2$ by a unital transformation $T$ if and only if $\sigma_1$ majorizes $\sigma_2$ i. e. [34]

$$T[\sigma_1] = \sigma_2 \leftrightarrow \sigma_1 \succ \sigma_2. \tag{2.82}$$

According to [34], $\sigma_1$ majorizes $\sigma_2$ if their spectra are in majorization order:

$$\sum_{i=1}^{k} \lambda_i^{\downarrow}(\sigma_1) \geq \sum_{i=1}^{k} \lambda_i^{\downarrow}(\sigma_2) \tag{2.83}$$

for all $k \geq 1$, where $\lambda_i^{\downarrow}(\sigma_1)$ denotes the eigenvalues of $\sigma$ arranged in non-increasing order.

By definition of Schur convexity, [35],

$$\vec{\lambda}(\sigma_1) \succ \vec{\lambda}(\sigma_2) \quad \rightarrow \quad G(\sigma_1) \geq G(\sigma_2), \tag{2.84}$$

with $G(x)$ defined by

$$G(x) := \sum_i g(x_i), \tag{2.85}$$

where $g$ is a convex function.

As a consequence, making $g(x) = -\log(x)$ a convex function and $x = \det[\rho]$, [17] showed that

$$\det\left(\rho(t)\right) \geq \det\left(\rho(0)\right). \tag{2.86}$$

In Fig. 15, with the dimension of the system of interest being $d = 3$, we present numerical results comparing between the determinant at $t$, i.e., $\det[\rho(t)]$ and the initial determinant, $\det[\rho(0)]$ for different dimensions of the environment representing Eq. (2.86). This and other results were obtained as follows: effective states were sampled by varying the parameter $p$ ranging in $[0.01, 1]$ with steps of 0.001. For each $\rho(0) \in \mathcal{L}(\mathcal{H}_d)$, considering no knowledge about the environment, we associated a pure average microscopic description in the extended space $\psi \in \mathcal{L}(\mathcal{H}_d \otimes \mathcal{H}_E)$. The number of microstates compatible with $\rho(0)$ is quantified through the volume in Eq. (2.52). The compatible microstates are evolved unitarily and an effective description at time t, $\rho(t) \in \mathcal{L}(\mathcal{H}_d)$, is obtained through the coarse-graining map. The evolved microstate is assigned to a set of compatible microstates, and the quantity of these is measured by volume.

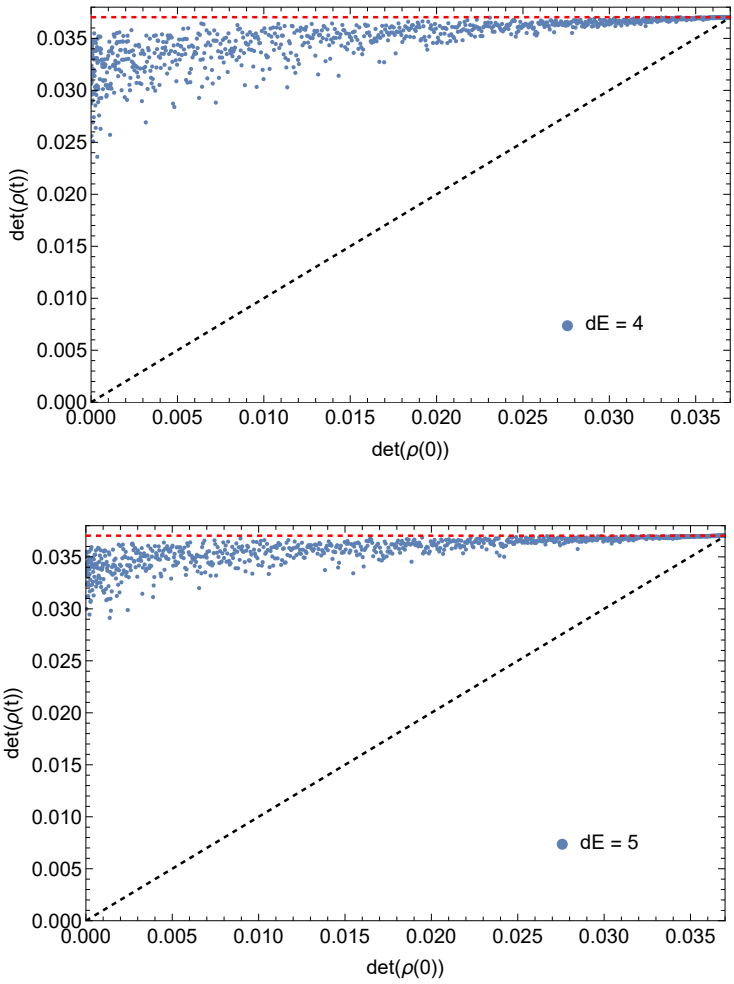


Figure 15 – We randomly sample effective states defined in Eq. (2.67) with system dimension $d = 3$ and parameter $p$ ranging from 0.01 to 1 in steps of 0.001. Each state is evolved under effective dynamics of the form $\Gamma[\rho(0)] = \Lambda \circ U \circ \mathcal{A}$, where $\Lambda$ and $\mathcal{A}$ correspond to the partial trace construction with environment dimensions $d_E = 4, 5$. The unitary operator $U$, acting on the composite space of dimension $3 \otimes d_E$ was choosen from CUE. The time dependence is entirely carried by the random unitary. For each realization, we compute the volume defined in Eq. (2.54) both at the initial time and after the effective evolution. The black curve indicates equality between the initial and final determinants, while the red curve marks the maximal determinant value.

We observe in Fig. 15 that the points for different dimensions of the environment, representing the comparation between $\det[\rho(t)]$ and $\det[\rho(0)]$ given different initial effective state, agree with the inequality (2.86), being above the reference line which marks the equality between the determinants and approaching the value of $\rho$ maximally mixed as $d_E$ increases.

Moreover, it is evident that increasing the size of the environment drives the recovered states closer to the maximally mixed state. This means that a larger environment, with no information about environment degrees of freedom, enhances the loss of information about the initial effective state, leading to a stronger washing out of its microscopic features.

Once it has been observed that the volume never decreases in the case of the effective dynamics induced by the partial trace when $d_E > d$ under our assumptions, we can observe the ratio between the volume associated with the ensemble characterized by the effective state at time $t$ ($\rho(t)$) and the volume of a set of microstates with the same initial effective state ($\rho(0)$)

$$\frac{\mathcal{V}(\rho(t))}{\mathcal{V}(\rho(0))} = \frac{\det[\rho(t)]^{d_E-d}}{\det[\rho(0)]^{d_E-d}}. \tag{2.87}$$

As before, we considered that the effective dynamics $\Gamma_t$ maps any statistical mixture $\rho(0)$ to states concentrated around the maximally mixed state, $\rho(t) \approx_{d_E \gg d} \frac{\mathbf{1}_d}{d}$ for random unitary evolutions, under the assumptions of no access to the environmental degrees of freedom, weak system-environment coupling, an environment dimension much larger than that of the system, and a sufficiently mixing interaction between the system and environment. The initial effective state is given by Eq. (2.67). Therefore, Eq. (2.87) can be written as

$$\frac{\mathcal{V}(\rho(t))}{\mathcal{V}(\rho(0))} = \frac{\det\left[\frac{\mathbf{1}_d}{d}\right]^{d_E-d}}{\det\left[(1-p)|\psi(0)\rangle\langle\psi(0)| + p\frac{\mathbf{1}_d}{d}\right]^{d_E-d}}, . \tag{2.88}$$

To compute the determinants at Eq.(2.88) we use the product of eigenstates ($\lambda_i$)

$$\det[\rho] = \prod_{i=1}^{d} \lambda_i \tag{2.89}$$

Then, the determinant of $\rho(t) \approx_{d_E \gg d} \frac{\mathbf{1}_d}{d}$ is straightforward:

$$\det\left[\frac{\mathbf{1}_d}{d}\right] = \left(\frac{1}{d}\right)^d \tag{2.90}$$

since the spectrum of $\mathbf{1}_d/d$ is $\{1/d, 1/d, ...\}$ $d$ times.

The eigenvalues of $\rho(0)$ can be obtained by choosing an orthonormal basis $\{|\psi(0)\rangle, |\psi_\perp^{(i)}\rangle\}$, where the vectors $|\psi_\perp^{(i)}\rangle$ span the subspace orthogonal to $|\psi(0)\rangle$. In this basis, the state

$$\rho(0) = (1-p)|\psi(0)\rangle\langle\psi(0)| + \frac{p}{d}\mathbb{I}_d \tag{2.91}$$

is diagonal. Acting on $|\psi(0)\rangle$, we obtain

$$\rho(0)|\psi(0)\rangle = \left[(1-p) + \frac{p}{d}\right]|\psi(0)\rangle, \tag{2.92}$$

which yields the eigenvalue

$$\lambda_1 = (1-p) + \frac{p}{d}. \tag{2.93}$$

For any vector orthogonal to $|\psi(0)\rangle$, the projector term vanishes and we obtain

$$\rho(0)|\psi_\perp^{(i)}\rangle = \frac{p}{d}|\psi_\perp^{(i)}\rangle, \tag{2.94}$$

leading to the remaining eigenvalues

$$\lambda_{2,\dots,d} = \frac{p}{d}. \tag{2.95}$$

Summarizing: the eigenvalues of $\rho(0)$ are $\lambda_1 = (1-p) + \frac{p}{d}$ when we project $\rho(0)$ over $\psi(0)$ and $\lambda_{2,\dots,d} = \frac{p}{d}$ when we project over an orthogonal vector. Thus, the determinant of $\rho(0)$ is

$$\det\left[(1-p)|\psi(0)\rangle\langle\psi(0)| + p\frac{\mathbf{1}_d}{d}\right] = \left(1 - \frac{d-1}{d}\right)\left(\frac{p}{d}\right)^{d-1}. \tag{2.96}$$

Therefore, the ratio between the volume associated with the ensemble characterized by the effective description $\rho(t)$ and $\rho(0)$ under our assumptions is

$$\frac{\mathcal{V}(\rho(t))}{\mathcal{V}(\rho(0))} = \frac{\left(\frac{1}{d}\right)^{d(d_E-d)}}{\left[\left(1 - \frac{d-1}{d}p\right)\left(\frac{p}{d}\right)^{d-1}\right]^{d_E-d}}, \tag{2.97}$$

Notice that $p \in [0,1]$. If $p \to 1$, $\rho(0) \to \frac{\mathbf{1}_d}{d}$ and the ratio $\frac{\mathcal{V}(\rho(t))}{\mathcal{V}(\rho(0))} \to 1$ given that the volumes are the largest possible. More generally, the condition $\mathcal{V}(\rho(0)) > \mathcal{V}(\rho(t))$ would require

$$\left(1 - \frac{d-1}{d}p\right)\left(\frac{p}{d}\right)^{d-1} > \left(\frac{1}{d}\right)^{d}. \tag{2.98}$$

To analyze whether inequality (2.98) can be satisfied for some $p \in [0,1]$, we multiply both sides by $d^d$, obtaining

$$\underbrace{(d-(d-1)p)\,p^{d-1}}_{f(p)} > 1. \tag{2.99}$$

We now study the function

$$f(p) = (d-(d-1)p)\,p^{d-1}. \tag{2.100}$$

At the boundary values, we find:

$$f(0) = 0, \qquad f(1) = 1. \tag{2.101}$$

Thus, neither boundary point satisfies inequality (2.99). Next, we compute the derivative

$$f'(p) = d(d-1)p^{d-2}(1-p). \tag{2.102}$$

For $p \in (0,1)$, all factors in $f'(p)$ are strictly positive, hence

$$f'(p) > 0. \tag{2.103}$$

Therefore, $f(p)$ is strictly increasing on the interval $[0,1]$. Since $f(1) = 1$ is the maximum extreme, it follows that

$$f(p) \leq 1 \tag{2.104}$$

for all $p \in [0,1]$. Consequently, inequality (2.99) cannot be satisfied in this interval. This shows again that, for this class of states, the volume associated with the effective dynamics induced by the partial trace never decreases.

For $d = 3$, as adopted in the numerical calculations, the volume ratio is

$$\frac{\mathcal{V}(\rho(t))}{\mathcal{V}(\rho(0))} = \frac{\left(\frac{1}{3}\right)^{3(d_E-3)}}{\left[\left(1-\frac{2}{3}p\right)\left(\frac{p}{3}\right)^2\right]^{d_E-3}}, \tag{2.105}$$

which depends on the mixing parameter $p \in [0,1]$ and the environment dimension.

The trace distance can also be expressed in terms of the parameter $p$ (see Eq.(2.76)), as discussed previously. For the dimension used in the numerical calculations ($d = 3$) and eigenvalues $\lambda_i \in \{-2/3, 1/3, 1/3\}$ the distance between $\rho(0)$ and $\rho_R(0)$ is

$$\mathcal{D}(\rho_R(0), \rho(0)) = \frac{2}{3}(1-p). \tag{2.106}$$

We present the behaviour of $\mathcal{D}(\rho_R(0), \rho(0))$ changing the parameter $p$ in the range $[0,1]$ in Fig. 16. We sampled effective states and assigned to each of them an average microscopic pure-state description in the extended Hilbert space $\psi \in \mathcal{L}(\mathcal{H}_d \otimes \mathcal{H}_E)$ compatible to it. These microscopic states were then evolved unitarily, and the corresponding effective state at time $t$, $\rho(t) \in \mathcal{L}(\mathcal{H}_d)$ was obtained through the coarse-graining map. Next, a set of microscopic states compatible with the evolved effective description was generated and evolved backward in time. Applying the coarse-graining map to the backward-evolved microscopic states yielded a recovered effective state 0, $\rho_R(0)$. Finally, the trace distance between the initial effective state and the recovered one was computed.

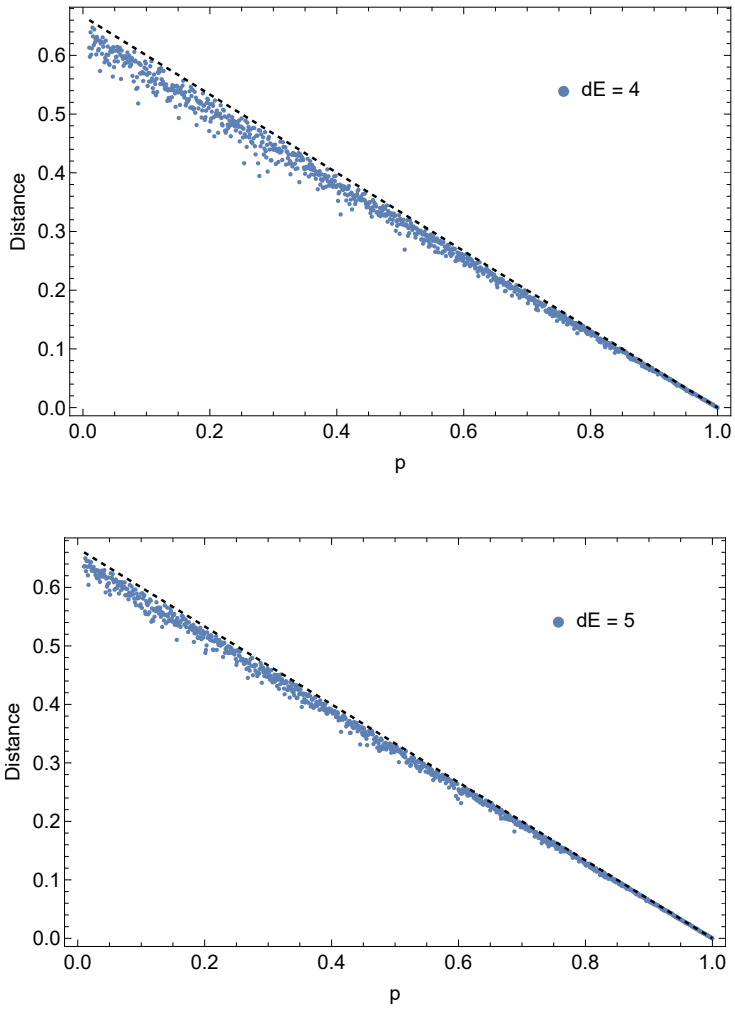


Figure 16 – From the initially sampled random effective states defined as (2.67) of dimension 3 and $p$ range equal to $[0.01, 1]$ with steps of 0.001, the respective determinants were obtained with $\mathcal{A}_{\Lambda_{tr_E}}$ given by Eq.(2.28) and random circular unitary of dimension $3 \otimes d_E$. We repeat the numerical calculation for different environment dimensions $d_E = 4, 5$. The dashed curve in black represents the theoretical curve of Eq.(2.106).

As shown in Fig. 16, for different environment dimensions, the numerical curves exhibit behavior consistent with the theoretical prediction of Eq. (2.106). As the environment dimension increases, the numerical results approach the reference curve more closely. This is expected under our assumptions since tracing out a larger environment leads to a greater loss of accessible information, rendering the effective description more mixed.

It is also instructive to analyze the probability density of the trace distance between the initial effective state and the recovered state $\rho_R(0)$, obtained through the composition of forward effective dynamics $\Gamma_t$ and backward dynamics $\Gamma_{-t}$. Since $\mathcal{D}(\rho_R(0), \rho(0))$ depends on the statistical weight parameter $p \in [0, 1]$, which is sampled uniformly, one expects the probability density intervals to reflect this uniform distribution for the class of states defined in Eq. (2.67).

Figure 17 shows the histogram representing the probability density distribution of the distances between $\rho(0)$ and $\rho_R(0)$, sampled for $p \in [0.01, 1]$ in steps of 0.001, for the environment dimension $d_E = 5$.

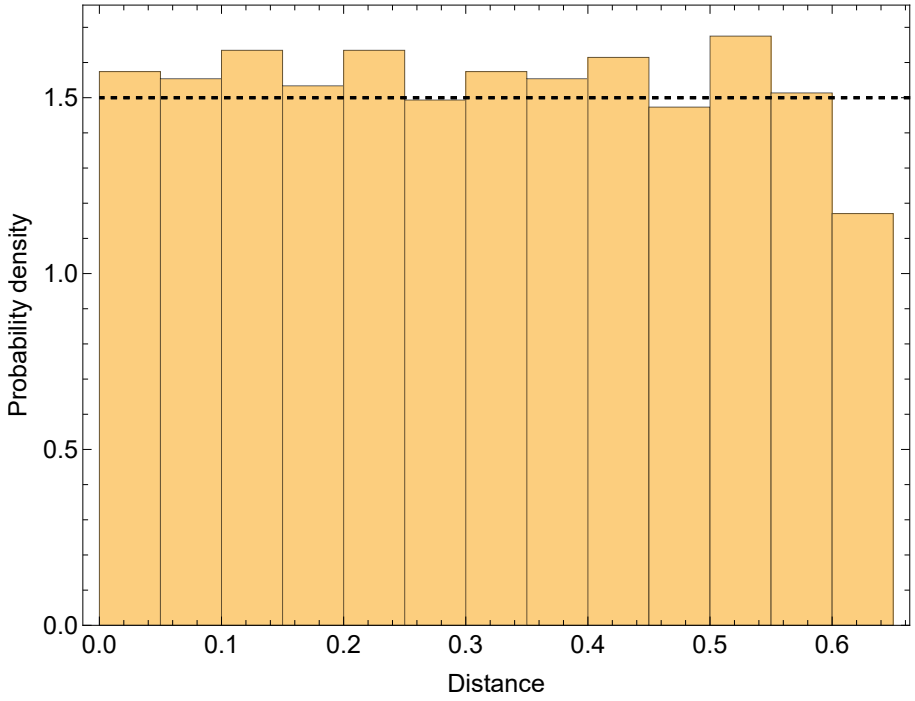


Figure 17 – Histogram of $\mathcal{D}(\rho_R(0), \rho(0))$ for environment dimension $d_E = 5$. For system dimension $d = 3$, the trace distance is bounded within the interval $[0, 2/3]$ (for $d_E >> d$). Since the mixing parameter $p$ is sampled uniformly in $[0, 1]$, and the distance varies smoothly and approximately linearly with $p$, the resulting probability distribution is expected to be approximately uniform over its allowed range. The larger the environment, the more uniform the behavior is expected to be.

We also analyze one correlation between the volume ratio in (2.105) and the trace distance in (2.106), both parameterized by $p$. Such a correlation allows us to identify the emergence of irreversibility: as the volume of the set of microscopic states associated with a single effective description grows according to the preparation of the effective description, the trace distance between the initial and recovered states also increases.

Using $p = 1 - \frac{3}{2}\mathcal{D}$, (where $\mathcal{D} = \mathcal{D}(\rho_R(0), \rho(0))$ is the distance between $\rho(0)$ and $\rho_R(0)$) the analytical expression relating the volume ratio (given by Eq. (2.105)) directly to the trace distance reads

$$\frac{\mathcal{V}(\rho(t))}{\mathcal{V}(\rho(0))} = \frac{\left(\frac{1}{3}\right)^{3(d_E-3)}}{\left[\left(\frac{1}{3}+\mathcal{D}\right)\left(\frac{1}{3}-\frac{\mathcal{D}}{2}\right)^2\right]^{d_E-3}}, \tag{2.107}$$

and the parametric curve at $p$ is shown in Fig. 18.

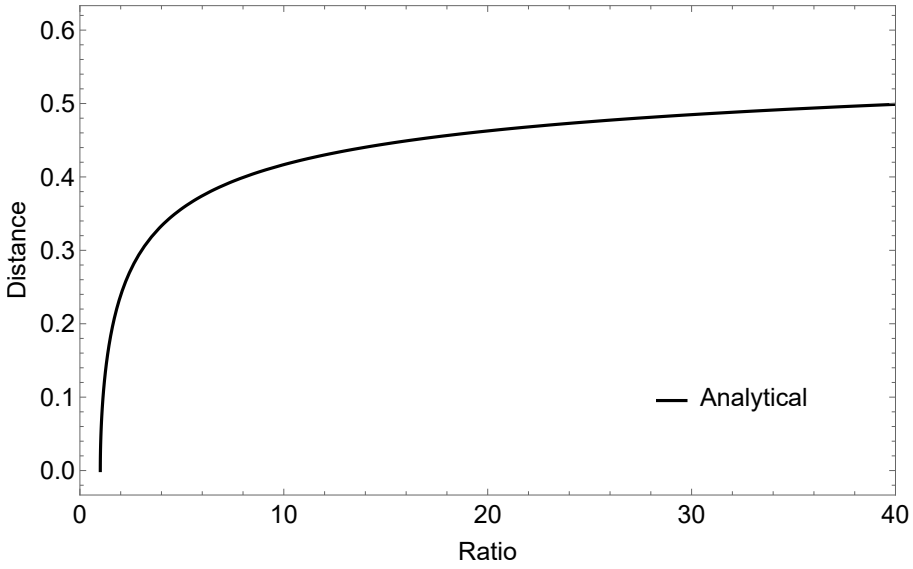


Figure 18 – Parametric curve showing the correlation between volume ratio of the sets of microstates associated with an effective description and trace distance between initial effective state and recovered effective state for $d_E = 5$.

Figure 18 shows that, for the partial trace case, the distance is increasing function of the volume ratio. In Fig. 19 we show the correlation between the increase in volume and in the distance comparing analytical curve with the datas obtained by numerical calculations for $d_E = 5$.

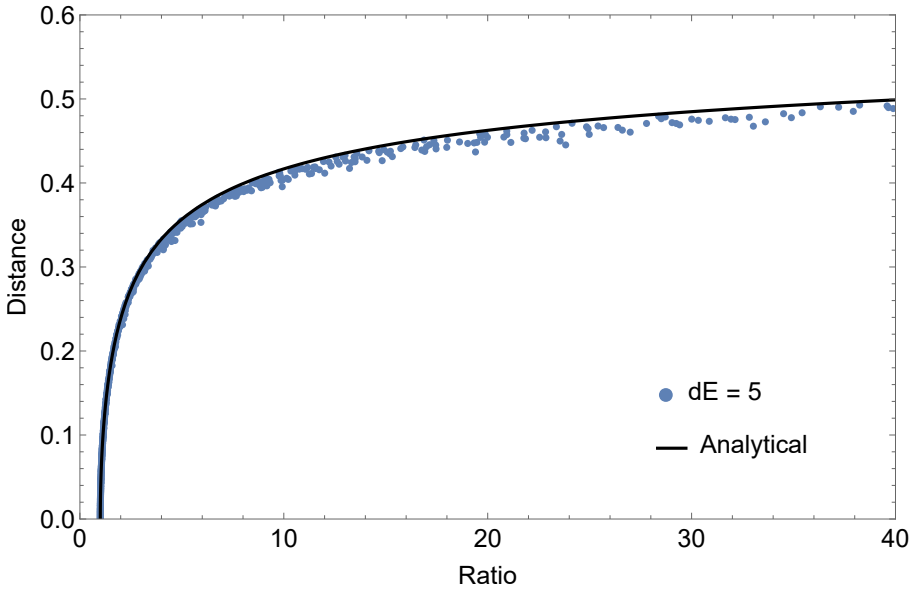


Figure 19 – Correlation between the increase in volume and the corresponding increase in trace distance. The black curve represents the theoretical prediction given by Eq. (2.107), while the blue points correspond to the sampled states defined in Eq. (2.67) where $\mathcal{D}(\rho_R(0), \rho(0))$ denotes the trace distance between $\rho(0)$ and $\rho_R(0)$. The plotted volumes and distances are obtained numerically following the procedure described in the text.

The correlation shown in Fig. 19 indicates the irreversible character of the effective dynamics in the case of the partial trace with $d_E > d$, since Eq. (2.107) is an increasing function of $\mathcal{D}(\rho_R(0), \rho(0))$. Therefore, larger values of the volumes ratios correspond to larger associated distance, signaling irreversibility in the effective dynamics.

### 2.4.2 Blurred and saturated detector

In this subsection, we present the irreversibility analysis for both blurred and saturated detectors. The effective dynamics is given by

$$\Gamma_t = \Lambda_{BnS} \circ \mathcal{U} \circ \mathcal{A}_{\Lambda_{BnS}}, \tag{2.108}$$

where $\mathcal{U}$ is a random unitary operator, and $\Lambda_{BnS}$ together with its associated assignment map $\mathcal{A}_{\Lambda_{BnS}}$ depend on the specific level-reduction scheme ($4 \to 2$ or $3 \to 2$). In both cases, the resulting effective map is not unital, but the effective dynamics by definition generates physical outputs, valid effective states.

The increase in volume following effective dynamics related to each macroscopic preparation should be understood in a statistical sense. In the case of $\Lambda_{BnS}$, both the effective and microscopic Hilbert spaces have very small dimensions, and the system is far from the thermodynamic limit. As a consequence, statistical fluctuations are large, which

allows for "atypical" realizations in which the volume of compatible microstates does not increase.

Even though this occurs only for a small fraction of states when compared to the typical volume increase under the action of the dynamics, there exist states whose associated volumes do not increase under the effective dynamics, as shown in Fig. 20. Effective states were sampled from the Bloch sphere. For each $\rho(0) \in \mathcal{L}(\mathcal{H}_d)$, and assuming no information about the environmental degrees of freedom, an average microscopic description in the extended Hilbert space $\psi \in \mathcal{L}(\mathcal{H}_D)$, was assigned. The number of microscopic states compatible with $\rho(0)$ is quantified by the volume given in Eq. (2.57) for the $4 \to 2$ reduction and in Eq. (2.58) for the $3 \to 2$.The corresponding microscopic description was evolved unitarily, and the coarse-graining map was then applied to obtain the effective state at time $t$, $\rho(t) \in \mathcal{L}(\mathcal{H}_d)$. A new set of microscopic states compatible with $\rho(t)$ was subsequently assigned, and its size was quantified through the corresponding volume. This procedure was repeated one thousand times.

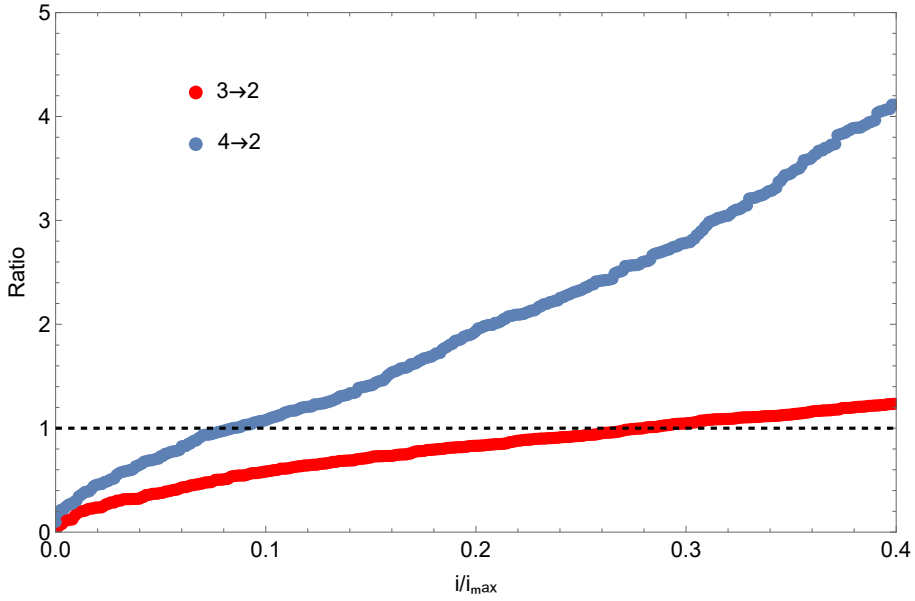


Figure 20 – Ordered ratio $\mathcal{V}(\rho^{(i)}(t))/\mathcal{V}(\rho^{(i)}(0))$ obtained from $i_{\max} = 1000$ independent realizations of the full protocol. In each iteration, a Bloch vector was randomly sampled to define an effective state $\rho(0)$. Its associated microscopic states was generated via the average assignment map, evolved under a random unitary drawn from the circular unitary ensemble, and mapped up to an effective state $\rho(t)$, from which the final volume was computed. The horizontal axis represents the normalized realization index $i/i_{\max}$. The blue curve corresponds to the $4 \to 2$ coarse-graining map, while the red curve corresponds to the $3 \to 2$ coarse-graining map.

From Fig. 20, one observes that the percentage of states for which the volume $\mathcal{V}(\rho(t))$ is smaller than $\mathcal{V}(\rho(0))$ is higher in the $3 \to 2$ detector case. This suggests that,

as the dimension of the initial system subjected to the coarse-graining map increases, the occurrence of atypical outcomes, those associated with volume reduction, becomes less frequent.

As in the case of the partial trace, we can observe the probability density of the distances of $\rho_R(0)$ with respect to an initial effective description $\rho(0)$. In scenarios involving small Hilbert space dimensions and non-unital effective dynamics, one should not expect the evolution to drive $\rho(0)$ towards the maximally mixed state. We sampled effective states from the Bloch sphere and assigned to each of them an average microscopic pure-state description in the extended Hilbert space, $\psi \in \mathcal{L}(\mathcal{H}_D)$, compatible with the given effective state. These microscopic states were evolved unitarily, and the corresponding effective description at time $t$ $\rho(t) \in \mathcal{L}(\mathcal{H}_d)$, was obtained through the coarse-graining map. A set of microscopic states compatible with $\rho(t)$ was then generated, and each of these states was evolved backward in time. Applying the coarse-graining map to the backward-evolved microscopic states yielded a recovered effective description $\rho_R(0))$. Finally, the trace distance between the initial effective state was obtained.

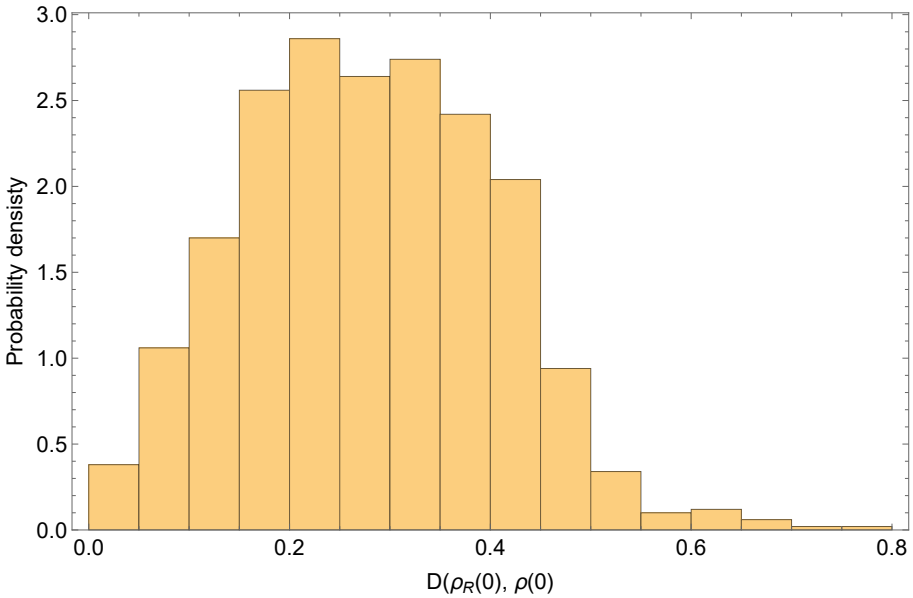


Figure 21 – Distribution of $D(\rho_R(0), \rho(0))$ for the $3 \to 2$ detector. The initial states $\rho(0)$ are uniformly sampled on the Bloch sphere, and $\rho_R(0) = \bar{\Gamma}[\rho(0)]$, where $\bar{\Gamma} = \Gamma_{-t} \circ \Gamma_t$. The map $\bar{\Gamma}$ is obtained from the composition of forward and backward effective dynamics, with the time dependence entirely carried by a random unitary. The mean value of distances is 0.280057.

In Fig. (21) we show the probability density for the case of $3 \to 2$ reduction.In Fig. (22), detector $4 \to 2$, the behavior of the probability density distribution of the distances between $\rho(0)$ and $\rho_R(0)$ has a higher mean when compared to that of detector $3 \to 2$ in Fig. (21).

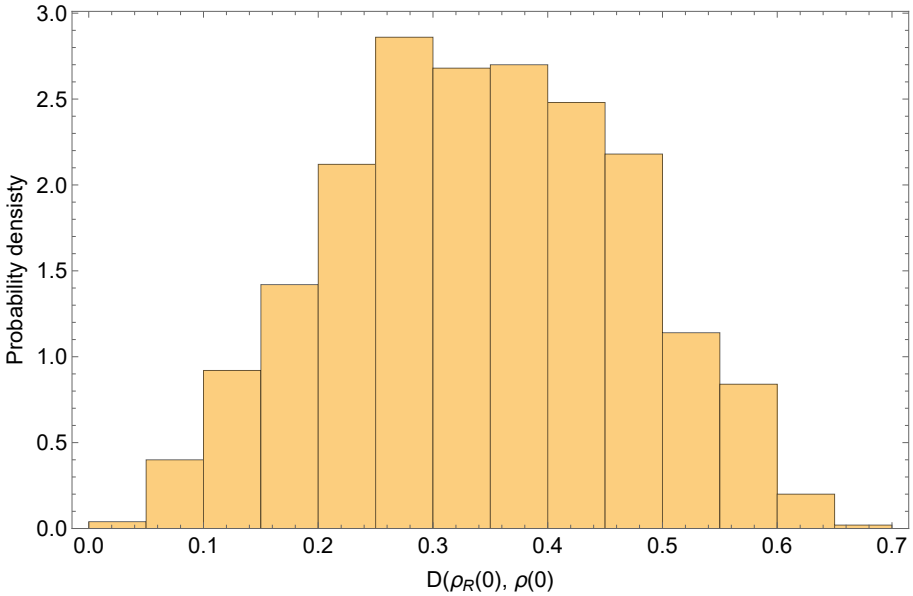


Figure 22 – Distribution of $D(\rho_R(0), \rho(0))$ from detector $4 \to 2$. Here, $\rho(0)$ was also uniformly sampled on the Bloch sphere, and $\rho_R(0) = \bar{\Gamma}_t[\rho(0)]$ was obtained through the recovered dynamics on the initial state with same parameters as Fig. 21. The mean value of distances is 0.341565.

Once the distances between $\rho(0)$ and $\rho_R(0)$ and the volumes of $\rho(0)$ and $\rho(t)$ are known, we can observe the behavior of the the distance as a function of volume ratio $\mathcal{V}(\rho(t))/\mathcal{V}(\rho(0))$, as shown in Figures 23 and 24. Each point represents a single numerical realization $i$, characterized by its volume ratio between $\rho(t)$ and $\rho(0)$ and the trace distance between $\rho(0)$ and $\rho_R(0) = \bar{\Gamma}_t[\rho(0)]$:

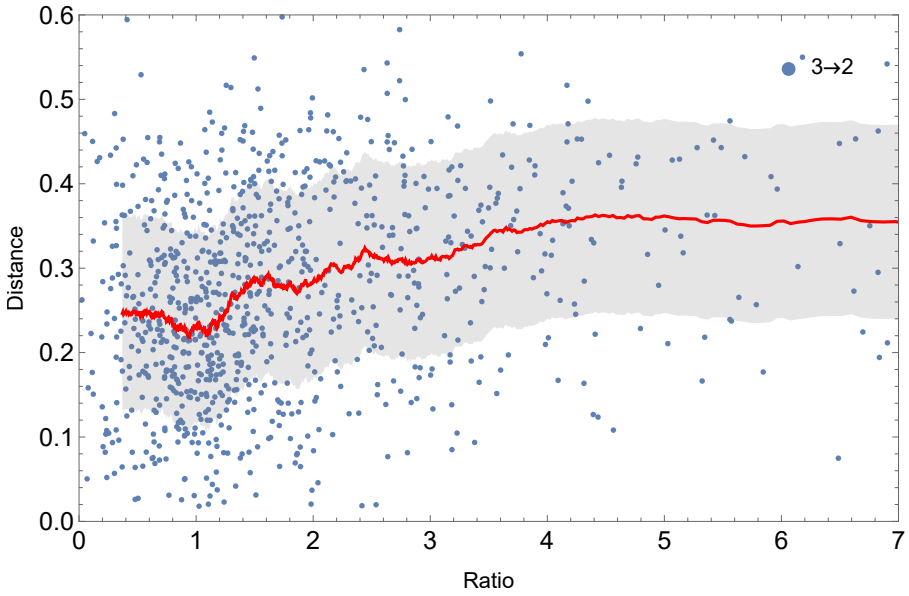


Figure 23 – Effective states were sampled randomly and uniformly in Bloch sphere. For each state, the following procedure was performed: application of the assignment map $\mathcal{A}$, unitary evolution drawn from the circular unitary ensemble of dimension 3, and subsequent coarse-graining via $\Lambda_{3\to 2}$. The initial and final volumes were then computed. By applying the inverse effective dynamics, $\Gamma_{-t}[\rho(t)]$, the state $\rho_R(0)$ was obtained, and the trace distance $D(\rho_R(0), \rho(0))$ was calculated, quantifying the distance between the initial and reconstructed states. Taking the red curve (the moving average considering 101 points) as a reference, we define the residuals as the differences between the y-coordinates of the data points and the corresponding values of the red curve. The grayed-out region represents the deviation area. The variance of these residuals is 0.0132121.

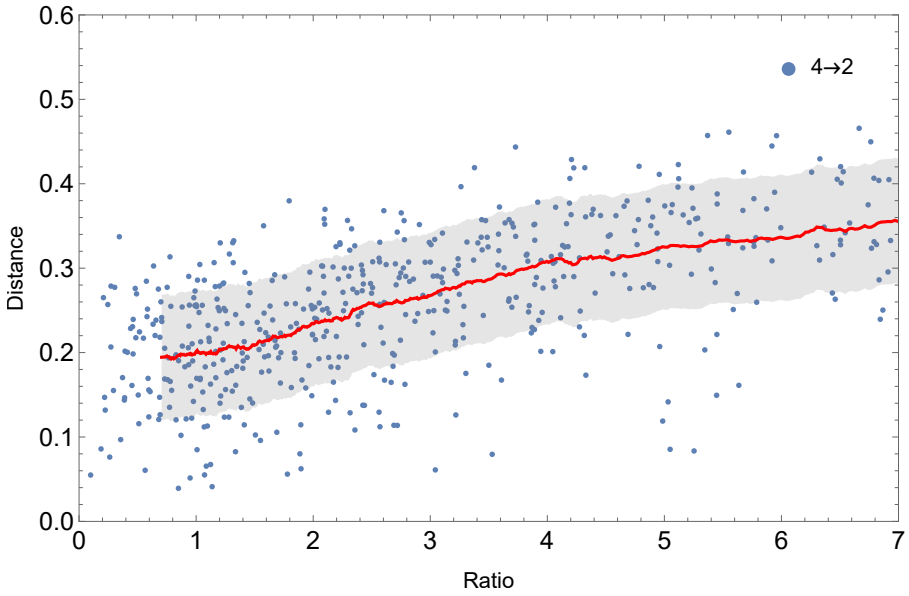


Figure 24 – In a very similar view to the previous figure, we obtained the initial and final volumes, where $U$ is a random CUE matrix of dimension 4. $\mathcal{A}$ was also generated from the average over the pure states and, in this case, the coarse-graining map was $\Lambda_{4\to 2}$. Taking the red curve (the moving average considering 101 points) as a reference, we define the residuals as the differences between the y-coordinates of the data points and the corresponding values of the red curve. The grayed-out region represents the deviation area. The variance of these residuals is 0.00550731.

Unlike the partial trace case, the behaviour of the data $D(\rho_R(0), \rho(0))$ as a function of the volume ratio $\mathcal{V}(\rho(t))/\mathcal{V}(\rho(0))$ does not exhibit a well-defined curve. Nevertheless, by comparing Fig. 23 with Fig. 24, one observes that the higher-dimensional detector displays a clearer tendency toward correlation between irreversibility, quantified by the distance, and volume increase. This suggests that the dimension of the underlying microscopic system plays a significant role in shaping the statistical structure of the problem, something that will be examined in greater detail in the next chapter.

## 2.5 Conclusion

The second law of thermodynamics governs all physical processes and, therefore, it is of utmost interest to investigate it from different perspectives. In classical statistical mechanics, the connection between microscopic and macroscopic descriptions is established through entropy, which quantifies the number of states compatible with a given macroscopic property. Here, we use an extension of the Boltzmann entropy concept to quantum systems by quantifying the number of accessible states in Hilbert space associated with a specific quantum preparation.

By employing the concepts of effective dynamics, which describe the macroscopic evolution accessible to an observer, the distance between effective states (initial and "recovered") as a criterion for irreversibility, and the volume of Hilbert space as a measure of the number of pure states compatible with a given effective description, we construct a framework that extends Boltzmann entropy to Hilbert space.

To assess whether processes induced by effective dynamics (defined through coarse-graining maps, unitary microscopic evolution, and average assignment maps) are irreversible, we analyze how the uncertainty associated with an effective description evolves in time. Generally the number of microscopic states compatible with the evolved effective description is larger than the number compatible with the initial preparation.

This happens once the microscopic set associated with $\rho(t)$ is not necessarily identical to the set of microscopic states obtained by evolving forward the microscopic preparation corresponding to $\rho(0)$. In other words, there may exist microscopic states whose effective description is $\rho(t)$ but which do not belong to the evolved image of the initial ensemble $\Omega_\Lambda(\rho(0))$. In such cases the uncertainty associated with the evolved effective state is greater than the one associated with the initial preparation.

This growth of uncertainty explains why the initial preparation and the recovered preparation (obtained by composing forward and backward effective dynamics) can be distinguishable, giving rise to irreversibility at the effective level. We characterized irreversibility through the correlation between the behavior of the Hilbert space volume associated with the preparation of the effective state after evolution, compared to the volume of the initial preparation, and the increase in distance between the initial and recovered effective states.

We observed, however, that there exist cases in which the volume does not increase. These situations arise when both the effective and microscopic Hilbert spaces have very small dimensions, and the system is far from the thermodynamic limit. As a consequence, atypical realizations are not sufficiently suppressed, allowing situations in which the volume of compatible microstates does not increase. In the next chapter, we consider systems with larger dimensions in order to suppress atypical behavior.

# 3 Dynamics of expectation values

In the previous chapter, we extended the Boltzmann entropy concept to quantum systems by quantifying the number of accessible states in Hilbert space associated with a given preparation. We showed that irreversibility is linked to the growth of this volume under dynamics induced by coarse-graining maps.

However, we also observed that this link is sensitive to the specific dynamics under consideration. When the microscopic Hilbert space has small dimension, the system is far from the thermodynamic limit and atypical behaviors may arise. In such cases, the volume associated with the effective density matrix may not increase after the dynamical process, and consequently the same may occur for entropy, which is an increasing function of the volume.

This chapter continues the analysis of effective dynamics, now formulated in terms of evolution of a fixed expectation value of an observable $A$. We consider the set

$$\Omega_A(a) = \{\phi \in \mathcal{H}_D \mid \langle\phi|A|\phi\rangle = a\} \tag{3.1}$$

consisting of all pure states that share the same expectation value of $A$, where $D$ denotes the Hilbert space dimension. The average over all macrostates defines the macroscopic quantity that characterizes the effective level of description. Although a single expectation value does not uniquely determine a density matrix, we adopt the same conceptual framework used previously: the expectation value specifies the macroscopic description, while the corresponding set of compatible pure states constitutes the underlying microscopic level.

Using the formalism of dynamical typicality of quantum expectation values developed by Bartsch and Gemmer [24] (see also [36]), together with a quantifier of irreversibility (the distance between expectation values) and the volume of the set of states sharing the same expectation value developed by Brody, Hook and Hughston [16], we quantify both the uncertainty associated with the set of microscopic states compatible with a given expectation value of an observable and the resulting irreversibility. Within this framework, we aim to show that irreversibility emerges naturally in the dynamics of large systems in connection with volume growth.

The central concept guiding this chapter is typicality. According to Refs. [6, 24, 36–38], an expectation value is said to be typical when most states in a given set produce values close to the ensemble average and rarely deviate significantly from it. Based on this idea, Ref. [24] introduced the concept of dynamical typicality: if pure states from such a set produce approximately the same expectation value of an observable $A$ at an initial instant $t = 0$, then, under unitary evolution, they will also produce approximately

the same expectation value at later times $t$. The importance of dynamical typicality is to characterize the dynamics of the expectation values, which will play the role of effective dynamics in this context.

When a system is prepared with a fixed expectation value of a given observable, a corresponding set of pure states is defined, namely the set of all states that share the same expectation value, as given in Eq.( 3.1). Since no further information about the microscopic state is available, we adopt the hypothesis of a uniform probability distribution over this set. This assumption reflects maximal ignorance beyond the prescribed expectation value and allows us to quantify the uncertainty associated with the number of microscopic states compatible with the preparation.

The volume associated with this uncertainty can be computed analogously to the procedure employed in the previous chapter. In particular, Ref. [16] defines the volume of the ensemble corresponding to a fixed expectation value for observables with equally spaced spectra. As will be discussed below, this leads to a simple analytical expression for the volume.

Within this framework, an analogue of the second law of thermodynamics can be analyzed through the behavior of the volume under a given dynamics. The expectation value at time $t$ defines a new set of microscopic states constrained to yield that expectation value. We can compare the volume associated with the initial preparation and the volume associated with the evolved macroscopic description. For generic dynamical evolutions, we expect the volume associated with the evolved expectation value to be larger than the volume associated with the initial preparation, which can be interpreted as a signature of irreversibility.

The way we define irreversibility is through the distance between expectation values. In analogy with the previous chapter, we compare forward and backward dynamics and compute the expectation value obtained after this process. The distance between the initial and the recovered expectation values then quantifies the degree of irreversibility. If the distance is nonzero, the initial and recovered values are distinguishable and the process is said irreversible for the given observable, initial states and dynamics.

In this chapter, we consider the observable defining the microscopic uncertainty set to be

$$A = \frac{\alpha J_z}{j}, \tag{3.2}$$

i.e., the angular momentum operator projected along the $z$ direction divided by the total angular momentum quantum number $j$. The normalization constant $\alpha$ is chosen as

$$\alpha = \sqrt{\frac{3j}{j+1}}. \tag{3.3}$$

This choice of $A$ is justified because the operator is traceless, can be properly normalized to satisfy the conditions required in Ref. [24], which allows for a simpler analytical treatment, and possesses an equally spaced spectrum. The last property allows us to apply the volume formula derived in Ref. [16].

To show the intuitive arguments presented above, we complement the analytical discussion with numerical simulations. The chapter is organized as follows. First, we present the formalism of dynamical typicality of expectation values to characterize the effective dynamics of interest. Next, we compute the volume associated with the set of states defined by a given expectation value following Ref. [16]. We then introduce the backward dynamics in order to define the recovered expectation value and the distance between the initial and recovered expectation values obtained from forward and backward dynamics. Subsequently, we discuss irreversibility in terms of volume growth, distance, and the connection between them. Finally, we present our conclusions.

## 3.1 Dynamical typicality

This section is dedicated to the effective dynamics of closed quantum systems described in terms of fixed expectation values of an observable associated with an ensemble of pure states. As in the previous chapter, instead of focusing on the complete microscopic evolution, we adopted a framework in which only macroscopic information is accessible. In the present case, however, this framework is based on the concept of typicality, which allows us to characterize effective dynamics through expectation values that are typical at each time $t$.

We begin by introducing the concept of dynamical typicality of expectation values, which provides the basis for defining an effective dynamics and for investigating the emergence of irreversibility. Building upon the notion of "static" typicality, Ref. [24] introduced the concept of dynamical typicality, referring to the typical behavior of expectation values under unitary time evolution.

To review this idea, consider the set of uniformly distributed normalized pure states (Haar states) $|\phi\rangle \in \mathcal{H}_D$, whose probability distribution is invariant under arbitrary unitary transformations. This invariance implies that all pure states are equally probable [24, 36]. We now restrict attention to the subset of states in the $D$-dimensional Hilbert space satisfying the constraint

$$\langle\phi|A|\phi\rangle = a. \tag{3.4}$$

This defines the set

$$\Omega_A(a) = \{|\phi\rangle \in \mathcal{H}_D \mid \langle\phi|A|\phi\rangle = a\}\,. \tag{3.5}$$

The fixed expectation value defines a subset of pure states $\Omega_A(a)$. Since no additional information about the microscopic state is available beyond the fixed expectation value, we assume a probability distribution that reflects only the symmetries of the constraint. In particular, we require the distribution to be invariant under all unitary transformations that preserve the condition $\langle\phi|A|\phi\rangle = a$. This requirement uniquely selects the uniform distribution restricted to the set $\Omega_A(a)$.

Ref. [24] showed that if pure states from such a set produce approximately the same expectation value of an observable $A$ at a instant $t = 0$, then, under unitary evolution, they will also produce approximately the same expectation value at later times $t$,

$$a_t \approx \left(\langle\phi(0)|U^\dagger\right) A \left(U|\phi(0)\rangle\right), \quad \forall\, |\phi(0)\rangle. \tag{3.6}$$

This property is known as dynamical typicality. Although there exists a set of atypical states that yield significantly different expectation values, this set is vanishing for large Hilbert spaces dimensions [36].

To demonstrate this, the autors of the Ref. [24] specified the observable $A$ solely through its moments, $c_i = \mathrm{tr}\{A^{(i)}/D\}$, with $D$ the Hilbert space dimension. The observable is required, for simplicity, to be traceless,

$$\frac{\mathrm{tr\{A\}}}{D} = c_1 = 0 \tag{3.7}$$

and normalized to

$$\frac{\mathrm{tr\{A^2\}}}{D} = c_2 = 1. \tag{3.8}$$

All higher moments $c_i$ for $i = 3, ..., 8$ are required to be to be of the order unity.

Instead of working directly with the ensemble of pure states constrained to yield a fixed expectation value of $A$, Ref. [24] introduced a substitute ensemble $\{|\omega\rangle\}$ whose expectation value of $A$ coincides with the prescribed one on average. This ensemble average provides a good approximation to the constrained ensemble average in the limit of large Hilbert space dimension and is significantly easier to handle analytically. Indeed, sampling uniformly from the set of pure states satisfying a fixed expectation value constraint corresponds to sampling from a restricted subset of the unit sphere in Hilbert space [38]. This geometric restriction makes the original ensemble $\{|\phi\rangle\}$ technically difficult to handle.

The set of states satisfying a constraint of the form Eq. (3.4) forms a lower-dimensional submanifold of the pure state space, as shown in Fig. 25. As a consequence, it has zero measure with respect to the Haar measure, and is therefore not sampled with nonzero probability under uniform Haar sampling. However, it is possible to define a conditional measure and perform the sampling consistently.

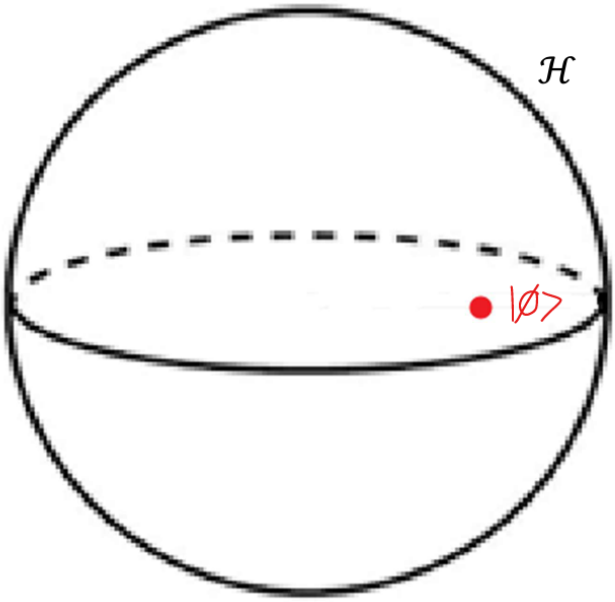


Figure 25 – Representation of the sphere of pure states and a submanifold corresponding to the set of pure states $|\phi\rangle$ compatible with a fixed expectation value. This constraint defines, in general, a lower-dimensional manifold in the space of pure states, which has zero measure with respect to the Haar measure. Consequently, such states cannot be obtained via direct uniform Haar sampling.

The "state" of this substitute ensemble is defined as

$$|\omega\rangle = \frac{1 + dA}{\sqrt{1 + d^2}}|\psi\rangle. \tag{3.9}$$

In Eq. (3.9), $|\psi\rangle$ is a Haar state, and $d$ (not to be confused with the smaller dimension introduced in the previous chapter) is a free parameter to be determined below. Although the notation suggests that $|\omega\rangle$ represents a physical quantum state, it should be emphasized that these vectors are normalized only on average with respect to the Haar measure.

$$\overline{\langle\omega|\omega\rangle} = 1 \tag{3.10}$$

and the variance of this normalization is [24]

$$\mathrm{Var}\left(\overline{\langle\omega|\omega\rangle}\right) = \frac{1}{D+1}\frac{4d^2 + 4d^3c_3 + d^4(c_4 - 1)}{(1 + d^2)^2}. \tag{3.11}$$

Thus, as $D$ grows the apparent abuse of notation corresponds to a convenient mathematical construction rather than to a set of strictly normalized quantum states. In the previous formulas the averages are done over the Haar states $|\psi\rangle$.

Regarding the substitute ensemble, the ensemble average of the expectation value of $A$ with respect to the ensemble $\{|\omega\rangle\}$ is given by [24]

$$\overline{\langle\omega|A|\omega\rangle} = \frac{2d + d^2c_3}{1 + d^2}. \tag{3.12}$$

We see that the mean expectation value is related to the parameter $d$. However, due to the specific structure of Eq. (3.12), the expectation values of $A$, when averaged over the ensemble $\{|\omega\rangle\}$, are constrained to remain small. For example, setting $c_3 = 0$, the mean expectation value initially increases with $d$, reaching a maximum at $d = 1$, and then decreases, returning to zero for large values of $d$, as shown in Fig. 26.

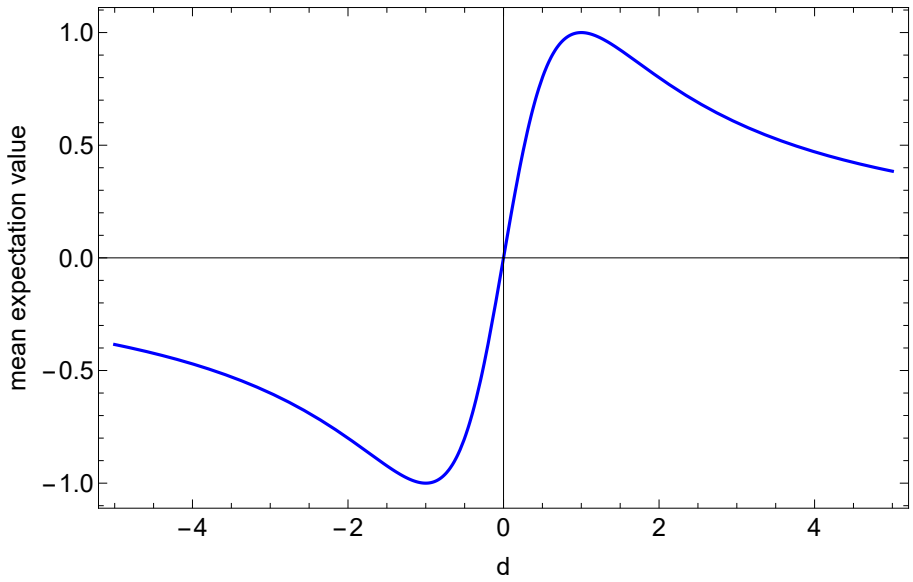


Figure 26 – Ensemble average expectation value of $A$ given by Eq. (3.12) as a function of the parameter $d$ for $c_3 = 0$. The mean value is bounded and remains smaller than one in modulus.

In Fig. 26, we observe that for each mean expectation value there are two corresponding values of $d$. We choose the smaller one, as this corresponds to the smallest distortion of the ensemble $\{|\omega\rangle\}$.

Moreover, Ref. [24] derived an upper bound on the variance of the expectation values at any time $t$,

$$\mathrm{Var}\left(\overline{\left(\langle\omega_0|U^\dagger\right) A \left(U|\omega_0\rangle\right)}\right) \leq \frac{1}{D+1}.\frac{1+4d\sqrt{c_4}+6d^2c_4+4d^3\sqrt{c_4}\sqrt[4]{c^4c^8}+d^4\sqrt{c_4c_8}}{(1+d^2)^2}, \quad (3.13)$$

which decreases as the Hilbert space dimension increases, ensuring typicality. The upper bound on the variance of the expectation values of $A$, given in Eq. (3.13), is valid for any time $t$. Therefore, according to [24], for sufficiently large systems, the curves describing the dynamics of the expectation values

$$\bar{a}_t = \left(\langle\omega(0)|U^\dagger\right) A \left(U|\omega(0)\rangle\right) \quad (3.14)$$

corresponding to the vast majority of states in the ensemble $\{|\omega\rangle\}$ are very close to each other and are concentrated around the ensemble mean at any time $t$.

Since, in the limit of large Hilbert space dimension, the expectation value of the substitute ensemble $\{|\omega\rangle\}$ provides an approximation to the constrained ensemble $\{|\phi\rangle\}$, it follows that the expectation values $\left(\langle\phi(0)|U^\dagger\right) A \left(U|\phi(0)\rangle\right)$ also exhibit a typical evolution. This property is referred to as dynamical typicality [24].

To explicitly illustrate dynamical typicality, we consider the observable

$$A = \frac{\alpha J_z}{j}. \tag{3.15}$$

The Hilbert space dimension is $D = 2j + 1$ and the eigenvalues of $A$ are $\alpha m/j$ with $m = -j, \ldots, j$. The constant $\alpha$ is a normalization factor.

The angular momentum operator has previously been related to a coarse-grained channel in Ref. [39] and later analyzed in Ref. [20], where the associated volume and assignment map were computed. In the present context, the choice of the operator in Eq. (3.15) is motivated by the fact that it is traceless, can be adjusted to satisfy the requirements of Ref. [24], and possesses an equally spaced spectrum, allowing the use of the volume formula derived in Ref. [16]. In addition, the Hilbert space dimension considered here may be choosen significantly larger than that treated in the previous chapter, hopefully bringing the system closer to the regime of most-of-times increasing entropy.

Recall that the conditions imposed for simplicity on the observable are that its moments satisfy $c_1 = 0$, $c_2 = 1$, and $c_i$ of order unity for $i = 3, 4, \ldots, 8$. With the normalization factor $\alpha$, the first two moments read

$$c_1 = \frac{\alpha}{D} \sum_{m=-j}^{j} \left(\frac{m}{j}\right) = 0, \tag{3.16}$$

$$c_2 = \frac{\alpha^2}{D} \sum_{m=-j}^{j} \left(\frac{m}{j}\right)^2 = \frac{\alpha^2(j+1)}{3j}. \tag{3.17}$$

Then, in order to make $c_2 = 1$ we must choose $\alpha$ such that

$$\alpha = \sqrt{\frac{3j}{j+1}}. \tag{3.18}$$

The higher moments of the observable in Eq. (3.15) can be also computed. It is straightforward to see the odd-numbered moments are zero. Consider $j = 1/2$, for example,

$$\begin{aligned} c_3 &= \frac{\alpha^3}{D} \sum_{m=-1/2}^{1/2} \left(\frac{m}{1/2}\right)^3 \\ &= \frac{\alpha^3}{D} \left[\left(\frac{-1/2}{1/2}\right)^3 + \left(\frac{1/2}{1/2}\right)^3\right] = 0. \end{aligned} \tag{3.19}$$

In the other hand, the even moments are

$$c_{2k} = \frac{\mathrm{tr}\{\alpha^{2k} J_z^{2k}/j^{2k}\}}{2j+1} = \frac{\alpha^{2k}}{(2j+1)j^{2k}} 2 \sum_{m=1}^{j} m^{2k}. \tag{3.20}$$

To find an expression that represents the even moments, consider $k = 1$, then

$$\sum_{m=1}^{j} m^2 = \frac{j(j+1)(2j+1)}{6}.$$

The order of this sum is $\sim j^3/3$. If $k = 2$, then

$$\sum_{m=1}^{j} m^4 = \frac{j(j+1)(2j+1)(3j^2+3j-1)}{30} \sim \frac{j^5}{5}$$

Extending to every $k$, it is suggested that

$$\sum_{m=1}^{j} m^{2k} \sim \frac{j^{2k+1}}{2k+1}.$$

in a way that even moments ($c_4, c_6$ and $c_8$) are of order

$$c_{2k} \sim \frac{3^k j^k}{j^k j^{2k+1}} \frac{j^{2k+1}}{2k+1} = \frac{3^k}{2k+1}$$

i.e of order 1. The higher moments have been highlighted here to be used in Eq. (3.13).

Now that the moments have been calculated, we can return to the case of the observable Eq. (3.15). Sampling an ensemble of pure states $\{|\phi\rangle\}$ subject to the constraint that all states share the same expectation value of the observable in Eq. (3.15),

$$\langle\phi|\alpha\frac{J_z}{j}|\phi\rangle = a, \tag{3.21}$$

is extremely difficult [38]. As stated previously, instead of explicitly constructing the constrained ensemble $\{|\phi\rangle\}$, we follow Ref. [24] and introduce a substitute ensemble $\{|\omega\rangle\}$ whose expectation value is equal to $a$.

With the aim of constructing the substitute ensemble, we first generate random Haar states $|\psi\rangle$ in a Hilbert space of dimension $D = 2j + 1$. The substitute ensemble $\{|\omega\rangle\}$ is then constructed from these Haar states in such a way that the expectation value is imposed only on average.

Given a target expectation value $a$, we define a parameter $d$ using Eq. (3.12). The left-hand side of that equation corresponds to the desired expectation value,

$$a = \frac{2d}{1+d^2}, \tag{3.22}$$

where we recall odd moments are null. Solving eq. (3.22) for $d$,

$$d = \frac{1 \pm \sqrt{1-a^2}}{a}, \tag{3.23}$$

and we we select the smaller root in order to ensure small values of $d$ (see Fig. 26),

$$d = \frac{1 - \sqrt{1 - a^2}}{a}. \tag{3.24}$$

With this choice, the states $|\omega\rangle$ are constructed according to Eq. (3.9). We then numerically compute the variance of the expectation values of the observable defined in Eq. (3.15) at time $t$ over the ensemble $\{|\omega\rangle\}$, and compare it with the analytical upper bound given in Eq. (3.13) of Ref. [24]. For a given initial expectation value $a_0$, the corresponding parameter $d_0$ is determined via Eq. (3.24). The resulting variance is then compared, for illustration purposes, with the theoretical bound, as shown in Fig. 27.

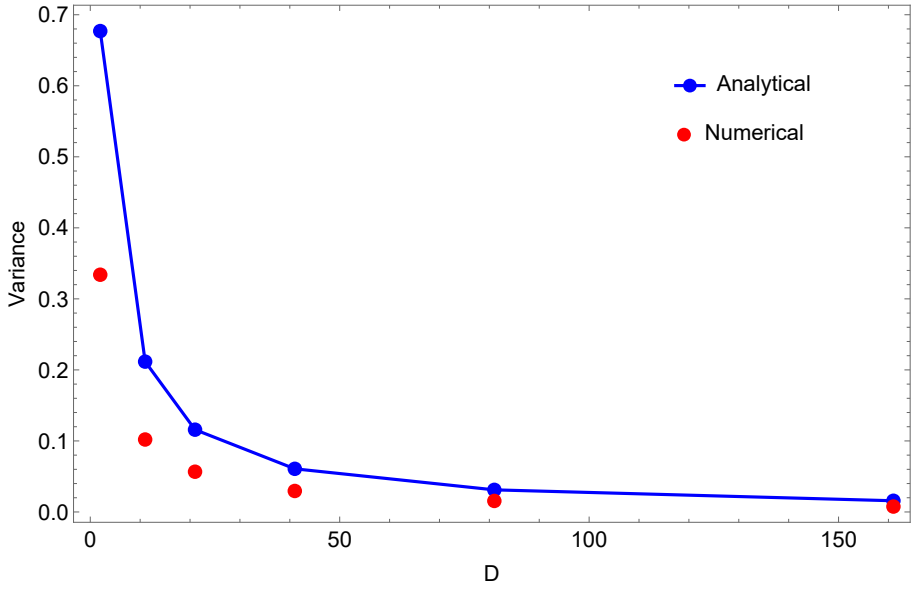


Figure 27 – Illustration of the variance of the operator $A = \alpha J_z/j$ for $j = \{1/2, 5, 10, 20, 40, 80\}$. Red points correspond to numerical data obtained by sampling one thousand substitute ensemble states according to a fixed expectation value $a = 0.441942$, with the corresponding parameter $d_0$ determined from Eq. (3.24). The blue curve represents the analytical upper bound variance (Eq. (3.13));

The variance of the expectation values of the observable $A$, defined in Eq. (3.12), at time $t$ satisfies the upper bound given by Eq. (3.13). Consequently, for sufficiently large Hilbert space dimension, the trajectories of the expectation values at time $t$ corresponding to the vast majority of states in the substitute ensemble remain very close to one another and hence close to the ensemble average at all times. In the large-dimensional limit, the time evolution of the expectation values of this observable therefore becomes typical. This behavior is illustrated in Fig. 28.

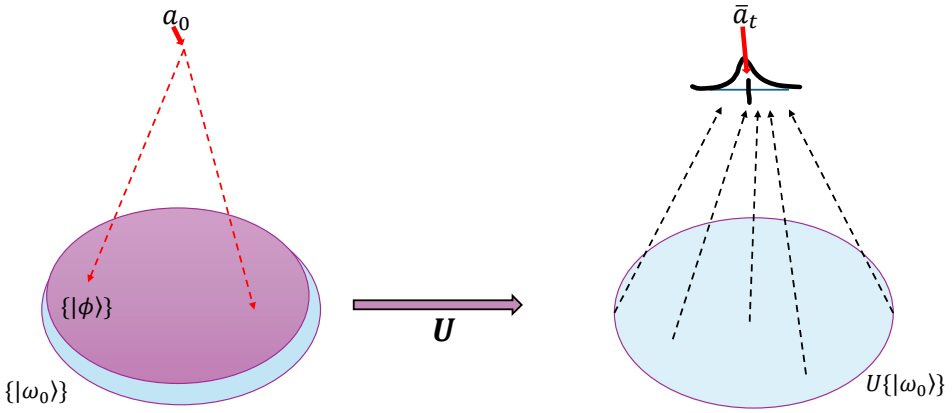


Figure 28 – Illustration of the forward dynamics for an ensemble prepared with initial expectation value $a_0$. This preparation defines an ensemble $\{|\phi\rangle\}$ and its substitute $\{|\omega\rangle\}$ whose states evolve unitarily in time. The ensemble averaged expectation value of the observable at time $t$ is denoted by $\bar{a}_t$, where the bar denotes average over the evolved set $\{U|\omega_0\rangle\}$. The black curve represents the distribution of the individual expectation average values.

Assuming dynamical typicality, the expectation values at later times concentrate around the ensemble average of the evolved states. Each expectation value at time $t$ may then be interpreted as defining an effective preparation, thereby specifying a new ensemble of compatible microscopic states. In the following sections, we investigate this idea in more detail by analyzing how the volume associated with these ensembles evolve in time and how this relates to the emergence of irreversibility.

## 3.2 Volume

The preparation of a system with a well-defined expectation value specifies the set of microscopic states compatible with it. Similarly to the previous chapter, we associate the number of compatible microstates with the uncertainty inherent in the preparation, since during the act of preparation no information about the specific microscopic state is available. Thus, the larger the number of states compatible with a given preparation, the

greater the uncertainty associated with it [17].

This section aims to define the uncertainty associated with the ensemble of pure states uniformly distributed and constrained to yield the same expectation value, $\langle\phi|A|\phi\rangle = a$, with $A = \alpha J_z/j$. This uncertainty is quantified by the number of microscopic states in the ensemble and is measured by the volume of the corresponding set. To this end, we rely on the results of Brody, Hook, and Hughston [16], who derived a closed-form expression for the general case and, in particular, for observables with equally spaced spectra.

So far, following Ref. [24], we have introduced the ensemble of pure states $|\phi\rangle$, that yield the exact expectation value, as well as a substitute ensemble of "states" $|\omega\rangle$. The expectation value of the operator $A$ with respect to states of the substitute ensemble is, on average, equal to that obtained from the ensemble of pure states $|\phi\rangle$. Moreover, as the dimension of the Hilbert space increases, the variance related to expectation values decreases. Although sampling from the constrained ensemble $\{|\phi\rangle\}$ is technically demanding, since it corresponds to a submanifold of the unit sphere of pure states [38], we have so far employed the substitute ensemble $\{|\omega\rangle\}$, which does not explicitly impose this constraint.

However, in order to calculate the volume associated with the microscopic states compatible with the preparation of an observable with a given expectation value, only the spectrum of the observable is required [16]. Therefore, in this section we focus on the volume of the original constrained ensemble. In particular, we consider

$$\Omega_A(\bar{a}_t) = \{|\chi\rangle \in \mathcal{H}_D \mid \langle\chi|A|\chi\rangle = \bar{a}_t\}\,, \tag{3.25}$$

which denotes the set of pure states defined by the expectation value at time $t$.

The number of microscopic pure states compatible with this macroscopic constraint is quantified with respect to the uniform (Haar) measure over all pure states, assuming all compatible states to be equally probable. This integral:

$$\mathcal{V}(a) = \int d\mu_\phi\ \delta(\langle\phi|A|\phi\rangle - a)\,, \tag{3.26}$$

defines the volume of uncertainty associated with microscopic configurations whose expectation values equal a given value. Analogously to the previous chapter, the integration is performed over the set of pure states with respect to the Haar measure.

In the case of a non-degenerate spectrum, Ref. [16] showed that the volume of uncertainty associated with microscopic configurations yielding a given expectation value can be expressed in terms of the eigenvalues of $A$ as

$$\mathcal{V}(a) = (-1)^n\,\pi^n \sum_{k=0}^{n} \delta^{(-n)}\,(a_k - a) \prod_{\substack{l=0 \\ l\neq k}}^{n} \frac{1}{a_l - a_k}, \tag{3.27}$$

where $D = n + 1$ is the dimension of the Hilbert space, $a_k$ denotes the $k$-th eigenvalue of $A$, and $a$ is the expectation value. The function

$$\delta^{(-n)}(x) = \begin{cases} 0, & x < 0, \\ \frac{1}{(n-1)!}\, x^{n-1}, & x \geq 0, \end{cases} \tag{3.28}$$

is the $n$-th antiderivative of the Dirac delta distribution, satisfying

$$\frac{d^n}{dx^n}\delta^{(-n)}(x) = \delta(x).$$

We remind the operator $A = \alpha\frac{J_z}{j}$, whose spectrum is

$$a_m = m\,\frac{\alpha}{j}, \qquad m = -j, \ldots, j, \tag{3.29}$$

where $\alpha$ is defined in Eq. (3.18). The corresponding volume of uncertainty is computed using Eq. (3.27). Substituting Eq. (3.29) into Eq. (3.27), we obtain

$$\mathcal{V}(a) = (-1)^{2j}\,\pi^{2j} \sum_{m=-j}^{j} \delta^{(-2j)}\left(\frac{\alpha}{j}m - a\right) \prod_{\substack{l=-j \\ l\neq m}}^{j} \frac{1}{\frac{\alpha}{j}(l-m)}. \tag{3.30}$$

This expression can be further simplified (see Appendix A) by introducing the substitutions

$$a' = a + \alpha, \qquad \omega = \frac{\alpha}{j}, \qquad n = 2j,$$

leading to

$$\mathcal{V}(a') = \frac{(-1)^n \pi^n}{(n-1)!\,\omega} \sum_{k=\lceil a'/\omega \rceil}^{n} \frac{(-1)^k}{k!(n-k)!} \left(k - \frac{a'}{\omega}\right)^{n-1}, \tag{3.31}$$

where $k = \lceil x \rceil$ define $k$ as the smallest integer that is greater than or equal to $x$.

The normalized volume of uncertainty, obtained by dividing Eq. (3.31) by the total volume of pure states, is therefore

$$\mu(a') = \frac{(-1)^n n}{\omega} \sum_{k=\lceil a'/\omega \rceil}^{n} \frac{(-1)^k}{k!(n-k)!} \left(k - \frac{a'}{\omega}\right)^{n-1}. \tag{3.32}$$

Ref. [16] showed that, as the dimension of the Hilbert space increases, the distribution of expectation values becomes increasingly concentrated around the mean value between the largest and smallest eigenvalues. In Fig. 29, we fit Gaussian distributions to investigate whether Eq. (3.30) approaches a Gaussian profile in the large-$j$ limit.

Then, consider the Gaussian distribution

$$f(a) = \frac{1}{\sigma\sqrt{2\pi}} e^{-\frac{1}{2}\left(\frac{a-\mu}{\sigma}\right)} \tag{3.33}$$

where $a$ is the expectation value, $\mu$ is the mean (do not confuse with the normalized volume Eq. (3.32)) and $\sigma$ is the standard deviation.

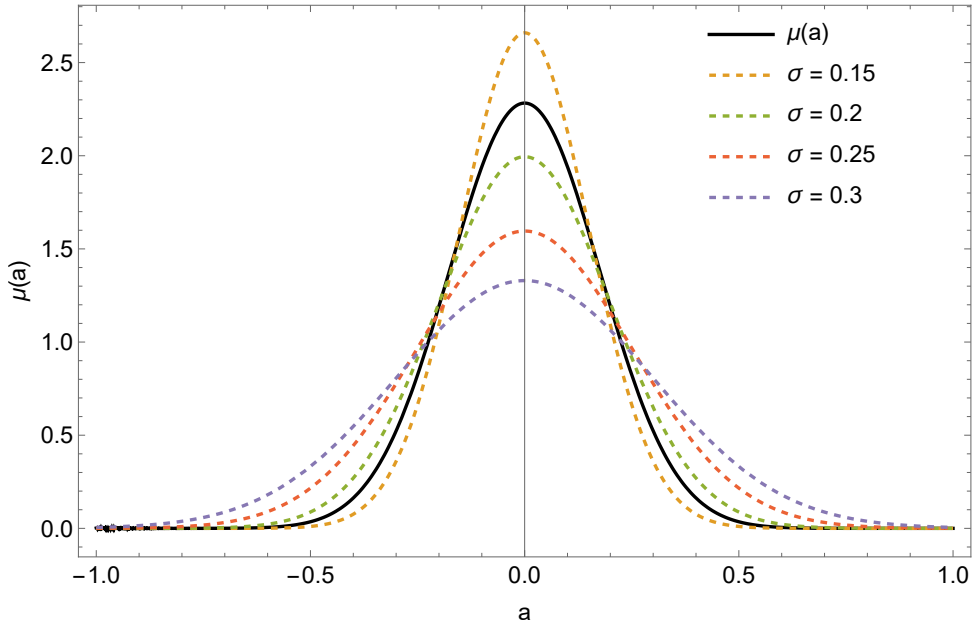


Figure 29 – This represents how the Gaussian distribution fits the curve that represents the volume for a given range of expected values. In this case, in dashed curves we used different values of standard deviation and the mean was taken as zero ($\mu = 0$). The black line is given by Eq. (3.32) with $j = 15$.

This fit with the Gaussian distribution motivated us to find the appropriate mean and standard deviation parameters. In Appendix B, we show how to compute this analytically. The Eq. (3.30) can be compared with a Gaussian distribution whose standard deviation and mean are given by

$$\sigma = \sqrt{\frac{\alpha^2}{6j}} \quad \text{and} \quad \mu = 0. \tag{3.34}$$

As shown in Fig. 30, the larger the dimension of the system, the closer the distribution for a given expectation value approaches a normal distribution.

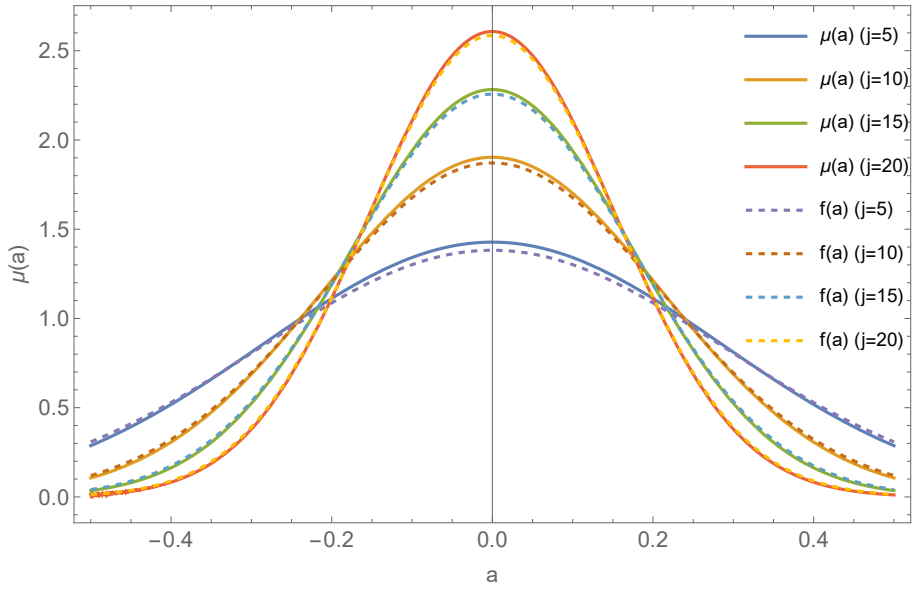


Figure 30 – For $j = \{5, 10, 15, 20\}$ we show a comparision of the theoretical expression for the normalized volume (Eq. (3.32), full lines) with the Gaussian approximations ($\sigma$ given by Eq. (3.34), $\mu = 0$; dashed lines)

This result is particularly useful, as it allows for a simplified evaluation of the volume associated with the uncertainty around a given expectation value. Such a volume plays a central role in characterizing irreversibility, as previously discussed in the chapter 2. In the present context, we will investigate how this volume increases when a large system undergoes a dynamical evolution of the set that yields the same expectation values.

## 3.3 Distance

This section is devoted to the characterization of irreversibility through the distance between expectation values of an observable. The central idea is to compare a given expectation value of an observable with the recovered expectation value obtained after a composition of forward and backward effective dynamics.

Let $a_0$ be a fixed expectation value of the preparation of $A$ at time $t = 0$ and its average related to $\bar{a}_0 = \langle\omega_0|A|\omega_0\rangle$, evaluated with respect to a state $|\omega_0\rangle$ drawn from the substitute ensemble $\{|\omega_0\rangle\}$. As discussed in the previous section, the ensemble can be evolved forward in time under the effective dynamics by applying a unitary operator $U_t$. The ensemble averaged expectation value of the observable at time $t$ is then given by

$$\overline{a}_t = \mathrm{tr}\{U_t\overline{|\omega_0\rangle\langle\omega_0|}U_t^\dagger\ A\}. \tag{3.35}$$

The average density operator associated with the substitute ensemble can be calculated

from its definition, Eq. (3.9). The result is [24]

$$\overline{|\omega_0\rangle\langle\omega_0|} = \frac{\mathbf{1} + 2d_0A + d_0^2A^2}{D(1+d_0^2)}, \tag{3.36}$$

where $d_0$ is a function of $a_0$ (see Eq. (3.31)). Substituting Eq. (3.36) into Eq. (3.35), the ensemble average expectation value at time $t$ can be expressed in terms of $d_0$ as

$$\overline{a}_t = \mathrm{tr}\left[U\left(\frac{\mathbf{1} + 2d_0A + d_0^2A^2}{D(1+d_0^2)}\right)U^\dagger\, A\right]. \tag{3.37}$$

Using the properties of the trace, this expression becomes

$$\overline{a_t} = \frac{1}{D(1+d_0^2)}\left[\mathrm{tr}\,(A) + 2d_0\mathrm{tr}\left(UAU^\dagger A\right) + d_0^2\mathrm{tr}\left(UA^2U^\dagger A\right)\right]. \tag{3.38}$$

Since the observable $A$ is traceless, as imposed by Eq. (3.7), the first term vanishes. Therefore, the ensemble-averaged expectation value at time $t$ can be written as

$$\overline{a}_t = \frac{d_0}{D(1+d_0^2)}\left[2\mathrm{tr}\left(UAU^\dagger A\right) + d_0\mathrm{tr}\left(UA^2U^\dagger A\right)\right]. \tag{3.39}$$

We now analyze the behavior of $\overline{a}_t$ under the forward effective dynamics. We consider a unitary evolution operator of the form $U(t) = e^{-iHt}$, where the Hamiltonian $H$ is drawn from the Gaussian Unitary Ensemble (GUE). The numerical results illustrated in Fig. 31 imply that the mean expectation value of the observable $A$ decays in time, in agreement with the predictions of Ref. [24].

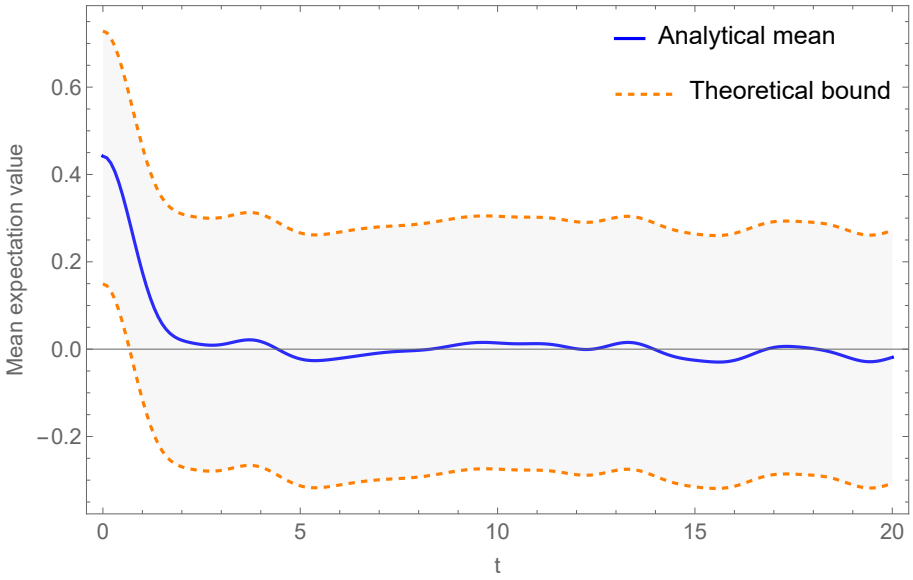


Figure 31 – Time evolution of the ensemble-averaged expectation value $\overline{a}_t$ (blue), obtained from Eq. (3.39) with unitary dynamics generated by a random but fixed GUE Hamiltonian of dimension $D$. The shaded region (orange) represents the theoretical upper and lower bounds given by Eq. (3.13), corresponding to $\overline{a}_t \pm \sqrt{\mathrm{Var}(\overline{a}_t)}$. The data were obtained for $j = 15$ and the time dependence is carried by the unitary $U_t = e^{-iHt}$.

In the same way that a preparation with expectation value $a_0$ defines the ensemble $\{|\phi\rangle\}$ together with its substitute ensemble $\{|\omega_0\rangle\}$, we may interpret the expectation value $\overline{a}_t$ as a new preparation defining another ensemble, denoted by $\{|\chi\rangle\}$, together with its corresponding substitute ensemble $\{|\omega_t\rangle\}$,

$$|\omega_t\rangle = \frac{1 + d_t A}{\sqrt{1 + d_t^2}}|\psi\rangle, \tag{3.40}$$

with $|\psi\rangle$ a Haar state and $d_t$ a function of $\overline{a}_t$.

All aforementioned ensembles are summarized in the Table 1:

| | |
|---|---|
| $\{\|\phi\rangle\}$ | $a_0 = \langle\phi\|A\|\phi\rangle$ |
| $\{\|\omega_0\rangle\}$ | $\overline{\langle\omega_0\|A\|\omega_0\rangle} = a_0$ |
| $\{\|\omega_t\rangle\}$ | $\overline{\langle\omega_t\|A\|\omega_t\rangle} = \bar{a}_t$ |
| $\{\|\chi\rangle\}$ | $\bar{a}_t = \langle\chi\|A\|\chi\rangle$ |

Table 1 – Summary of the ensembles discussed in the text. The value $a_0$ defines the constrained ensemble $\{|\phi\rangle\}$, while $\bar{a}_t$ defines $\{|\chi\rangle\}$. The substitute ensembles are constructed such that their average expectation values satisfy $\overline{\langle\omega_0|A|\omega_0\rangle} = \bar{a}_0$ and $\overline{\langle\omega_t|A|\omega_t\rangle} = \bar{a}_t$.

Although two ensembles may be constructed to reproduce the same expectation value of the observable $A$, they are not, in general, identical. In particular, the set of states obtained by evolving the ensemble $\{|\omega_0\rangle\}$ forward in time does not necessarily coincide with the set of states whose expectation value is exactly $a_t$. While the evolved ensemble $\{U_t|\omega_0\rangle\}$ yields a distribution of expectation values whose average is $\bar{a}_t$, there exist states with expectation value exactly $\bar{a}_t$ that are not contained in $\{U_t|\omega_0\rangle\}$, as illustrated in Fig. 32. We represent the set whose expectation value is exactly $\bar{a}_t$ greater than $\{U_t|\omega_0\rangle\}$ but with an intersection between them.

The ensemble $\{|\omega_t\rangle\}$ can be evolved backward in time by applying the inverse unitary operator $U_t^\dagger$, as shown in Fig. 32. Since the upper bound on the variance of the expectation values of $A$, given in Eq. (3.13), holds for arbitrary times, the dynamics remains typical both in the forward and backward directions.

Under this backward evolution, we define the recovered expectation value at time $t = 0$, denoted by $\overline{a}_0^R$. Following steps analogous to those leading to Eq. (3.39), we find that the recovered expectation value, averaged over the ensemble, is given by

$$\overline{a}_0^R = \frac{d_t}{D(1 + d_t^2)}\left[2\mathrm{tr}\left(U_t^\dagger A U_t A\right) + d_t \mathrm{tr}\left(U_t^\dagger A^2 U_t A\right)\right]. \tag{3.41}$$

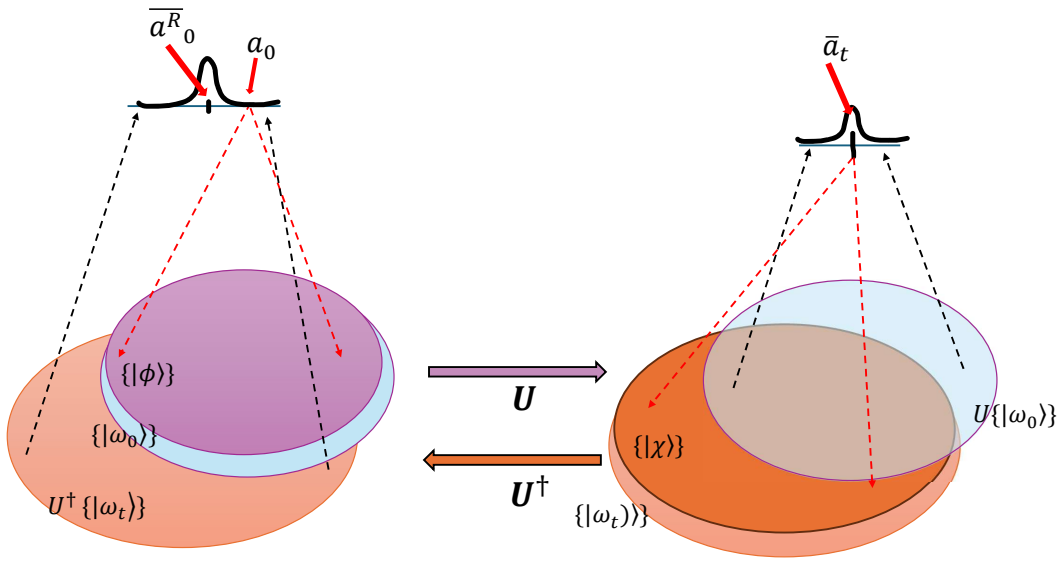


Figure 32 – Schematic representation of the forward and backward dynamics of expectation values. A preparation with expectation value $a_0$ defines the ensemble $\{|\phi\rangle\}$ and the substitute ensemble $\{|\omega_0\rangle\}$, whose forward evolution (purple) under $U_t$ produces a distribution of expectation values with average $\bar{a}_t$. The preparation defined by $\bar{a}_t$ corresponds to a different ensemble $\{|\chi\rangle\}$, substituted by $\{|\omega_t\rangle\}$, whose volume is generally larger than that of the dynamically evolved ensemble $\{U_t|\omega_0\rangle\}$, although the two sets intersect. Evolving $\{|\omega_t\rangle\}$ backward in time (orange) using $U_t^\dagger$ yields a recovered expectation value $\bar{a}_0^R$, which does not necessarily coincide with the initial value $a_0$.

To quantify the difference between the initial and recovered expectation values, $a_0$ and $\bar{a}_0^R$, respectively, we introduce distance

$$\mathcal{D}(\bar{a}_0^R, a_0) = |\bar{a}_0^R - a_0|. \tag{3.42}$$

Our goal is to relate the distance defined in Eq. (3.42) to irreversibility, in close analogy with the approach adopted in the previous chapter. If $\mathcal{D}\left(\bar{a}_0^R, a_0\right) = 0$, the expectation values are indistinguishable. In this case, the effective dynamics is said reversible with respect to $A, a$ and $H$, the hamiltonian. Conversely, if $\mathcal{D}\left(\bar{a}_0^R, a_0\right) \neq 0$, the backward dynamics cannot recover the original ensemble. The expectation values then become distinguishable, signaling the emergence of irreversibility in the effective dynamics. This irreversibility scenario will be explored in detail in the next section.

## 3.4 Irreversibility

The second law of thermodynamics states that the entropy of an isolated system does not decrease in the thermodynamic limit [13, 25, 26, 30–33]. In the present framework, entropy is associated with the volume of the ensemble of pure states that share the same expectation value of a given observable.

A signature of irreversibility, in this case, is the increase of the volume of the set related to the expectation value after a generic dynamic,

$$\frac{\mathcal{V}(\{|\chi\rangle\})}{\mathcal{V}(\{|\phi\rangle\})} > 1, \tag{3.43}$$

where the volume is computed according to Eq. (3.31), with $a' = a + \alpha$. Here, $\mathcal{V}(\{|\phi\rangle\})$ denotes the volume of the ensemble of states $|\phi\rangle$ whose exact expectation value is $a_0$, while $\mathcal{V}(\{|\chi\rangle\})$ corresponds to the volume of the ensemble of states $|\chi\rangle$ with exact expectation value $\overline{a}_t$.

In the previous section, we showed that the volume defined in Eq. (3.31) can be approximated by a Gaussian distribution with variance and mean given in Eq. (3.34). Using this Gaussian approximation, the ratio between the volumes in Eq. (3.43) becomes

$$\frac{\mathcal{V}(\overline{a}_t)}{\mathcal{V}(a_0)} \approx \frac{\frac{\exp\left\{-\overline{a}_t^2/2\sigma^2\right\}}{\sigma\sqrt{2\pi}}}{\frac{\exp\left\{-a_0^2/2\sigma^2\right\}}{\sigma\sqrt{2\pi}}},$$

where $\sigma = \sqrt{\frac{\alpha^2}{6j}}$. This expression simplifies to

$$\frac{\mathcal{V}(\overline{a}_t)}{\mathcal{V}(a_0)} \approx \exp\left\{1/2\sigma^2\ (a_0^2 - \overline{a}_t^2)\right\}. \tag{3.44}$$

For the ratio in Eq. (3.44) to be greater than unity, it is necessary that $|a_0| > |\overline{a}_t|$, implying that the absolute value should decrease in time.

Previously, we showed that the mean expectation value decays toward zero as time increases, such that $|a_0| > |\bar{a}_t|$ for $t > 0$. In Fig. 33, we compare the analytical prediction obtained from Eq. (3.39) with numerical results of $a_t$ over time for the operator $A = \alpha J_z/j$. The analytical curve used here can be regarded as analytical, since it employs the same values of $a_0$ and $d_0$ extracted from the numerical calculations, as well as the same set of random unitaries generated from a GUE Hamiltonian. By contrast, the numerical results are obtained by explicitly sampling states from the ensemble and computing the mean expectation value as the average over all sampled expectation values.

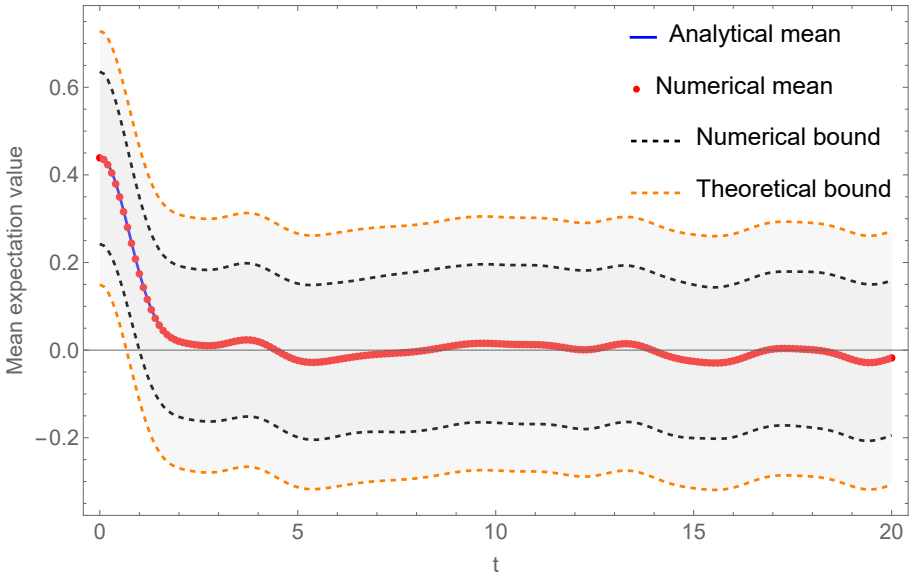


Figure 33 – Mean expectation values at each time t. On blue analytical mean expectation value obtained by Eq. (3.39) where the $U = e^{-iHt}$, with $H$ a random Hamiltonian of dimension $D$. On red numerical calculations for mean expectation value with $j = 15$ and $a_0 = 0.441942$ and considering 10000 states of the ensemble. The theoretical upper and lower bounds given by Eq. (3.13), corresponding to $\overline{a}_t \pm \sqrt{\mathrm{Var}(a_t)}$. The numerical bound correspond to the variance of numerical data..

Since $|\overline{a}_t|$ is smaller than the initial fixed expectation value $|a_0|$ and thus $|\bar{a}_t| < |a_0|$ for any $t > 0$, the ratio of volumes given in Eq. (3.44) remains greater than unity throughout the entire time interval, as shown in Fig. 34.

To generate the numerical results shown in Fig. 34 and subsequent figures, we fix $j = 15$ and an initial expectation value $a_0 = 0.441942$. We then determine the corresponding parameter $d_0$ (see Eq. (3.12)) and construct the initial ensemble of states $|\omega_0\rangle$. Each state is evolved unitarily under a realization of a fixed random Hamiltonian of dimension $D = 2j + 1$, for times $t \in [0, 20]$ with step size 0.2. At each time step, we compute the expectation value of $A$ and its ensemble average. The resulting mean expectation value at time $t$ is interpreted as defining an effective new preparation, which determines a new parameter $d_t$ and a new ensemble of states $|\omega_t\rangle$. Finally, we compare the volume associated with the initial value $a_0$ to that corresponding to $\bar{a}_t$.

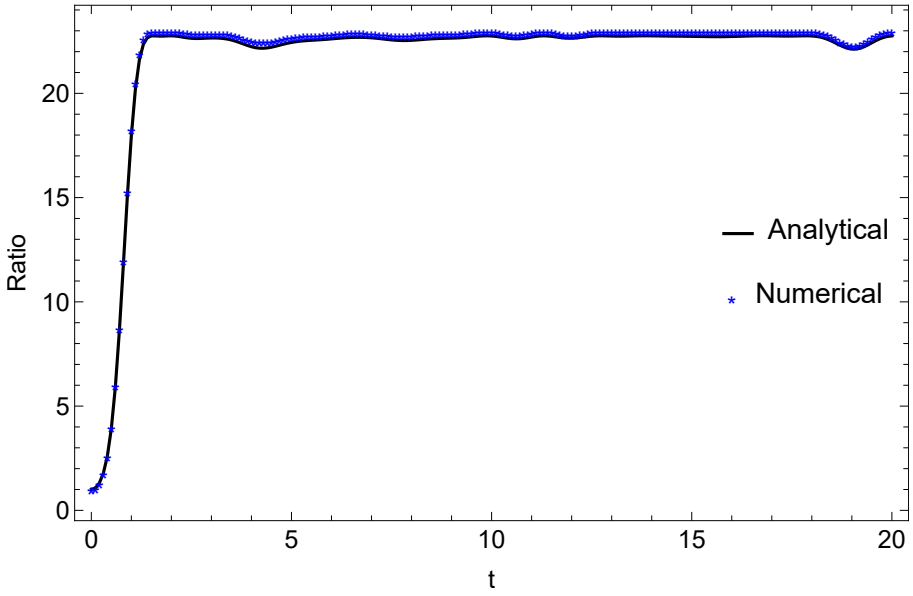


Figure 34 – Ratio $\mathcal{V}(\bar{a}_t)/\mathcal{V}(a_0)$ at each time t is obtained by Eq. (3.44) for $j = 15$ and all the settings already mentioned in Fig. 33.

Recalling the concept of volume of uncertainty introduced in the previous chapter, the volume $\mathcal{V}(\bar{a}_t)$ quantifies the number of microscopic pure states compatible with the macroscopic expectation value $\bar{a}_t$. The larger this volume, the greater the number of microscopic configurations associated with the same macroscopic value, and consequently, the larger the microscopic uncertainty underlying the measured observable.

In Fig. 35, we show the time dependence of the distance between the initial fixed expectation value $a_0$ and the recovered value $\bar{a}_0^R$ obtained after a forward and backward evolution generated by the unitary operator $U = e^{-iHt}$ and $U^\dagger = e^{iHt}$ where $H$ is a random Hamiltonian drawn from the GUE and $t \in [0, 20]$. At each time step, the mean expectation value $\bar{a}_t$ is interpreted as defining an effective preparation of the system, which determines a new parameter $d_t$ and an associated ensemble $|\omega_t\rangle$. Each state $|\omega_t\rangle$ is then evolved backward in time using the same Hamiltonian used for the forward evolution. For the backward evolved states, we compute the expectation value of $A$ and its mean value, denoted $\bar{a}_0^R$. Finally, we evaluate the distance between the initial fixed expectation value $a_0$ and the recovered one $\bar{a}_0^R$.

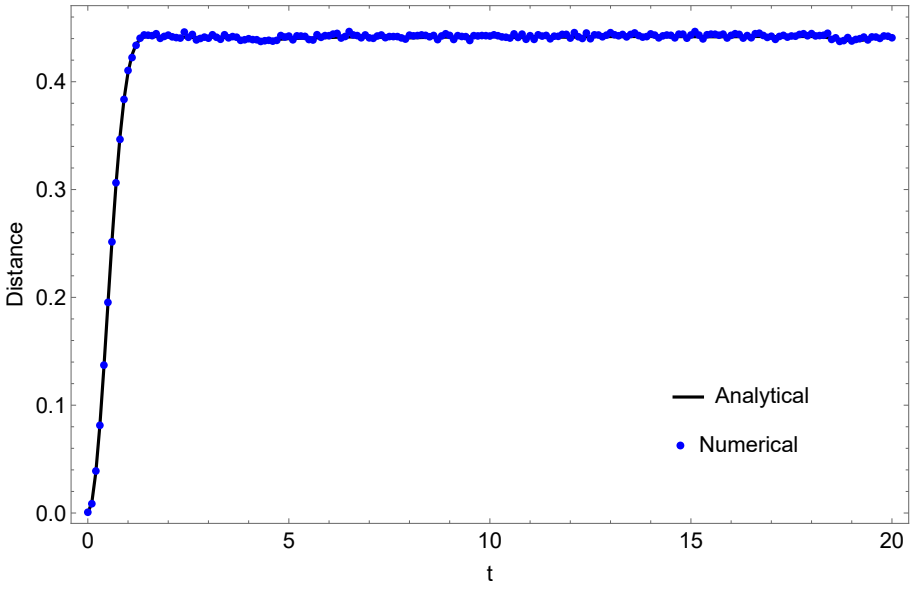


Figure 35 – Distance between $a_0$ and $\bar{a}_0^R$ as a function of time $t$. The blue curve corresponds to numerical results obtained with the same parameters used in Fig. 34. Starting from an initial expectation value $a_0$, the corresponding $d_0$ was used to generate an ensemble of 10000 states $|\omega_0\rangle$. These states were evolved forward in time under the unitary operator $U_t$, yielding the mean expectation value $\bar{a}_t$. The resulting states $|\omega_t\rangle$ were then evolved backward, and the recovered expectation value $\bar{a}_0^R$ was obtained. The distance between $a_0$ and $\bar{a}_0^R$ was subsequently computed. The black curve represents the analytical prediction, obtained from Eq. (3.41), using the same initial value $a_0 = 0.441942$ as in the numerical simulations.

As stated previously, our definition of irreversibility is based on the distance between the initial expectation value $a_0$ and the expectation value obtained after the composition of forward and backward typical dynamics, denoted by $\bar{a}_0^R$. An important advantage of this approach is that it does not require access to microscopic level in order to detect the emergence of irreversibility in the process.

If $\mathcal{D}(\bar{a}_0^R, a_0) = 0$, the effective dynamics is said to be reversible with respect to the observable $A$. In contrast, if $\mathcal{D}(\bar{a}_0^R, a_0) \neq 0$, the backward dynamics fails to recover the original preparation. In this case, the ensemble $\{|\chi\rangle\}$ defined by the recovered expectation value is no longer equivalent to the image of the initial ensemble $\{|\phi\rangle\}$ under forward evolution, and the effective dynamics is therefore irreversible.

These results motivate us to check where there is a correlation between the volume ratio defined in Eq. (3.44) and the distance introduced in Eq. (3.42). Such a correlation provides a clear signature of irreversibility: as the volume of the ensemble associated with a given expectation value increases, the Euclidean distance between the initial and recovered expectation values also increases.

With the observable $A = \alpha J_z/j$, the initial expectation value $a_0 = 0.441942$, $j = 15$, and considering a random Hamiltonian, the parametric plot obtained by combining Eqs. (3.44) and (3.42) is shown in Fig. 36.

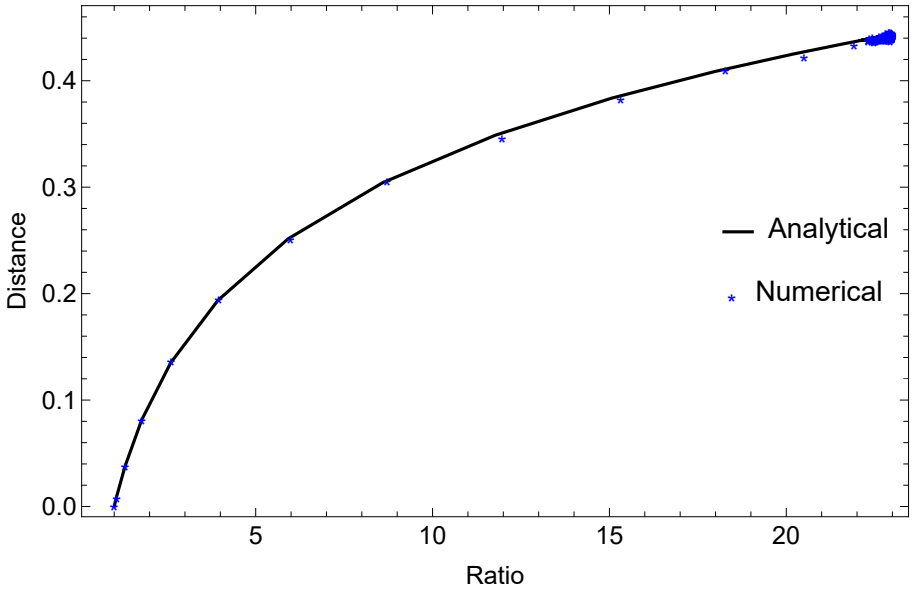


Figure 36 – Correlation between the Euclidean distance $\mathcal{D}(\overline{a}_0^R, a_0)$, obtained from Eq. (3.41), and the volume ratio $\mathcal{V}(\overline{a}_t)/\mathcal{V}(a_0)$, obtained from Eq. (3.44), for $j = 15$ and an ensemble of 10000 states $|\omega\rangle$.

The correlation displayed in Fig. 36 highlights the irreversible character of the effective dynamics of expectation values. As the evolution time increases, both the expectation value $\overline{a}_t$ and the recovered value $\overline{a}_0^R$ decay toward zero, leading to a strictly positive distance $\mathcal{D}(\overline{a}_0^R, a_0)$. At the same time, the ratio of ensemble volumes remains greater than unity.

Taken together, these results reveal a clear correlation between the increase in ensemble volume and the distance between the initial and recovered expectation values. Larger Hilbert-space volumes (corresponding to a greater number of microscopic states compatible with the evolved expectation value) are associated with greater distinguishability between the initial and reconstructed preparations. This behavior suggests the existence of an analogue of a second law for the effective dynamics: the quantum Boltzmann entropy, defined through the Hilbert-space volume of compatible microstates, tends to increase under expectation-value dynamics. In this sense, irreversibility is not merely a qualitative feature, but is quantitatively captured by entropy growth and its operational manifestation through a nonvanishing distance between initial and recovered expectation values.

## 3.5 Conclusion

In this chapter, we investigated irreversibility in the dynamics of expectation values within the framework of dynamical typicality. Focusing on observables with equally spaced spectra, we analyzed how ensembles of pure states constrained by a fixed expectation value evolve under unitary dynamics.

The central mechanism behind irreversibility arises from the mismatch between two ensembles: the forward-evolved ensemble associated with the initial preparation and the ensemble defined by the evolved expectation value. Although both correspond to the same macroscopic quantity ($\bar{a}_t$), they are not microscopically identical. As a consequence, the number of microscopic states compatible with the evolved expectation value is typically larger than the number compatible with the initial one.

This enlargement of the compatible set leads to an increase in the associated Hilbert-space volume. The growth of this volume implies that, after composing forward and backward effective dynamics, the recovered expectation value generally differs from the initial preparation. Irreversibility therefore manifests itself operationally through a nonvanishing distance between the initial and recovered expectation values.

Finally, we showed that volume growth and distinguishability are correlated: larger increases in volume correspond to larger distances between initial and recovered effective descriptions. This establishes a direct connection between entropy growth in Hilbert space and macroscopic irreversibility for expectation-value dynamics.

An important direction for future work is the extension of this analysis to more general classes of observables beyond those with equally spaced spectra.

# 4 Conclusion

The second law of thermodynamics stands as one of the most robust and universally applicable principles in physics. Its persistence, despite the time-reversal invariance of the fundamental microscopic laws, continues to raise fundamental questions about the origin of macroscopic irreversibility. This thesis addressed this tension by investigating whether irreversibility can emerge in closed quantum systems when the dynamics are described at an effective, macroscopic level.

The central result of this work is that irreversibility can arise naturally from the structure of effective dynamics, even when the underlying microscopic evolution is strictly unitary and reversible. The key mechanism responsible for this emergence is the mismatch between the forward-evolved microscopic ensemble and the ensemble defined by the evolved effective description. This structural mismatch leads to a growth in the number of microscopic states compatible with the macroscopic description after the evolution, thereby increasing uncertainty and generating effective irreversibility.

To formalize this idea, we used an analog of the Boltzmann notion of entropy for quantum systems by defining entropy through the volume of compatible microscopic states in Hilbert space. Within this framework, entropy growth corresponds to an increase in the volume of the ensemble associated with an effective description. Importantly, this growth does not require any fundamental violation of microscopic reversibility; it emerges from the loss of accessible information inherent in the transition between microscopic and macroscopic levels.

Two complementary realizations of effective dynamics were analyzed. In the first, irreversibility emerged from dynamics induced by coarse-graining channels, unitary evolution, and assignment maps. In the second, the same phenomenon was investigated through the framework of dynamical typicality, where macroscopic descriptions are expressed in terms of expectation values. Both approaches revealed the same structural origin of irreversibility: the enlargement of the set of compatible microscopic states under effective evolution.

A central contribution of this thesis is the definition of irreversibility through distinguishability. We demonstrated that the growth of ensemble volume i.e, the quantum Boltzmann entropy, is directly correlated with the increase in distance between the initial and recovered effective descriptions. This establishes a concrete link between volume increase in Hilbert space and distinguishability. If this distance vanishes, the process is reversible at the macroscopic level. This definition is experimentally meaningful, as it relies solely on quantities accessible at the macroscopic level.

It is crucial to emphasize that the irreversibility discussed here is emergent rather than fundamental. The microscopic dynamics remain unitary and reversible at all times. Irreversibility arises because effective descriptions do not retain complete information about the microscopic state space. From the macroscopic standpoint — the level at which physical observations are made — this loss of accessible information manifests itself as entropy growth and as the impossibility of perfectly recovering the initial preparation.

The results obtained here suggest that the second law of thermodynamics can be understood as a structural consequence of effective description in quantum systems. Rather than requiring environmental coupling or explicit dissipation, irreversibility can emerge from the internal architecture of effective dynamics.

Future investigations may extend this framework to more general classes of observables, different coarse-graining procedures, and larger many-body systems closer to the thermodynamic limit. Such extensions may further clarify the universality and limitations of the mechanisms identified here.

# Bibliography


[1] E. Melhoramentos, *Michaelis: dicionário escolar de lingua portuguesa*. Editora Nobel, 2009.

[2] o. ROCHA, JFM., *Origens e evolução das idéias da física [online]*. EDUFBA, 2002.

[3] C. Cercignani and R. Penrose, *Ludwig Boltzmann: The Man Who Trusted Atoms*. OUP Oxford, 2006.

[4] W. Greiner, D. Rischke, L. Neise, and H. Stöcker, *Thermodynamics and Statistical Mechanics*. Classical Theoretical Physics, Springer New York, 2000.

[5] J. Bricmont, "Probabilistic explanations and the derivation of macroscopic laws," *arXiv:1906.01836v2*, 2019.

[6] J. L. Lebowitz, "From time-symmetric microscopic dynamics to time-asymmetric macroscopic behavior: An overview," *arXiv:0709.0724 [cond-mat.stat-mech]*, 2007.

[7] J. Loschmidt, "Über den zustand des wärmegleichgewichtes eines systems von körpern mit rucksicht auf die schwerkraft," *Wiener Berichte, 73, 139*, 1876.

[8] W. Thomson, "The kinetic theory of the dissipation of energy," *Proceeding of the Royal Society of Edinburgh, 8, 325–34*, 1874.

[9] E. Zermelo, "Über einen satz der dynamik und die mechanische wärmetheorie," *Wiedemann's Annalen, 57, 485–94 (1886) [English translation in: S.G. Brush, Kinetic theory, Vol. 2, Irreversible processes, pp. 208–17, Pergamon Press, Oxford]*, 1966.

[10] L. Boltzmann, "Entgegnung auf die wärmetheoretischen betrachtungen des hrn. e. zermelo," *Wiedemann's Annalen, 57, 773–84 (1896) [English translation in: S.G. Brush, Kinetic theory, Vol. 2, Irreversible processes, pp. 218–28, Pergamon Press, Oxford*, 1966.

[11] R. T. Sheldon Goldstein, Joel L Lebowitz and N. Zangh'ı, "Gibbs and boltzmann entropy in classical and quantum mechanics. in statistical mechanics and scientific explanation: Determinism, indeterminism and laws of nature," *World Scientific*, p. 519–581, 2020.

[12] M. Nielsen and I. Chuang, *Quantum Computation and Quantum Information: 10th Anniversary Edition*. Cambridge University Press, 2010.

[13] M. Kardar, *Statistical Physics of Particles*. Cambridge University Press, 2007.

[14] H. Breuer and F. Petruccione, *The Theory of Open Quantum Systems*. Oxford University Press, 2002.

[15] A. Wehrl, "General properties of entropy," *Rev. Mod. Phys.*, vol. 50, pp. 221–260, Apr 1978.

[16] D. Brody, D. Hook, and L. Hughston, "Microcanonical distributions for quantum systems," 07 2005.

[17] I. B. L. Veeren, *Micro vs Macro: Probing the frontiers between quantum and classical regimes*. PhD thesis, Centro Brasileiro de Pesquisas Físicas, 2023.

[18] P. S. Correia, P. C. Obando, R. O. Vallejos, and F. de Melo, "Macro-to-micro quantum mapping and the emergence of nonlinearity," *Phys. Rev. A*, vol. 103, p. 052210, 2021.

[19] C. Duarte, G. D. Carvalho, N. K. Bernardes, and F. de Melo, "Emerging dynamics arising from coarse-grained quantum systems," *Phys. Rev. A*, vol. 96, p. 032113, Sep 2017.

[20] R. O. Vallejos, P. S. Correia, P. C. Obando, N. M. O'Neill, A. B. Tacla, and F. de Melo, "Quantum state inference from coarse-grained descriptions: Analysis and an application to quantum thermodynamics," *Phys. Rev. A*, vol. 106, p. 012219, Jul 2022.

[21] J. Watrous, *The Theory of Quantum Information*. Cambridge University Press, 2018.

[22] M. M.Wolf, "Quantum channels and operations," *[available at https://www-m5.ma.tum.de/foswiki/pub/M5/Allgemeines/MichaelWolf/]*, 2012.

[23] R. Alicki, M. Fannes, and M. Pogorzelska, "Quantum generalized subsystems," *Phys. Rev. A*, vol. 79, p. 052111, May 2009.

[24] C. Bartsch and J. Gemmer, "Dynamical typicality of quantum expectation values," *Phys. Rev. Lett.*, vol. 102, p. 110403, Mar 2009.

[25] J. Casquilho and P. Teixeira, *Introduction to Statistical Physics*. Cambridge University Press, 2015.

[26] S. Salinas, *Introdução a Física Estatística Vol. 09*. EDUSP, 1997.

[27] P. Silva Correia and F. de Melo, "Spin-entanglement wave in a coarse-grained optical lattice," *Phys. Rev. A*, vol. 100, p. 022334, Aug 2019.

[28] C. Cohen-Tannoudji, J. Dupont-Roc, and G. Grynberg, *Atom-Photon Interactions: Basic Processes and Applications*. A Wiley-Interscience publication, Wiley, 1992.

[29] I. Bloch, "Quantum coherence and entanglement with ultracold atoms in optical lattices," *Nature*, vol. 453, 2008.

[30] H. Callen, *Thermodynamics and an Introduction to Thermostatistics*. Wiley, 1991.

[31] K. Huang, *Statistical Mechanics, 2nd Ed.* Wiley India Pvt. Limited, 2008.

[32] R. Kubo, R. Kubo, H. Ichimura, T. Usui, and N. Hashitsume, *Statistical Mechanics*. North-Holland Personal Library, Elsevier Science, 1990.

[33] F. Reif, *Fundamentals of Statistical and Thermal Physics*. Waveland Press, 2009.

[34] A. Streltsov, H. Kampermann, S. Wölk, M. Gessner, and D. Bruß, "Maximal coherence and the resource theory of purity," *New Journal of Physics*, vol. 20, p. 053058, may 2018.

[35] G. Gour, M. Müller, V. Narasimhachar, R. Spekkens, and N. Yunger Halpern, "The resource theory of informational nonequilibrium in thermodynamics," *Physics Reports*, vol. 583, 09 2013.

[36] P. Reimann, "Dynamical typicality of isolated many-body quantum systems," *Phys. Rev. E*, vol. 97, p. 062129, Jun 2018.

[37] P. Reimann, "Typicality for generalized microcanonical ensembles," *Phys. Rev. Lett.*, vol. 99, p. 160404, Oct 2007.

[38] M. Mueller, D. Gross, and J. Eisert, "Concentration of measure for quantum states with a fixed expectation value," *Commun. Math. Phys.*, vol. 303, p. 785, 2011.

[39] I. Saideh, A. D. Ribeiro, G. Ferrini, T. Coudreau, P. Milman, and A. Keller, "General dichotomization procedure to provide qudit entanglement criteria," *Phys. Rev. A*, vol. 92, p. 052334, Nov 2015.

[40] C. Tian and C. Kalia, "Stirling numbers of the second kind," *MIT PRIMES Circle Spring*, 2023.

# A Volume associated with microcanonical ensemble

We consider the operator

$$A = \alpha \frac{J_z}{j},$$

with spectrum

$$a_m = m\,\frac{\alpha}{j}, \quad m = -j, \ldots, j. \tag{A.1}$$

From Brody's construction, the volume of the set constrained by a given expectation value of an observable with non-degenerate energy spectrum can be written as [16]

$$\mathcal{V}(a) = (-1)^n\,\pi^n \sum_{m=0}^{n} \delta^{(-n)}\,(a_m a) \prod_{l=0, l\neq m}^{n} \frac{1}{a_l - a_m} \tag{A.2}$$

where $D = n + 1$ is the dimension of the system, $a_m$ is the $m$-th eigenvalue of $A$ and the $n$-th antiderivative of the Dirac delta distribution is

$$\delta^{(-n)}(x) = \begin{cases} 0, & x < 0 \\ \frac{1}{(n-1)} x^{n-1}, & x \geq 0 \end{cases} \tag{A.3}$$

Substituting Eq. (A.1) in Eq. (A.2) and focusing in the productory, we have

$$\begin{aligned} \prod_{l=-j, l\neq m}^{j} \frac{1}{\frac{\alpha}{j}^{2j}(l-m)} &= \left(\frac{j}{\alpha}\right)^{2j} \left[\prod_{l=-j}^{m-1} \frac{1}{(l-m)}\right] \left[\prod_{l=m+1}^{j} \frac{1}{(l-m)}\right] \\ &= \left(\frac{j}{\alpha}\right)^{2j} (-1)^{j+m} \prod_{l=-j}^{m-1} \frac{1}{(m-l)} \prod_{l=m+1}^{j} \frac{1}{(l-m)} \\ &= \left(\frac{j}{\alpha}\right)^{2j} \frac{(-1)^{j+m}}{(j+m)!(j-m)!}. \end{aligned} \tag{A.4}$$

The antiderivative in this case is

$$\delta^{(-2j)}\left(\frac{\alpha}{j} m - a\right) = \left(\frac{j}{\alpha}\right)^{2j-1} \frac{1}{(2j-1)!} \left[m - \frac{j}{\alpha} a\right]^{2j-1}, \qquad m \geq \tfrac{j}{\alpha} a \tag{A.5}$$

Substituting Eq. (A.4) and Eq. (A.5) in Eq. (A.2)

$$\mathcal{V}(a) = \frac{\pi^{2j} j}{(2j-1)!\,\alpha} \sum_{m \geq \lfloor ja/\alpha \rfloor}^{j} \frac{(-1)^{j+m}}{(j+m)!(j-m)!} \left(m - \tfrac{ja}{\alpha}\right)^{2j-1}. \tag{A.6}$$

It's possible to change variables and get closer to [16] formulation. If we set

$$\begin{aligned} k = j + m, \quad k = 0, ..., 2j \\ n = 2j \\ a' = a + \alpha \\ \omega = \alpha / j \end{aligned}$$

the Eq. (A.6) becomes

$$\mathcal{V}(a') = \frac{(-1)^n \pi^n}{(n-1)!\omega} \sum_{k \geq \lceil a'/\omega \rceil}^{n} \frac{(-1)^k}{k!(n-k)!} \left(k - a'/\omega\right)^{n-1}, \tag{A.7}$$

where $k = \lceil x \rceil$ define $k$ as the smallest interger that is freater than or equal to $x$. The normalized volume, obtained dividing Eq. (A.7) by the total volume of pure states, is

$$\mu(a') = \frac{(-1)^n n}{\omega} \sum_{k \geq \lceil a'/\omega \rceil}^{n} \frac{(-1)^k}{k!(n-k)!} \left(k - a'/\omega\right)^{n-1} \tag{A.8}$$

for a given expectation value.

# B Gaussian form of Eq. (3.30)

Consider

$$f(a) = \frac{(-1)^n \pi^n}{(n-1)!\omega} \sum_{m \geq \lceil \frac{E+\alpha}{\omega} \rceil}^{n} \frac{(-1)^m}{m!(n-m)!} \left( m - \frac{a+\alpha}{\omega} \right)^{n-1}, \tag{B.1}$$

where $a' = a + \alpha$. We can write the moments associated with Eq. (B.1) as

$$\gamma_k = \int_{a_{min}}^{a_{max}} da\ a^k f(a). \tag{B.2}$$

Substituting Eq. (B.1) in Eq. (B.2)

$$\gamma_k = \int_{-\alpha}^{m} da\ a^k \frac{(-1)^n \pi^n}{(n-1)!\omega} \sum_{m \geq \lceil \frac{a+\alpha}{\omega} \rceil}^{n} \frac{(-1)^m}{m!(n-m)!} \left( m - \frac{a+\alpha}{\omega} \right)^{n-1}. \tag{B.3}$$

Changing variables,

$$x = \frac{a+\alpha}{\omega} \tag{B.4}$$

$$x_{min} = 0 \tag{B.5}$$

$$x_{max} = m \tag{B.6}$$

$$\omega dx = da \tag{B.7}$$

And for each fixed $m$, the integral over $x$ should only include those $x$ with $x \leq m$. Then, we can rewrite Eq. (B.3)

$$\gamma_k = \frac{(-1)^n \pi^n}{(n-1)!\omega} \sum_{m \geq 0}^{n} \frac{(-1)^m}{m!(n-m)!} \int_0^m \omega dx\ (\omega x - \alpha)^k\ (m-x)^{n-1}. \tag{B.8}$$

The normalization is when $k = 0$. So,

$$\gamma_0 = \frac{(-1)^n \pi^n}{(n-1)!} \sum_{m \geq 0}^{n} \frac{(-1)^m}{m!(n-m)!} \int_0^m dx\ \ (m-x)^{n-1}. \tag{B.9}$$

That integral in Eq. (B.9) we can resolve by substitution

$$\int_0^m dx\ \ (m-x)^{n-1} = \frac{m^n}{n}$$

than Eq. (B.9) becomes

$$\begin{aligned} \gamma_0 &= \frac{(-1)^n \pi^n}{n(n-1)!} \sum_{m \geq 0}^{n} \frac{(-1)^m m^n}{m!(n-m)!} \\ &= \frac{(-1)^n \pi^n}{nn!(n-1)!} \sum_{m \geq 0}^{n} (-1)^m \binom{n}{m} m^n \end{aligned} \tag{B.10}$$

where we used the definition of binomial coefficient

$$\binom{n}{m} = \frac{n!}{m!(n-m)!}.$$

Using *Mathematica* to resolve the summation,

$$\sum_{m\geq 0}^{n} (-1)^m \binom{n}{m} m^n = (-1)^n n!$$

Thus, we can simplify $(-1)^n$ and $n!$ in Eq. (B.10) and we find

$$\gamma_0 = \frac{(-1)^n \pi^n}{nn!(n-1)!}(-1)^n n! = \frac{\pi^n}{n!}. \tag{B.11}$$

Similarly, to $k = 1$, the first moment is

$$\begin{aligned}\gamma_1 &= \frac{(-1)^n \pi^n}{(n-1)!} \sum_{m\geq 0}^{n} \frac{(-1)^m}{m!(n-m)!} \int_0^m \omega dx \, (\omega x - \alpha) \, (m-x)^{n-1} \\ &= \frac{(-1)^n \pi^n}{(n-1)!} \sum_{m\geq 0}^{n} \frac{(-1)^m}{m!(n-m)!} \left[\omega \int_0^m dx \, x \, (m-x)^{n-1} - \alpha \int_0^m dx \, (m-x)^{n-1}\right]. \end{aligned} \tag{B.12}$$

We can resolve the first integral in Eq. (B.12) by integration by parts

$$\int_0^m dx \, x \, (m-x)^{n-1} = \frac{m^{n+1}}{n(n+1)},$$

and Eq. (B.12) becomes

$$\begin{aligned}\gamma_1 &= \frac{(-1)^n \pi^n}{(n-1)!} \sum_{m\geq 0}^{n} \frac{(-1)^m}{m!(n-m)!} \left[\omega \frac{m^{n+1}}{n(n+1)} - \alpha \frac{m^n}{n}\right] \\ &= (-1)^n \pi^n \left\{ \left[\frac{\omega}{(n+1)!} \sum_{m\geq 0}^{n} \frac{(-1)^m m^{n+1}}{m!(n-m)!}\right] - \left[\frac{\alpha}{n!} \sum_{m\geq 0}^{n} \frac{(-1)^m m^n}{m!(n-m)!}\right] \right\} \end{aligned} \tag{B.13}$$

where we simplified $(n-1)!$ and we split the summation into two pieces. Using *Mathematica* again to resolve the summation

$$\sum_{m\geq 0}^{n} \frac{(-1)^m m^n}{m!(n-m)!} = \sum_{m\geq 0}^{n} (-1)^m \binom{n}{m} m^n = (-1)^n n! \tag{B.14}$$

$$\sum_{m\geq 0}^{n} \frac{(-1)^m m^{n+1}}{m!(n-m)!} = \sum_{m\geq 0}^{n} (-1)^m \binom{n}{m} m^{n+1} = (-1)^n n! S(n+1,n) = (-1)^n n! \frac{n(n+1)}{2}, \tag{B.15}$$

where

$$S(n+1,n) = \frac{n(n+1)}{2} \tag{B.16}$$

is a Stirling number of second kind. Therefore, Eq. (B.13) becomes

$$\begin{aligned}\gamma_1 &= \frac{(-1)^n \pi^n}{n!} \left\{ \left[\frac{\omega}{(n+1)!} \, (-1)^n n! \frac{n(n+1)}{2}\right] - \left[\frac{\alpha}{n!}(-1)^n n!\right] \right\} \\ &= \frac{\pi^n}{n!} \left(\frac{\omega n}{2} - \alpha\right) \end{aligned} \tag{B.17}$$

Recovering $n = 2j$ and $\omega = \alpha/j$, we obtain

$$\gamma_1 = 0 \tag{B.18}$$

Finally, for $k = 2$, the second moment is

$$\gamma_2 = \frac{(-1)^n \pi^n}{(n-1)!} \sum_{m\geq 0}^{n} \frac{(-1)^m}{m!(n-m)!} \int_0^m \omega dx \, (\omega x - \alpha)^2 \, (m-x)^{n-1} \,, \tag{B.19}$$

where

$$\int_0^m \omega dx \, (\omega x - \alpha)^2 \, (m-x)^{n-1} = \tag{B.20}$$

$$\left[\omega^2 \int_0^m dx \, x^2 \, (m-x)^{n-1} - 2\omega\alpha \int_0^m dx \, x \, (m-x)^{n-1} + \alpha^2 \int_0^m dx \, \, (m-x)^{n-1}\right]. \tag{B.21}$$

Resolving each integral by substitution or integration by parts methods, we get

$$\int_0^m dx \, \, (m-x)^{n-1} = \frac{m^n}{n} = \frac{m^n (n-1)!}{n!}$$

$$\int_0^m dx \, x \, (m-x)^{n-1} = \frac{m^{n+1}}{n(n+1)} = \frac{m^{n+1}(n-1)!}{(n+1)!}$$

$$\int_0^m dx \, x^2 \, (m-x)^{n-1} = \frac{2m^{n+2}}{n(n+1)(n+2)} = \frac{2m^{n+2}(n-1)!}{(n+2)!}$$

Splitting the summation into three parts,

$$\sum_{m\geq 0}^{n} \frac{(-1)^m}{m!(n-m)!} \frac{m^n}{n!} = \frac{1}{n!} \sum_{m\geq 0}^{n} (-1)^m \binom{n}{m} m^n = (-1)^n S(n,n) \frac{n!}{n!}$$

$$\sum_{m\geq 0}^{n} \frac{(-1)^m}{m!(n-m)!} \frac{m^{n+1}}{(n+1)!} = \frac{1}{(n+1)!} \sum_{m\geq 0}^{n} (-1)^m \binom{n}{m} m^{n+1} = (-1)^n S(n+1,n) \frac{n!}{(n+1)!}$$

$$\sum_{m\geq 0}^{n} \frac{(-1)^m}{m!(n-m)!} \frac{2m^{n+2}}{(n+2)!} = \frac{2}{(n+2)!} \sum_{m\geq 0}^{n} (-1)^m \binom{n}{m} m^{n+2} = (-1)^n S(n+2,n) \frac{2n!}{(n+2)!}$$

and the Stirling numbers of second kind are [40]

$$S(n,k) = \sum_{i=0}^{k} \frac{(-1)^{k-i} i^n}{(k-i)!i!}.$$

Thinking of boxes, if we want to number to partition a set of $n+2$ objects into $n$ non-empty boxes, two options are available:

- One subset contains 3 elements, and the rest are singletons.

$$\binom{n+2}{3} = \frac{n(n+1)(n+2)}{6}$$

- Two subsets contain 2 elements each, and the rest are singletons. It is, 4 elements will be paired, then partition them into 2 pairs in 3 different ways.

$$3\binom{n+2}{4} = \frac{(n-1)n(n+1)(n+2)}{8}.$$

So,

$$S(n+2,n) = \frac{n(n+1)(n+2)}{6} + \frac{(n-1)n(n+1)(n+2)}{8} = \frac{(3n+1)n(n+1)(n+2)}{24}.$$

Thus the second moment is, after some simplifications of $(n-1)!$ and $(-1)^n$,

$$\begin{aligned}\gamma_2 &= \frac{\pi^n}{n!}\left[\frac{2\omega^2 n!}{(n+2)!}\frac{(3n+1)n(n+1)(n+2)}{24} - 2\omega\alpha\frac{n!n(n+1)}{2(n+1)!} + \alpha^2\right] \\ &= \frac{\pi^n}{n!}\left[\frac{\omega^2(3n+1)n}{12} - \omega\alpha n + \alpha^2\right]. \end{aligned} \tag{B.22}$$

Once the moments are defined, we write the variance recovering $n = 2j$ and $\omega = \alpha/j$ as

$$\sigma^2 = \frac{\gamma_2 - \gamma_1^2}{\gamma_0} = \frac{\alpha^2}{6j}. \tag{B.23}$$